INFORMATION TO USERS

This reproduction was made from a copy of a document sent to us for microfilming. While the most advanced technology has been used to photograph and reproduce this document, the quality of the reproduction is heavily dependent upon the quality of the material submitted.

The following explanation of techniques is provided to help clarify markings or notations which may appear on this reproduction.

1. The sign or "target" for pages apparently lacking from the document photographed is "Missing Page(s)". If it was possible to obtain the missing page(s) or section, they are spliced into the film along with adjacent pages. This may have necessitated cutting through an image and duplicating adjacent pages to assure complete continuity.

2. When an image on the film is obliterated with a round black mark, it is an indication of either blurred copy because of movement during exposure, duplicate copy, or copyrighted materials that should not have been filmed. For blurred pages, a good image of the page can be found in the adjacent frame. If copyrighted materials were deleted, a target note will appear listing the pages in the adjacent frame.

3. When a map, drawing or chart, etc., is part of the material being photographed, a definite method of "sectioning" the material has been followed. It is customary to begin filming at the upper left hand corner of a large sheet and to continue from left to right in equal sections with small overlaps. If necessary, sectioning is continued again—beginning below the first row and continuing on until complete.

4. For illustrations that cannot be satisfactorily reproduced by xerographic means, photographic prints can be purchased at additional cost and inserted into your xerographic copy. These prints are available upon request from the Dissertations Customer Services Department.

5. Some pages in any document may have indistinct print. In all cases the best available copy has been filmed.

University Microfilms International
300 N. Zeeb Road
Ann Arbor, MI 48106

Hart, Dale

AN EVALUATION OF FLUID INCLUSION TECHNIQUES AS TOOLS IN MINERAL EXPLORATION AS APPLIED AT THE YELLOW ASTER GOLD MINE, CALIFORNIA

University of Alaska, Fairbanks M.S. 1986

PLEASE NOTE:

In all cases this material has been filmed in the best possible way from the available copy. Problems encountered with this document have been identified here with a check mark __√__.

1. Glossy photographs or pages _____
2. Colored illustrations, paper or print _____
3. Photographs with dark background _____
4. Illustrations are poor copy _____
5. Pages with black marks, not original copy _____
6. Print shows through as there is text on both sides of page _____
7. Indistinct, broken or small print on several pages √
8. Print exceeds margin requirements _____
9. Tightly bound copy with print lost in spine _____
10. Computer printout pages with indistinct print _____
11. Page(s) _____ lacking when material received, and not available from school or author.
12. Page(s) _____ seem to be missing in numbering only as text follows.
13. Two pages numbered _____. Text follows.
14. Curling and wrinkled pages _____
15. Dissertation contains pages with print at a slant, filmed as received _____
16. Other _____

_____

_____

University
Microfilms
International

AN EVALUATION OF FLUID INCLUSION TECHNIQUES AS TOOLS IN MINERAL EXPLORATION AS APPLIED AT THE YELLOW ASTER GOLD MINE, CALIFORNIA

A

THESIS

Presented to the Faculty of the University of Alaska
in Partial Fulfillment of the Requirements
for the Degree of

MASTER OF SCIENCE

BY

DALE HART B.Sc.Hons. ARSM, DIC

Fairbanks, Alaska

May 1986

AN EVALUATION OF FLUID INCLUSION TECHNIQUES AS TOOLS IN MINERAL EXPLORATION AS APPLIED AT THE YELLOW ASTER GOLD MINE, CALIFORNIA

RECOMMENDED:

Chairman, Advisory Committee

Department Head

APPROVED:

Dean, School of Mineral Engineering

Director of Graduate Programs

4 August 1986

Date

Abstract

Fluid inclusions have the potential to provide useful data during a minerals exploration program. Three fluid inclusion techniques were applied at the former Yellow Aster gold mine in California, which produced 500,000 troy ounces of gold until 1923. The techniques evaluated independently were; decrepitate linked induction coupled plasma emission spectrographic analysis (DICP), fluid inclusion mapping and fluid inclusion microthermometry.

Approximately 100 analyses of quartz revealed DICP to be an inappropriate technique at Yellow Aster. Fluid inclusion mapping of 100 thin sections was a relative success and highlighted the increased inclusion abundance in quartz associated with gold mineralization. Conclusions based on greater than 1200 microthermometric measurements suggest gold-sulfide mineralization is a result of fluid boiling. Successive generations of inclusions record the loss of 20 mole percent carbon dioxide from the fluid regime and the overall cooling from 330°C to 240°C. Redox reactions controlled gold deposition in the near surface zones.

Acknowledgements

The author gratefully acknowledges the help and advice of all those involved with the evolution of this thesis.

At Imperial College of Science, London, England warm thanks to former colleagues Dr.Alexandra Kay, Dr.Elizabeth Jones, Dr.Stephen Chryssoulis, and Dr.Chris Wellings. Special thanks to Dr.Andy Rankin supervisor and co-worker on various projects. Thanks also to the technical staff of the Mining Geology Section at the Royal School of Mines for their high quality sample preparation work.

At British Petroleum Minerals special thanks to Dr.Michael Harris for his encouragement and for suggesting the Yellow Aster mine as a suitable topic. Warm thanks to Dr.J.P.N.Badham whose enthusiasm and continuing interest were very much appreciated.

At Amselco Exploration Inc., USA, thanks are due principally to Mr. Edgar Lockhart, Steve Kay and Dr.Barry Rayment, for financial support and cooperation.

At Memorial University, Newfoundland, Canada thanks are due to Dr's Simon Jackson and David Strong for their help, advice and cooperation.

At the University of Alaska, thanks to fellow student Roger Burleigh for helpful discussion. Thanks also to my committee particularly Dr.Sam Swanson for his sound advice. Special thanks are due to Paul Metz, chairman of my committee, for his support and suggesting Alaska as a place to study. Financial support through the Mineral Industry Research Laboratory is gratefully acknowledged.

Finally, thanks to Curtis Freeman for his thorough reviews and to my wife Cathy, for a splendid job of typing, and her unfailing support.

TABLE OF CONTENTS

List of Figures

List of Tables

General Introduction

This thesis is based on work carried out at Imperial College of Science and Technology, London, England and at the University of Alaska, Fairbanks, Alaska between 1982 and 1986.

During the period December 1982 to August 1984 the author was employed as a Research Assistant on two separate though related research projects, sponsored by British Petroleum Minerals International Ltd., (BPMIL) at the Royal School of Mines, London. Data from both of these projects are included in this thesis with the permission of BPMIL and Imperial College.

The projects were entitled:

a) 'application of induction coupled plasma (ICP) emission spectrography to the evaluation of steam aureoles as prospecting guides to intrusive hosted mineralization'. The project ran from February to December 1983 under the joint direction of Dr.Andrew Rankin (Imp.Col.) and Dr.Michael Harris (BPMIL-Edinburgh, Scotland).

b)'Fluid inclusions in gold deposits', which ran from January to August 1984, under the joint direction of Dr.Andrew Rankin (Imp. Col.) and Dr.Nick Badham (BPMIL), and subsequently on a consultancy basis until December

1984.

The technique of fluid inclusion decrepitate analysis by linking to an induction coupled plasma and emission spectrophotometer (abbreviated to DICP herein) was first developed at Imperial College, London in 1979. Funding from the European Economic Community (EEC) and National Environmental Research Council (NERC) until 1982 established DICP as an almost routine analytical technique. The results produced are of a semi-quantitative nature based on the chemical analysis of bulk decrepitable inclusion contents. The rationale underlying the technique assumes fluid inclusions provide a direct method of assessing whether metal rich and potentially ore forming fluids have passed through a body of host rock.

Encouraging results from studies on tin mineralized granites of the Cornubian Province (Rankin and Alderton, 1982) created 'industrial interest' in fluid inclusions. A project to test rigorously any precious metal exploration potential of fluid inclusions was developed by Dr.Mike Harris (BPMIL) in conjunction with Dr.Andy Rankin (see above). The Yellow Aster mine, in the Randsburg Mining District, Kern County, California was suggested as a suitable field site. The Yellow Aster

mine had a reported visual fluid inclusion abundance anomaly and widespread gold mineralization (M.Harris, 1980b). The field site also offered the logistical support of an active exploratory program being conducted by Amselco Exploration Inc., (a BPMIL subsidiary).

During late 1983, Dr.Nick Badham, BPMIL research manager initiated a global project to investigate several geological aspects of hydrothermal gold deposits. The author was employed to investigate fluid inclusion in gold deposits at Imperial College. Yellow Aster in California was chosen as one of the suitable field sites.

At the commencement of this second project at Imperial College, permission was gained from BPMIL and Amselco Exploration Inc., to continue the study of the Yellow Aster mine and surrounding area for my proposed Master of Science thesis in Geological Engineering at the University of Alaska.

Chapter 1

FLUID INCLUSIONS IN MINERALS EXPLORATION

Introduction

Fluid inclusions are small, generally less than 100μm pockets of fluid trapped within crystalline materials. These small fluid-filled cavities may be sealed off during the growth of the surrounding crystal yielding primary inclusions. However, they may be introduced post-crystallization in association with a fracturing and rehealing process, yielding secondary inclusions (Roedder 1984a).

Irrespective of their geneses, fluid inclusions are samples of a fluid (or fluids) present at some stage in a crystal's geological history. Consequently, they have been used to obtain data on the PTX regime of the prevailing fluid present either during crystal growth or some later alteration event. The potential for the application of fluid inclusions in minerals exploration becomes obvious should a discrete inclusion population be associated with economic mineralization. Roedder (1977) presents an excellent review of the potential applications of fluid inclusions in mineral exploration.

This chapter briefly outlines some of the applications, basic premises, and shortcomings of fluid inclusions as exploration tools for economic mineralization, principally gold.

Primary, secondary and pseudosecondary inclusions

The recognition of primary inclusions, i.e those trapped during the period of crystal growth, is critical to any fluid inclusion study. Consequently, secondary inclusions are often not studied. However, it should be kept in mind that many if not most mineralizing events are episodic. Petrographic studies on many gold-quartz veins indicate the gold has been introduced later than the bulk of quartz, often associated with a fracturing episode(Roedder, 1984b: Smith and Kesler, 1985). Thus, at least some of the secondary inclusions contain the actual gold depositing fluid (Boyle, 1954). In this study the composition of the various generations of secondary inclusions were suspected to be a key factor in understanding the evolution of the fluid regime at the Yellow Aster mine in California.

Excellent descriptions of the petrographic features used to distinguish primary and non-primary inclusions can be found in Roedder (1972 and 1984b, Appendix I).

Applying the criteria in practice is often more difficult, and a clear distinction between genetic types may require a thorough microthermometric investigation in tandem with morphological description (Rankin and Hart, 1985).

Possible applications for fluid inclusions in the exploration environment

Unfortunately much of the work in this field has been published in Russian and is not generally available in English (except as abstracts). Ermakov (1965) observed that hydrothermal ore deposits were commonly surrounded by various alteration halos. He suggested that in an ideal case an inner macroscopic alteration halo would decrease in intensity with increasing distance from mineralization becoming a trace element or geochemical halo.This alteration halo could be exceeded in extent by a distinctive fluid inclusion halo shown schematically in figure 1.1

The zonation represents the migration of a hydrothermal fluid through a body of rock. At some distance from the mineralization, macroscopically visible alteration would cease but the fluid might retain the potential to heal fractures in the host rocks and become

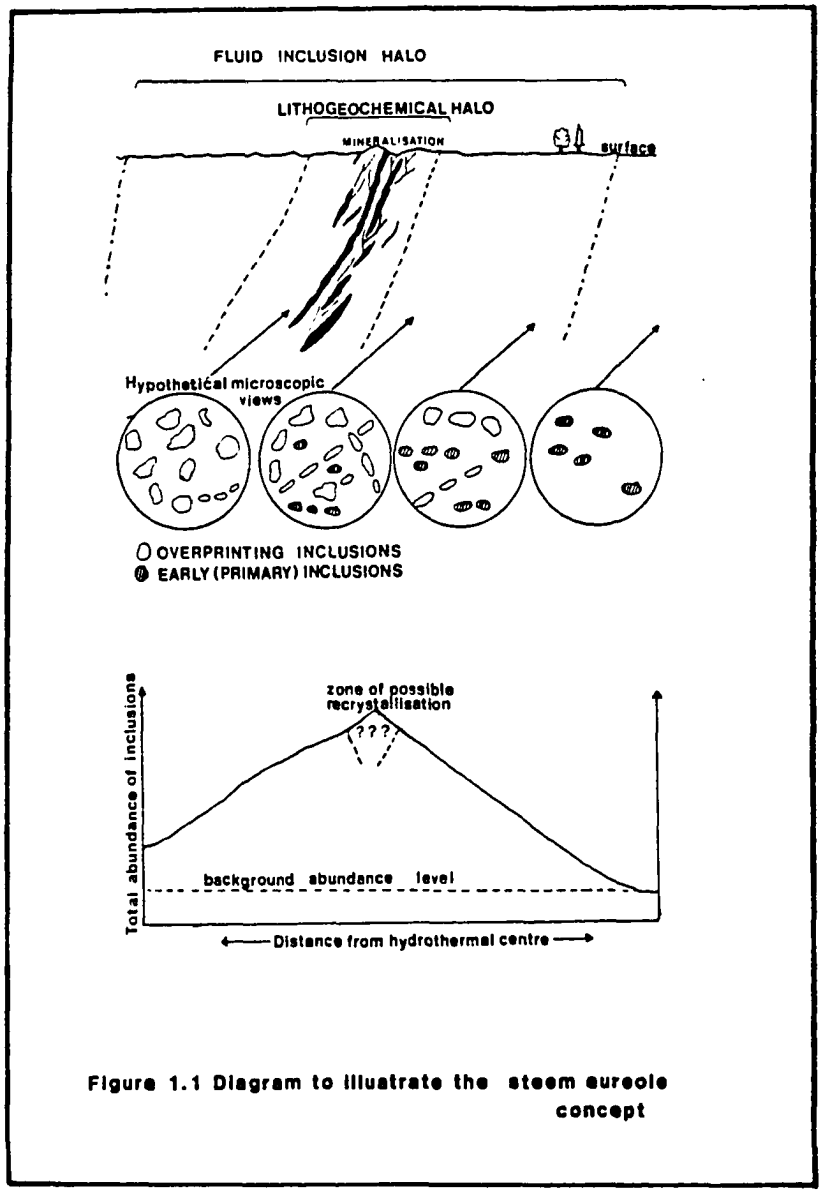

Figure 1.1 Diagram to illustrate the steam aureole concept

trapped as secondary or overprinting inclusions (figure 1.1).

This concept has obvious exploration potential particularly for hidden ore bodies, theoretically providing a larger target area than even the trace element halo associated with mineralization. The inclusion halo might be detected by either:
a) variation in the total abundance of fluid inclusions, increasing towards the palaeo-fluid focus, or by
b) compositional variation between the earlier (indigenous) and the later overprinting generations of inclusions.

Rankin and Alderton (1983) observed both a variation in the total abundance and compositional variation of fluid inclusions associated with the tin mineralized granites of southwestern England, in ordinary petrographic thin sections of igneous quartz from the granites. They concluded that fluid inclusion petrography (fluid inclusion mapping) provided a good record of the complex and temporally restricted nature of hydrothermal events, as exemplified in S.W. England.

Roedder (1984a) suggests the main potential for applications of fluid inclusions to gold exploration are:
1) fluid inclusions can help clarify the regional or local geology
2) fluid inclusions can provide a larger target area in the search for concealed ore-bodies, or provide directional information for design of a drilling program.
3) Fluid inclusions can aid in the recognition of hidden deposits because characteristic inclusions might still be found in resistant minerals in stream sediments or weathered outcrops.
4) Fluid inclusions can be used to clarify the P-T-X environment of ore deposition and perhaps help characterize a distinctive genetic model.

Application of fluid inclusions to the characterization and recognition of mineralizing fluids

Many of the problems of ore genesis which stimulated the polemic interpretations of earlier years have been resolved. Fluid inclusion science has made a significant contribution to these advances. For example, fluid inclusions were particularly important in the debate that centered on the origin of the fluids responsible for Mississippi Valley-type ores (Roedder, 1967). Numerous inclusion studies revealed the ore fluids to have

homogenization temperatures in the range of 100 to 150°C, being essentially sodium-calcium chloride brines, often containing appreciable dissolved methane in solution (Hutchinson, 1985). These observations are felt to preclude the surface or sea water syngenetic origin for lead-zinc mineralization popular in Western Europe (Skinner and Barton, 1973: Roedder, 1976: Roedder, 1984b), and also probably discount a primary magmatic source (Roedder, 1976).

Fluid inclusion studies of the porphyry copper mineralization of the southwestern U.S.A also revealed that these hydrothermal systems had evolved through a boiling stage and were characterized by highly saline inclusions (Nash, 1973: Nash, 1976: Moore and Nash, 1976: Theodore and Nash, 1973: Roedder, 1971 and Blake and others, 1978).

Fluid inclusion evidence bearing on the environments of gold deposition is the subject of an excellent paper by Roedder (1984a). Based on a review of the pre-1978 literature (dominantly Russian) Roedder concludes that most gold-mineralizing fluids are in the 100-400 °C temperature range. The mineralizing solutions are generally dilute (<10 wt% for the total of the major ions) although carbon dioxide is present in many

solutions, sometimes as a major constituent. Roedder notes that carbon-dioxide bearing inclusions are ubiquitous in gold ores from metamorphic environments. An attempt to quantify the character of ore fluids associated with various types of gold mineralization is shown in Table 1.1.

Since 1978, the literature has contained more frequent reports of carbon-dioxide bearing inclusions in gold bearing environments. Kay and Strong (1983) report a high abundance of carbon dioxide-bearing inclusions in gold-bearing quartz veins at the Moretons Harbour area, Newfoundland, Canada. Harris (1979 and 1980) observed carbon dioxide-bearing inclusions, possibly indicating boiling, in the gold mineralized portions of a Hercynian granodioritic complex at Salave in northwestern Spain. Leake and others (1979) and Hart (1984) report a carbon dioxide-bearing fluid inclusion assemblage in the quartz-arsenopyrite-gold veins at the margins of the Loch Doon granite complex in southwestern Scotland. Metz (1983) has established a positive correlation between the molar proportion of carbon dioxide in fluid inclusions and the amount of gold in quartz veins of the Fairbanks mining district, Alaska. Burleigh (in press) reports a very important component of carbon dioxide to the gold - telluride mineralizing fluids at the Independence Mine,

Table 1.1. Fluid inclusion compositions associated with gold mineralization.

Deposit type	TH (°C) Range	Fluid Composition	Comments	References
Archean greenstone (gold-quartz carbonate veins.	250-400	H_2O-CO_2 $\pm CH_4$ ($\leqslant$25 Mole % CO_2)	Boiling not common. Depth usually >6 km.	Smith, Cloke and Kessler, 1984; Boyle, 1979; Boyle and others, 1975
Epithermal lode gold Mesozoic volcanic association).	200-300	H_2O-NaCL 3-20 Eq. Wt % NaCL $\pm CO_2$	Boiling very common.	Berger and Eimon, 1982; Buchanan, 1981; Hayba, 1983; Giles and Nelson, 1982; Walthier, Sirvas and Araneda, 1985
Hot Springs 'type' gold deposits.	150-200	$H_2O >> CO_2$ CO_2 as dissolved gas	Boiling common.	Schnorr and others, 1984; Rankin and Hart, 1985
Carlin 'type' deposits.	175-200	$H_2O \pm CO_2$ ±NaCL	Dilute low salinity fluids.	Nash, 1972; Radtke, Rye and Dickson, 1981
Intrusive hosted gold deposits.	250-350	$H_2O \pm CO_2$ ±NaCL	Boiling sometimes observed.	Harris, 1979; Hart and Rankin, 1983; Rankin and Hart, 1985

in the Willow Creek Mining District, Alaska. Masterman (in press) suggests that carbon dioxide bearing fluids played an important role in the evolution of the tin-gold mineralized plutons of the Circle Mining District, Alaska.

Smith and Kesler (1985) studied fluid inclusions in quartz-carbonate veins of the Hollinger-McIntyre gold mine at Timmins, Ontario, Canada. Gas chromatographic analyses of fluid inclusions in ore-bearing veins have higher carbon dioxide contents than those in non-ore veins. Extensive sampling and analyses of veins from the surrounding area revealed a well developed zonation of carbon dioxide contents about the main zone of mineralization. Low carbon dioxide levels (1-3 mole percent) were detected in peripheral veins, increasing to a maximum of greater than 12 mole percent in mineralized zones. The importance of a carbon dioxide component to the mineralizing fluid in Archean greenstone gold terranes is also suggested by Boyle (1979), Kerrich (1980), Kerrich and Fyffe (1981), Fyon and Crocket (1980).

Schnorr and others (1984) conclude that carbon dioxide-bearing inclusions have a potential application in gold exploration. They utilized decrepitation linked

gas chromatographic analyses of jasperoid outcrops around the Pueblo Viejo gold-silver ore body in the Dominican Republic to delineate an anomalous carbon dioxide depletion over the ore zone.

These studies suggest that any exploration technique using chemical analyses of fluid inclusion contents should be able to analyze for carbon dioxide, or its constituent elements. However carbon dioxide, though very important in some gold-bearing systems, is not associated with all types of gold mineralization (Table 1). Rankin and Hart (1985) observed carbon dioxide-bearing fluid inclusions very infrequently in a study of 150 samples from approximately 15 gold mines or prospects in established gold mining locations (including Transvaal, S. Africa: the Coromandel Peninsula in New Zealand: several `porphyry' type gold mines/prospects in the southwestern U.S.A). Thus the mere presence or absence of carbon dioxide (based on observation only) within fluid inclusions is not an adequate criterion for assessing the gold mineralization potential of a prospect. This illustrates that fluid inclusions are not a panacea for exploration but should be used in conjunction with other evaluatory techniques to better understand the environment of ore deposition.

Limitations and practical aspects of inclusion studies

Some of the more serious limitations to the widespread application of fluid inclusion studies to gold deposits are listed below:

a) many fine grained gold-bearing quartz veins do not contain inclusions suitable for study (Roedder, 1984b: Rankin and Hart, 1985).

b) Most inclusions in gold-bearing quartz are small and difficult to study. Rankin and Hart (1985) found gold deposits to be characterized by their abundance of less than 10 μm inclusions, commonly with irregular morphology. Of the 150 samples investigated, approximately 20 percent contained inclusions suitable for microthermometric study.

c) To fully utilize the pressure - temperature - composition data provided by inclusions, and its implications for the ore depositional environment, the specific generation of inclusions associated with mineralization must be established. This task is very difficult in regions of episodic fluid activity and multiple overprinting.

Chapter 2

GEOLOGIC SETTING AND MINERALIZATION IN THE RANDSBURG-JOHANNESBURG-ATOLIA AREA OF THE RAND MINING DISTRICT, CALIFORNIA

Introduction

The selection of a suitable field site to evaluate the potential application of some fluid inclusion technologies to gold exploration was made in conjunction with BPMIL (see general introduction).

A field site for which precious metal assay data were freely available and also having a well developed inclusion assemblage was necessary. The Yellow Aster mine area in Kern County, California satisfied both criteria. The general area also had significant past production in both silver and tungsten from the Kelly and Atolia groups of mines respectively (Table 2.1). These mineralizations were spatially separate and it was felt might allow characterization of the hydrothermal fluid associated with each, elucidating or negating any genetic link.

This chapter outlines the detailed geology of the study area. It is felt that the potential applications and drawbacks of fluid inclusions in exploration programs can only be accurately evaluated in light of a sound

Table 2.1. Estimated production figures for mines in the Randsburg Mining District.

Mine Name	Metal	Production Period	Production (lode source)	$ 1985 production value	Source
A. Gold Mines					
Yellow Aster	Au	1895-1924	500,000 oz.	162.5×10^6	Hulin, 1925
Sunshine	Au		53,000 oz.		Clark 1970
Little Butte	Au		20,000 oz.		Clark, 1970
Butte Wedge	Au		25,000 oz.		Hess, 1910
Baltic	Au		1430-2500 oz.		Clark, 1970
Black Hawk	Au		35,000 oz.		Clark, 1970
Bully boy	Au		6,000 oz.		Clark, 1970
Consolidated	Au		2,500 oz.		Clark, 1970
King Solomon	Au		25,000 oz.		Clark, 1970
Lucky Boy	Au		6,000 oz.		Clark, 1970
Big Dike	Au		10,000 oz.		Clark, 1970
Big Gold	Au		25,000 oz.		Clark, 1970
Butte	Au		100,000 oz.		Clark, 1970
Buckboard	Au		25,000 oz.		Clark, 1970
Minnehaha	Au		5,000 oz.		Clark, 1970
Operator Divide	Au		30,000 oz.		Clark, 1970
Sidney	Au		12,500 oz.		Clark, 1970
			882,500 oz.	287.7×10^6	

Table 2.1 (Continued)

Mine Name	Metal	Production Period	Production (lode source)	$ 1985 production value	Source
B. Silver Mines					
"Kelly Mines"	Ag	1919-1937	18,000,000 oz.	108×10^6	Hulin, 1925
C. Tungsten Mines					
Union Mine	WO_3	1915-1939	4433 tons		Lemmon and Dorr, 1940

geological framework. Some of the work reported in this chapter is taken from other authors.

Location

The Randsburg Mining District is located about 241 air kilometers NNE of Los Angeles, California, in the northern portion of the Mojave desert geomorphic province (figure 2.1). The towns of Randsburg and Johannesburg are serviced by U.S. Highway 395 and lie along the Kern County-San Bernadino County divide.

Past mineral production

Production in the Randsburg Mining District probably began with the discovery of placer gold at Goler Wash 9 miles northwest of Randsburg in the winter of 1893-94 (Hess, 1910). Gold was discovered at the Yellow Aster (formerly the Olympus) mine in 1895 resulting in a small gold rush. Production from the Yellow Aster mine between 1895-1924 (Hulin,1925) is estimated to exceed 500,000 troy ounces. Several other significant gold mines were located near the Yellow Aster mine, (figure 2.2) and their estimated production is given in Table 2.1.

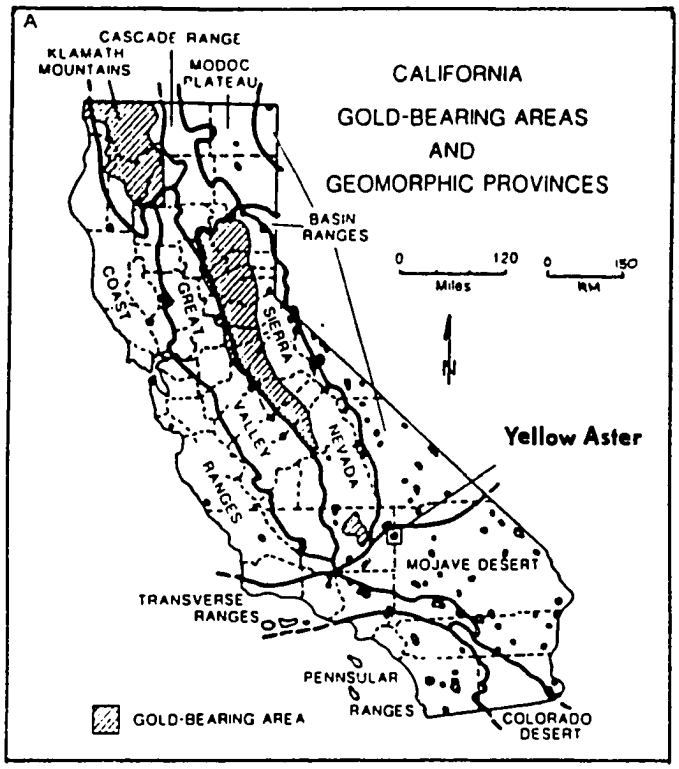

Figure 2.1 Physiographic setting of the study area

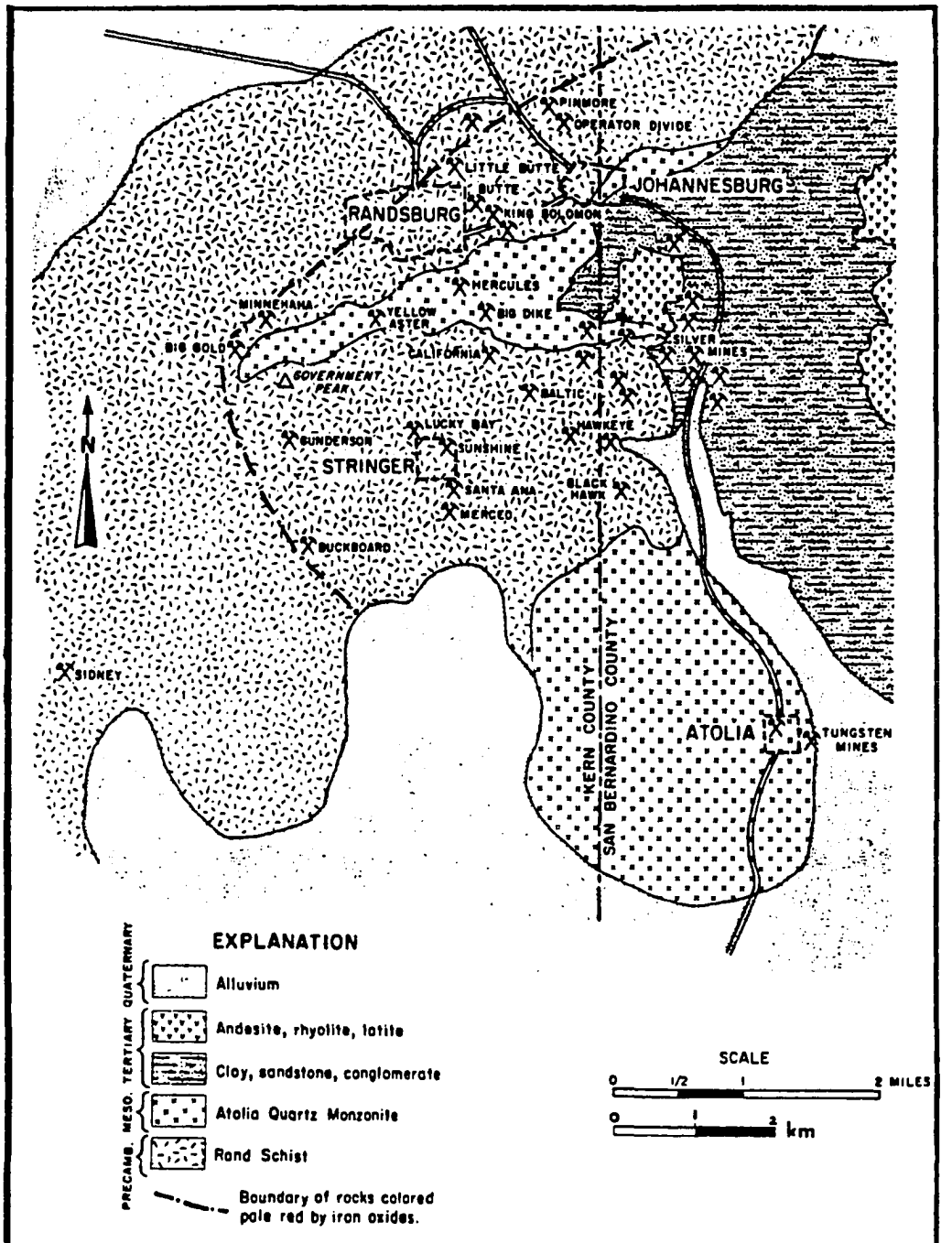

Figure 2.2 Location of mines with significant past production in the Rand Mining District (after Troxel and Morton 1962)

World War I created a demand for tungsten which resulted in the discovery of placer and subsequently lode scheelite in the Atolia region to the south of Johannesburg (figure 2.2). Total production is estimated at 10,000 short ton units of WO3 (Morehouse, 1984). The mines have been worked intermittently for the past 10-15 years. Production figures for some mines are given in Table 2.1.

Silver production at the Kelly mine (formerly the California Rand Silver mine) began in 1919 following the passing of the Pittman Act guaranteeing a $1.00 per troy ounce price for domestic silver (Tucker and Sampson, 1940). Total production from the Kelly and associated silver mines is estimated at 18 million troy ounces (Table 2.1 and figure 2.2). Production has been limited since about 1940.

Current exploration activity is centered on the Stringer District south of the Yellow Aster pit where recent drilling has delineated a potential low grade gold orebody. Estimated reserves are 27 million metric tons at an average grade of 0.03 oz/ton (Sassos, 1986).

Previous work

Hulins 1925 Ph.D thesis submitted at the University of California, subsequently issued as California Division of Mines and Geology Bulletin 95, is the only comprehensive work on the geology and mineralization of the Randsburg Mining District. This excellent text and geological map guided most of the initial sampling carried out in the Yellow Aster region.

More recently, as a result of renewed economic interest in the region several investigations have been initiated. Dr. Simon Jackson of Memorial University Newfoundland, Canada is currently investigating the major, trace, and rare earth element geochemistry associated with the mineralization in the Randsburg area. Reference will be made to the unfinished Masters thesis of the late Jeff Morehouse, who prior to his untimely death in a climbing accident in 1985 was evaluating the role of structural control on alteration and mineralization in the Randsburg District.

Regional geology

The Rand Mountains, of reported Precambrian age, (Clark, 1970) form an approximately southwest trending chain some eighteen kilometers long and six kilometers wide. The rocks are known as the Rand Schist (greenschist facies), which have been intruded by later stocks of quartz monzonite, granodiorite and rhyolite compositions (figure 2.2). To the east of the Rand section are poorly consolidated sediments of the Rosamond Series (Hulin, 1925) which consist of clays, feldspathic sandstone and conglomerate of probable continental derivation. Rosamond Series of Miocene Age rocks are overlain to the east by a flat sequence of dominantly andesitic volcanics, approximately five million years old, (Hulin, 1925) which forms the prominent Red Mountain overlooking US Highway 395.

The Garlock fault, a major structure associated with the San Andreas fault system, occurs eight miles north of the Rand Mountains, approximately parallel to the south west trend. The history of faulting in the region is complex and is intimately associated with mineralization events (Morehouse, 1984).

Morehouse (1984), based on Rb/Sr dating of the Rand Schist, suggests that it was metamorphosed 160 ±25 Ma, although mariposite indicates an 80 Ma metamorphic event. Jacobson (1983) suggests that the deformation of the Pelona, Orocopia and Rand Schists of southern California occurred during a northeastward directed thrust event approximately 50-60 Ma. An upper plate of Precambrian, Palaeozoic, and Mesozoic igneous and metamorphic rocks of continental character is interpretted to have been thrust over a Pelona-Orocopia-Rand Schist lower plate (Jacobson, 1983). The lower plate, comprised of greywacke, shale, basaltic volcanics, chert and ultramafic rock is considered to be oceanic in nature. Morehouse (1984) also considers the Rand Thrust, which is exposed south of the study area, to be coeval with the metamorphism of the Rand Schist, and that the rocks are subduction related. Jackson and Strong (1985) observed possible mafic and ultramafic olistoliths within the schist at the Yellow Aster open pit further supporting a possible subduction related origin for the schist protolith.

Geology of the Yellow Aster, Kelly and Atolia mine areas.

Recent radiogenic isotope work by Jackson and Strong (1985) and Morehouse (1984) has led to a revision of the ages generally associated with the intrusions of the mineralized areas (i.e. those of Hulin 1925). Prior to a geochronologic account of the events defined by this work, a petrographic descriptive report on the various lithologies present is warranted.

Petrology

This section is based on descriptions of a suite of approximately 100 thin sections cut from samples collected by the author in the area (figure 2.3) during 1983 and 1984. Some reference to similar work undertaken by Jackson and Strong (1985) will also be made. The geologic base map showing the areal extent of the lithologic units discussed is used with the kind permission of Amselco Exploration Incorporated (Appendix II).

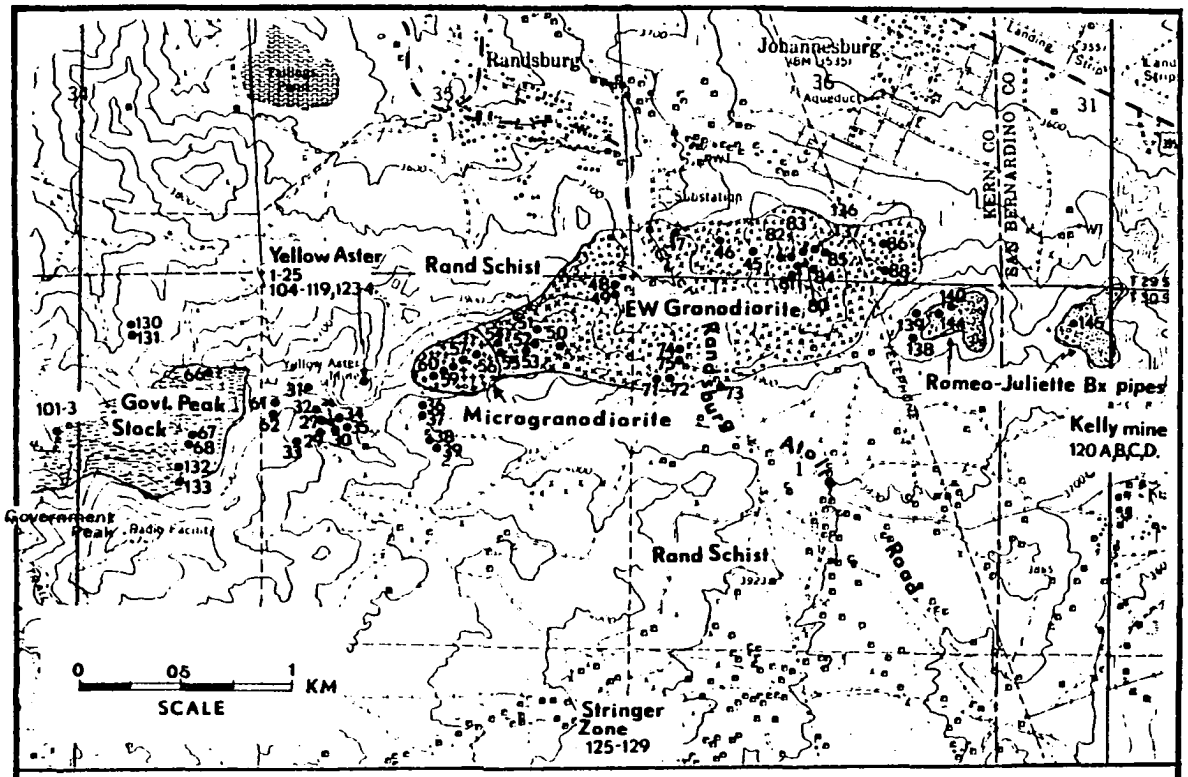

Figure 2.3 Location of samples taken

Rand Schist

The Rand Schist is comprised dominantly of biotite - albite, biotite - hornblende - albite, and biotite - chlorite - albite - quartz schists,with lesser amounts of amphibolite and quartzite. In thin section they typically contain subhedral albite porphryoblasts and lenses of quartz usually surrounded by elongated masses of biotite or chlorite. Locally muscovite and actinolitic schists are also observed within the Yellow Aster open pit. The amount of quartz observed in the schistose rocks seemed to increase with proximity to the intrusive bodies and may indicate a slight silicification concomitant with thermal metamorphism. Jackson and Strong (1985) report the mafic and ultramafic rocks observed within the schist are comprised almost entirely of talc, although some primary igneous plagioclase is possibly retained. Whole rock and trace elemental analyses reveal these rocks to have high chromium and nickel contents (Appendix II - data from Jackson and Strong, 1985) supporting a mafic/ultramafic protolith.

Intrusive rocks

The Rand Schist has been intruded by several igneous plutonic bodies and dikes of varied composition (Appendix II). These are described as:

a) Atolia quartz monzonite,

b) EW granodiorite,

c) Microgranodiorite,

d) Government Peak Stock,

e) Romeo and Juliette, silicified breccia and felsic intrusive pipes respectively (Jackson and Strong, 1985).

f) Dikes.

Atolia Quartz Monzonite

This rock type underlies a large area (figure 2.2) to the south of the Rand Mountains. In hand specimen it is a light-grey, medium to coarsed-grained rock, exhibiting fresh black biotite and an abundant distinctive honey colored sphene. In thin section the rock is comprised of approximately equal proportions of potassium feldspar, quartz and plagioclase, with about 15 percent combined biotite and hornblende. Potassium feldspar sometimes forms large grains which poikilitically enclose most other phases, but is typically observed as an interstitial phase. Magnetite,

apatite and lesser zircon are observed as minor, though relatively common, accessory minerals.

Post-crystallization deformation is suggested by the common observation of strained biotite flakes, fractured/strained plagioclase, undulatory extinction of quartz, and localized recrystallization observed in thin section. Hulin (1925) suggests this deformation is probably associated with the abundant east-west oriented fracturing associated with scheelite mineralization discussed later.

EW Granodiorite

This term is proposed to cover a range of intrusive phases from quartz diorite through granite. The EW granodiorite is the major intrusive lithology in the vicinity of the Yellow Aster open pit. It is so named as it forms the prominent east-west ridge between the Yellow Aster pit and the Johannesburg-Atolia road. (figure 2.3)

In hand specimen the rock is characterized by fine grained secondary biotite resulting in a variably developed 'gneissic' texture. The rock is typically medium-grained equigranular, containing biotite, plagioclase and quartz. Localized areas of intense silicification of hydrothermal brecciation associated

with abundant fine-grained biotite result in white and black varieties of the granodiorite (figure 2.4).

In thin section the rock has a medium-grained, aphyric texture. It is composed of plagioclase (>40 %), quartz (<20%), potassium feldspar (>10%), biotite (10%) and hornblende (<5%). Sphene, magnetite, apatite and less commonly garnet form the accessory minerals. Alteration minerals include biotite, sericite, hematite, pyrophyllite and chlorite.

Potassium feldspar is often perthitic, and forms large grains poikilitically enclosing plagioclase crystals. These rocks also exhibit features suggesting a post-crystallization deformation event. Deformed albite twin lamellae and undulatory quartz extinction are ubiquitous. The abundance of secondary biotite which often forms discrete narrow veinlets through plagioclase, and rims primary igneous biotite (figure 2.5) is interpretted to be the result of remobilization due to deformation. Jackson and Strong (1985) indicate that the potassium content of the rocks is typical of grandodioritic rocks and suggest no potassic addition (Appendix II). Jackson and Strong (1985) also suggest the deformation probably occurred while the intrusion was still hot, in the presence of a fluid phase.

Figure 2.4 Black variety of EW granodiorite

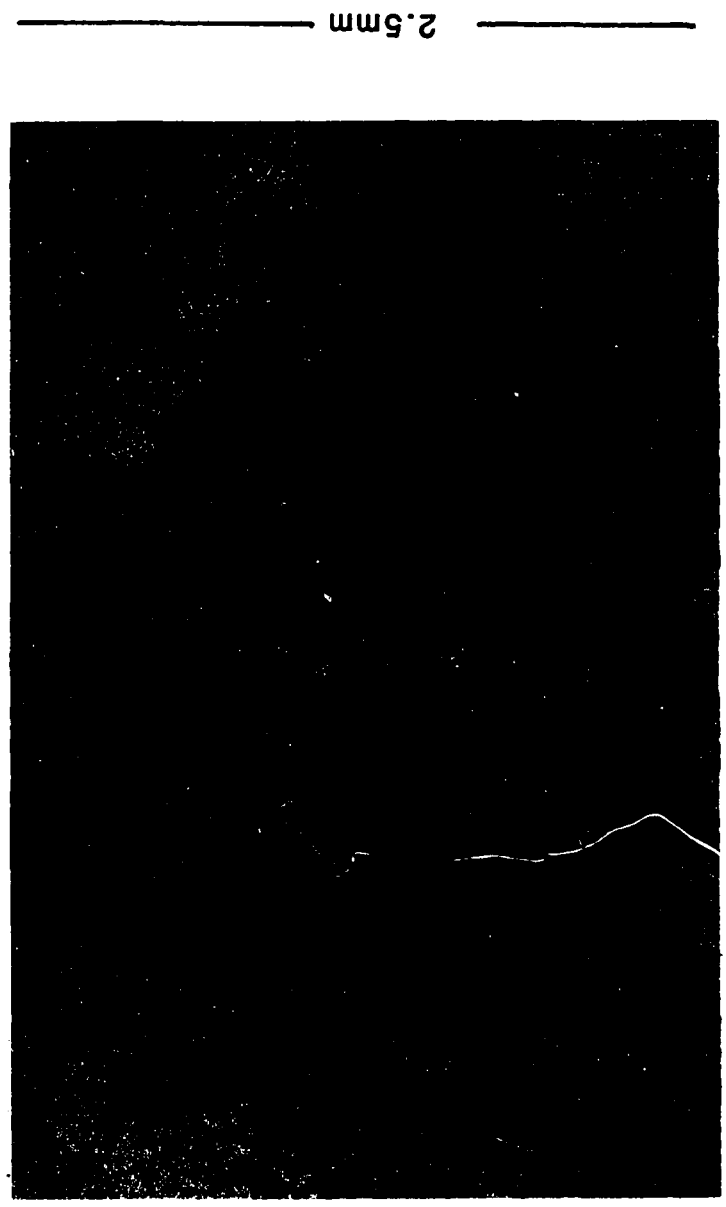

Figure 2.5 Fine grained secondary biotite cutting across primary biotite

Microgranodiorite

This rock type occurs in several localities proximal to the Yellow Aster open pit. It forms the prominent hill to the southeast of the open pit and also outcrops on the northern and northwestern edges of the pit.

Microgranodiorite has its type locality at YA 56-60 (figure 2.3). In hand specimen it is typically a light yellow-brown color, relatively fine grained, equigranular rock containing biotite, hornblende and plagioclase as phenocrysts.

In thin section the rock exhibits an allotriomorphic granular texture, characterized by the growth of dark green porphyroblastic alkali amphibole and porphyroblastic biotite which enclose small, often rounded crystals of quartz and plagioclase feldspar (figure 2.6). Plagioclase, biotite and potassium feldspar form phenocrysts (< 2mm) usually set in an equigranular interlocking matrix of quartz, plagioclase and potassium feldspar. The plagioclase and potassium feldspar phenocrysts exhibit secondary overgrowths, probably subsolidus, the onset of which is marked by zones of rounded quartz inclusions (figure 2.6 b). Modal proportions are estimated at potassium feldspar <15%, plagioclase <50%, quartz <20%, hornblende <10%, biotite

Figure 2.6a Alkali amphibole phenocryst in microgranodiorite

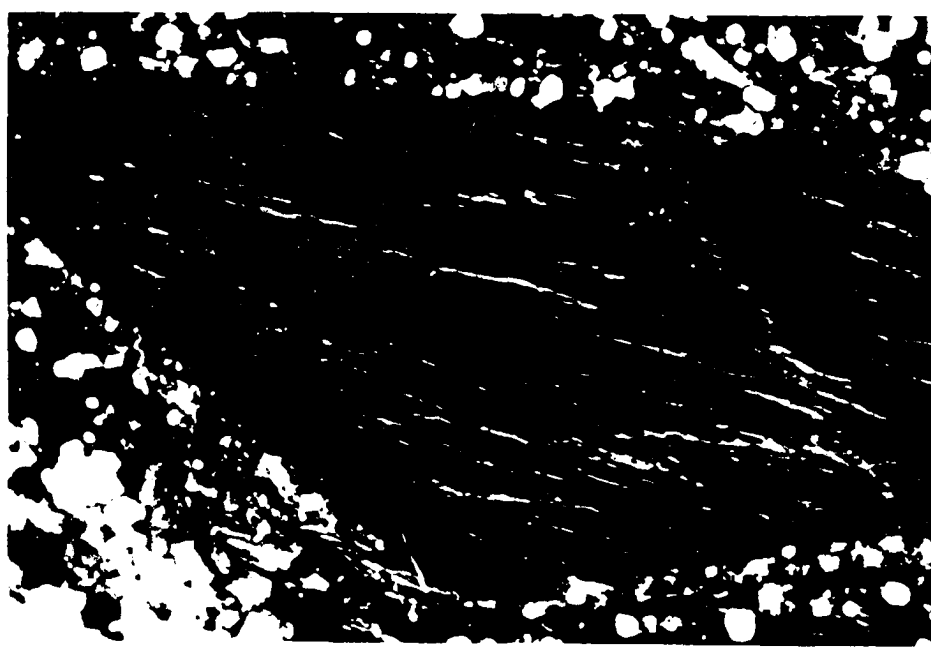

Figure 2.6b Quartz inclusions in alkali feldspar

<10%, with accessory magnetite, sphene and apatite.

Late magmatic growth of amphibole is suggested by several features. Primary igneous colorless amphibole exhibits an overgrowth of dark green amphibole. Amphibole overgrowths on primary igneous biotite and amphibole replacing plagioclase are also observed. The growth of the porphyroblastic alkali amphibole is felt to be strong evidence for late magmatic growth. The fine grained-equigranular nature of the groundmass suggests rapid cooling.

The Government Peak Stock

This intrusive unit occurs west of the Yellow Aster pit (figure 2.3), and is well exposed on the north-facing slope of Government Peak. Several variationss in the intrusive were recognized by Amselco staff geologists. Most of the intrusion is a fine-grained, gray, porphyritic diorite. It consists of small phenocrysts of plagioclase (< 3mm long) and slightly smaller biotite and augite, in a fine-grained equigranular groundmass of quartz, feldspar and biotite. Pyroxene is variably replaced by amphibole which in turn is replaced by biotite.

The stock also contains a more felsic variant exhibiting a medium to fine-grained, equigranular, texture comprising quartz, plagioclase, microperthite, biotite and minor amphibole.

Romeo and Juliette intrusive pipes

Romeo pipe (figure 2.3) is a silicified breccia pipe outcropping to the east of the Yellow Aster pit, approximately 0.8 Km south of Johannesburg. Hand specimen observation revealed angular fragments of 'granitic rock' cemented by milky white microcrystalline quartz veins. Romeo pipe also contains areas of cellular-honeycomb quartz attesting to an intense silicification. In thin section the clastic nature of the rock is evident as well as the result of intense silicification (figure 2.7) evidenced by intergrowths of quartz and potassium felspar.

The Juliette pipe adjacent to the Romeo pipe (figure 2.3), is a large plug of rhyolitic composition. In thin section euhedral phenocrysts of potassium feldspar and sodic plagioclase occur in a siliceous groundmass. Quartz and biotite also form phenocrysts but exhibit resorption and chloritic alteration respectively.

Figure 2.7 Quartz-feldspar intergrowth in Romeo breccia

Dike rocks

Numerous felsic dikes occur throughout the study area. Basic to intermediate dikes are less common. The felsic dikes are commonly quartz-feldspar porphyries, or quartz - biotite - feldspar porphyries. Hulin (1925) noted that many of the dikes appear to emanate radially from the Romeo and Juliette intrusive complex.

Alteration and mineralization

A detailed account of the distribution of hydrothermal alteration facies is not warranted. However an attempt to briefly describe the characteristic alteration minerals and ore, gangue minerals associated with the gold, silver and tungsten mineralization is presented.

Gold mineralization and associated alteration assemblages

Gold mineralization is more widespread (figure 2.2) than either silver or tungsten mineralization. However, the major production (approximately 500,000 troy ounces) has been from the Yellow Aster mine and those mines located in the 'Stringer Zone' (Hulin, 1925).

Mineralization at the Yellow Aster mine is intimately associated with intense fracturing and faulting. Troxel and Morton (1962) indicate gold mineralization at Yellow Aster is confined to a fault bound wedge containing two thirds quartz monzonite, one-third Rand Schist with minor rhyolite dikes (figure 2.8). Gold is found in both the schist and quartz monzonite. Hulin (1925) concluded the attitude of gold bearing structures were variable although a strong development of northwest-southeast gold-bearing quartz veins was described at Yellow Aster. Gold often is disseminated in the the country rock in the footwall of faults of various orientations. Hulin (1925) also indicated that gold was often associated with the margins of dikes (felsic or diabase) and that gold visibly post-dates these intrusions. Hulin indicates the Butte, Kenyon, Wedge and Little Butte mines were located along a single large diabase dyke (figure 2.2). The Big Dike Mine was located proximal to a felsic dike, emphasizing the importance of these structures.

Gold is commonly associated with quartz veins but also occurs in quartz-free fractures. Associated gangue minerals are arsenopyrite, pyrite, iron oxides and calcite. Most gold was recovered from areas with an intense red-brown coloration probably resulting from the

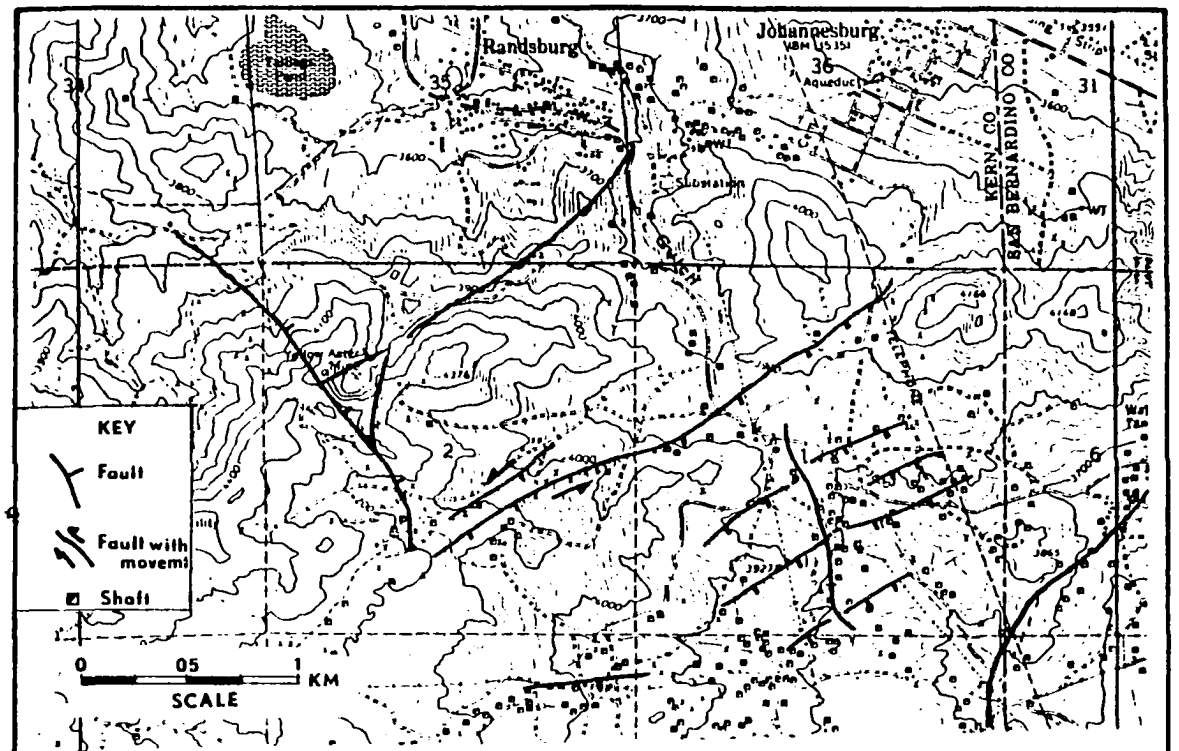

Figure 2.8 Major structures proximal to the Yellow Aster mine (after Morehouse 1984)

oxidation of arsenopyrite and pyrite. Hulin (1925) reports scheelite was also found in the gold ores, though a relative age relationship was not discerned.

Phyllic alteration with minor arsenopyrite and pyrite

Phyllic alteration at the Yellow Aster mine is very similar to that described for the porphyry coppers of the southwestern U.S.A. and is dominantly associated with areas of gold mineralization within the Yellow Aster pit. Appendix III contains geochemical analyses for gold, silver, tungsten, antimony, arsenic, and mercury for rocks from Yellow Aster and several other mineralized localities.

This alteration type progresses from selecte to pervasive resulting in the the complete obliteration of original igneous texture (figure 2.9). The progression of alteration reflects the change from a regime where host rock mineralogy is the controlling factor on the alteration assemblage produced to a regime whereby the host rock is inundated by a fluid which alters the rock to a uniform assemblage of quartz and sericite, with minor arsenopyrite and pyrite occupying fractures. Increasing alteration results in the local (up to tens of meter scale) redistribution of quartz as ragged patches

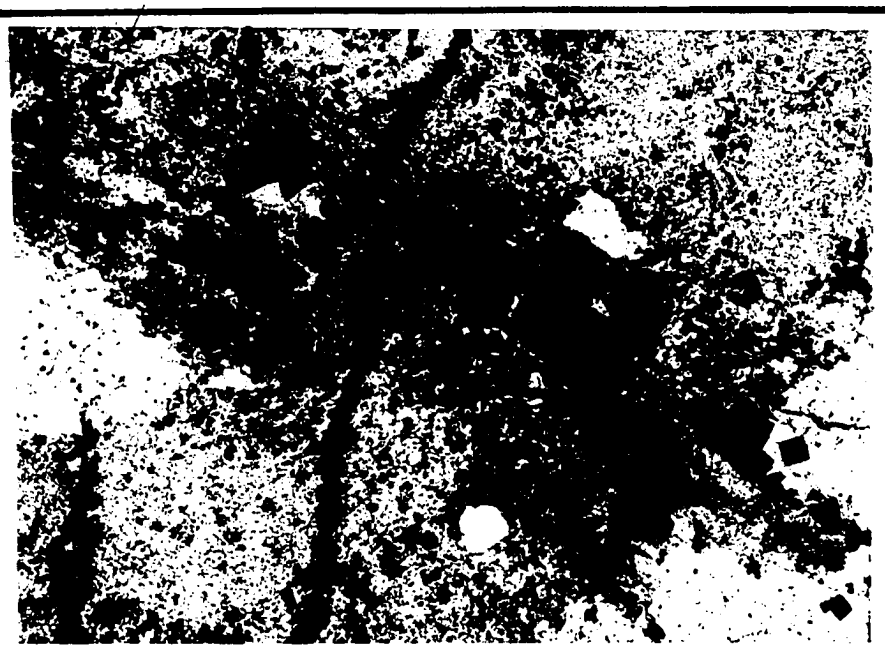

Figure 2.9a Quartz-pyrite-sericite alteration of EW granodiorite

Figure 2.9b Calcite cementing clasts of iron oxides

and centimeter scale veinlets.

The decomposition of pyrite and arsenopyrite as a result of oxidization results in discrete veinlets of iron oxide and the ubiquitous red - brown staining observed to accompany gold mineralization.

However, some of the more intense and pervasive hematization observed at the Yellow Aster mine (YA119 and YA123) appeared to be a hypogene hydrothermal alteration event. Pervasively hematized rocks are commonly cut by clean unstained veins of quartz and calcite (figure 2.9). Discrete gold particles were occasionally observed within fractures cutting such iron oxide-rich rock. Thus, field and microscopic observation suggest some fraction of the iron oxides observed at Yellow Aster are of hypogene - hydrothermal origin, post dating the pyrite - sericite alteration event but preceeding the quartz - carbonate veinlets. The picture is somewhat confused by supergene oxides after iron - sulfides.

Late stage calcite, and calcite with quartz veins post date the mineralizing event/s. Intense local carbonatization results in calcite cemented breccias (figure 2.9). Figure 2.10 schematically summarizes the alteration and geochemical characteristics of the gold mineralizing events at Yellow Aster.

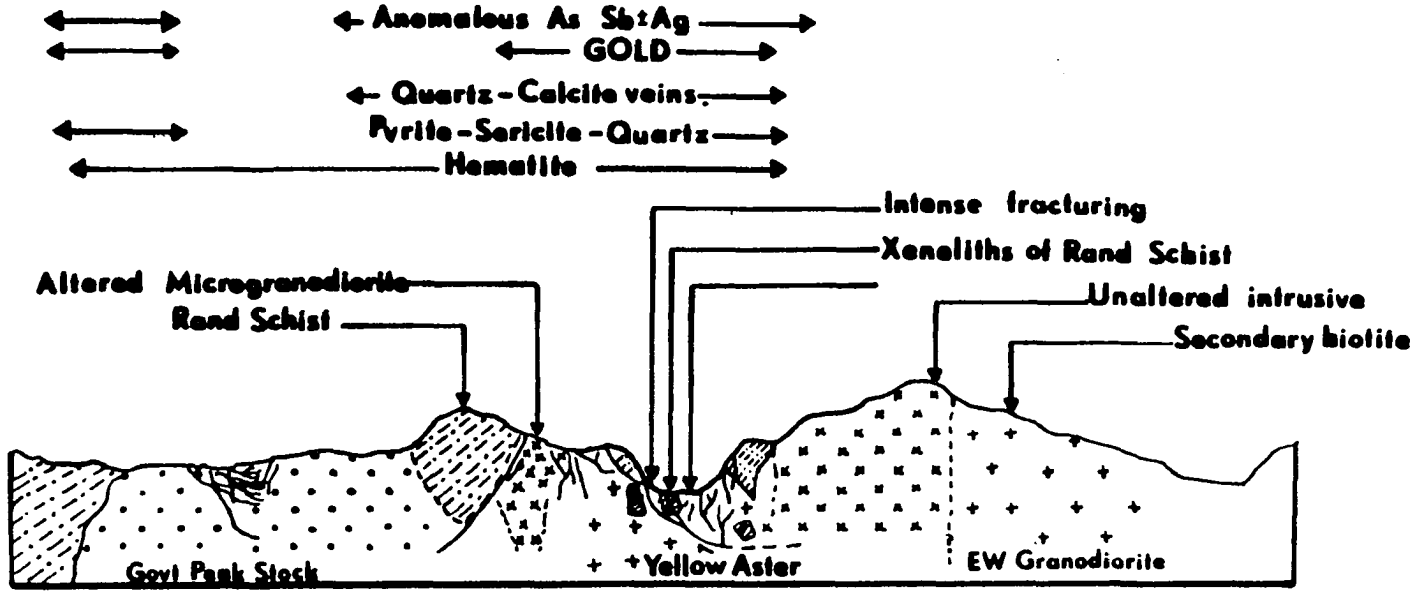

Figure 2.10 Schematic summary of alteration and geochemical characteristics associated with mineralization at Yellow Aster

Silver mineralization and associated assemblage

Silver mineralization within the Randsburg area has a more limited spatial distribution than gold (figure 2.2). The petrographic descriptions in this section are a synthesis based on rocks collected from the Kelly Mine dump, and the detailed work of Hulin (1925).

All of the commercial silver orebodies were located in siliceous veins within the Rand Schist. Two orientations were recognized, one approximately north-south and the second, more economically significant, northwest-southwest (Hulin, 1925). An idealized section through the vein system is illustrated in figure 2.11. The Footwall Vein was the largest and was exposed at surface for over 1,091 meters of strike length, averaging 15.6 meters thick. Hulin (1925) reports that several of the silver veins could be traced for short distances into the pre-mineral fault gouge shown in figure 2.11 and demonstrably post date the low angle structure.

Silver mineralization is accompanied by strong silicification of the Rand Schist which commonly appears deep grey blue proximal to the veins. Silver bearing minerals identified by Hulin were miargyrite, argentiferous tetrahedrite, with lesser pyrargyrite and

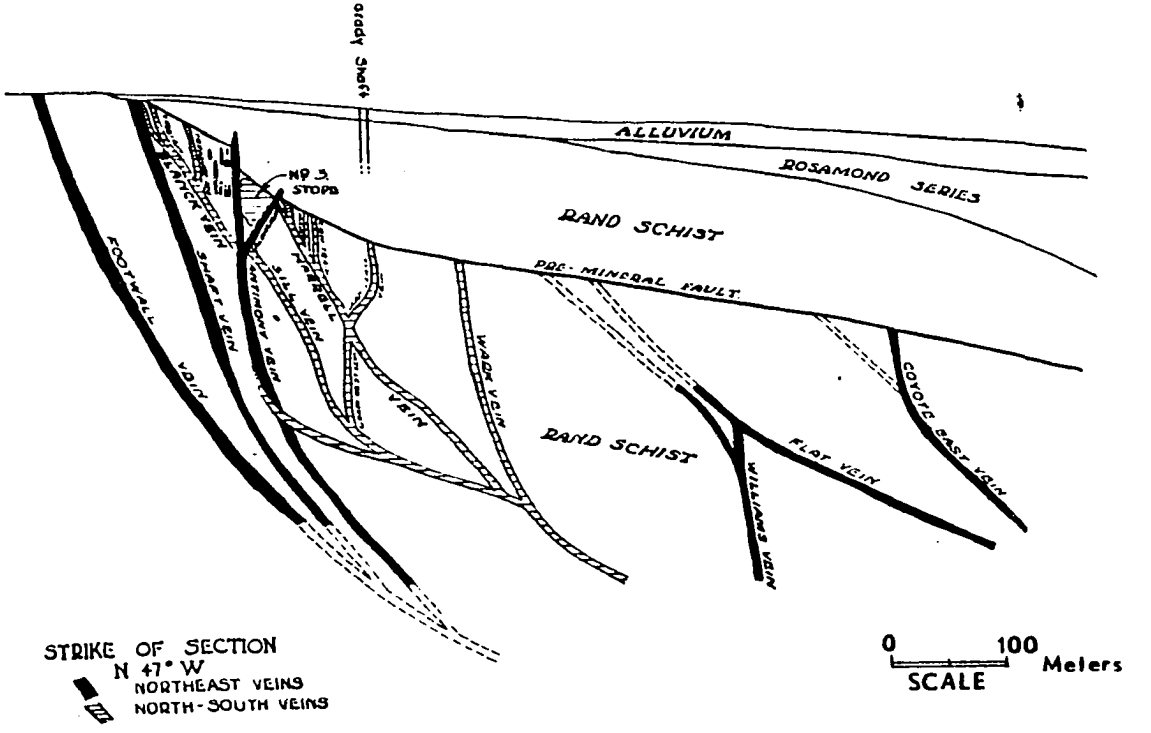

Figure 2.11 Idealized section through the Kelly silver veins
(AFTER HULIN, 1925)

proustite. Cerargyrite was the only positively identified secondary silver mineral. Gangue minerals include pyrite, arsenopyrite, stibnite, lesser amounts of chalcopyrite and quartz. Silica occurs as fine grained cryptocrystalline chalcedony and also as a later more euhedral vein filling quartz (figure 2.12). Geochemical data for rocks from the Kelly mine dump are contained in Appendix III. The silver mineralization is accompanied by elevated values for Sb, As, Au and Hg as might be anticipated from the ore mineralogy.

Hulin (1925) observed silver mineralized veinlets cutting, and thus post - dating diabase dikes of Miocene age. He also concluded that gold mineralization preceded the silver mineralization based on a cross cutting relationship observed in the Kelly mine (then the California Rand Silver Mine).

Figure 2.12 Typical quartz vein textures observed for Kelly Mine samples

Tungsten mineralization and associated alteration assemblage

Tungsten mineralization occurs centered around Atolia (figure 2.3). Scheelite-bearing quartz veins form a sub-parallel system approximately 150 meters wide and 4 kilometers long, striking N80E. The veins are generally less than 2 meters thick and dip 70-76 to the north. Scheelite has an erratic distribution within the veins forming complex shoots and chimneys (Lemmon and Dorr, 1940). Economic vein concentrations of scheelite were usually between 0.3 and 1.5 meters thick. The longest ore shoot discovered, the north vein of the Union Mine (Table 2.1), was 340 meters long at surface but which 'pinched out' at a depth of 200 meters (Hulin, 1925). Typical ore grades were 3.5% to 4% WO3 (Lemmon and Dorr, 1940).

Scheelite forms the only tungsten-bearing mineral in the veins. Fine grained quartz and subordinate calcite are the dominant gangue minerals. The veins typically appear fined grained milky white, with calcite and scheelite occasionally exhibiting cleavage faces. Pyrite and more rarely stibnite are reportedly abundant in some veins (Lemmon and Dorr, 1940). Pyrite is an ubiquitous mineral in the wall rock alteration assemblage.

Petrographic studies reveal at least two ages of quartz growth. A very fine grained microcrystalline quartz is post-dated by a more euhedral medium to coarse grained quartz. Hulin (1925) observed scheelite also occuring in two distinct morphological varieties which correlated with those of quartz, i.e. an early fine grained variety, succeeded by later coarser crystals, although this was not observed by the author. Calcite post dates both quartz-scheelite textural varieties.

Wall rock alteration of the quartz monzonite is characterized by a pyrite - 'sericitic' plagioclase - chlorite assemblage (figure 2.13). Minor silicification and redistribution of quartz is also evident. Alteration selvedges range from a few centimeters for narrow veins, up to several meters surrounding the larger veins. Decomposition of pyrite in the weathering environment results in a variably developed brown coloration.

Hulin suggested that the low temperature epithermal textures of the quartz-scheelite veins and the presence of tungsten in post - Miocene gold bearing structures of the 'stringer zone' precluded any genetic association with the Atolia quartz monzonite. He felt scheelite mineralization was directly related to later Miocene igneous activity.

Figure 2.13 Chlorite-pyrite alteration assemblage

A brief review of the geologic history of the Randsburg mineralized areas

Morehouse (1984) indicates a 160 Ma ±25Ma date for the lithification of the Rand Schist based on Rb/Sr dating. He suggests Rand Schist metamorphism is related to a regional low angle thrusting event at approximately 80Ma.

Jackson and Strong (1985a, 1985b) consider the Atolia quartz monzonite to be emplaced during tectonic activity with 40 Ar/39 Ar ages on biotite and hornblende mineral separates indicating a 74-84 Ma emplacement age. Subsequent Rb/Sr dates on corresponding rocks indicate a similar age (Jackson and Strong, 1985b). Morehouse (1984) reports a U-Pb date from a zircon separate from the Atolia Quartz Monzonite at 85 Ma. This age range correlates with the final stages of the emplacement of the Sierra Nevada batholith.

The suite of intrusive rocks proximal to the Yellow Aster pit were correlated by Hulin (1925) with the Atolia quartz monzonite. Recent age dating by Jackson and Strong (1985a, 1985b) indicate a more complex intrusive history, and is reported below.

Rb/Sr dates for the EW granodiorite (deformed) give a 77.5±41.6 Ma age with an initial 87Sr/86Sr of .708-.709 (the large error bar being a function of restricted range of Rb/Sr and the young age of the rocks). The age dates of the EW granodiorite appear to broadly correlate with those of the Atolia quartz monzonite.

Intrusive activity resumed at approximately 20 Ma. The high level intrusions such as the Microgranodiorite, Government Peak Stock, and various felsic dykes all giving 40 Ar/39 Ar dates of 20 Ma ± 1Ma. Intrusive activity culminates with the emplacement of the Juliette rhyolite pipe and associated Romeo breccia pipe about 18.5Ma. Serictic alteration accompanying gold mineralization, and that in the intrusive pipe halo, gave 40 Ar/39 Ar ages coincident with the final phase of intrusive activity (Jackson and Strong, 1985).

Sericitic alteration associated with silver mineralization at the Kelly Mine gave a 15.3Ma age, distinctly later than the final phase of intrusive activity. However, consideration of the geographic distribution of metals associated with the various intrusive phases (Appendix III) suggests silver mineralization probably is related to the intrusion of the rhyolite pipes. Appendix III, Table A3.1 illustrates

that the rocks of the Romeo - Juilette sericitic alteration halo have elevated antimony, silver and mercury values. Gold and arsenic also show elevated values though they are markedly lower than those present at the Yellow Aster pit and the Government Peak Stock.

Chapter 3

DECREPITATION INDUCTION COUPLED PLASMA ANALYSIS OF ATOLIA - RANDSBURG QUARTZ (METHODOLOGY, INSTRUMENTATION AND INTERPRETATION OF RESULTS).

Introduction

Inductively-coupled plasma emission spectrometry (ICP) is a suitable method of examining the chemical composition of small volumes of fluid. In the standard ICP method, a nebulized test solution is injected into a toroidal plasma formed in a stream of argon gas. The nebulized solution is subjected to a temperature of about 9000 degrees Kelvin and completely atomized. At this temperature many atoms emit their characteristic radiation/s. By linking the plasma source to an emission spectrophotometer the concentration of the atomic species present in the the plasma can be quantified (the basic assumption of quantitative emission spectroscopy being that the intensity of a characteristic radiation is proportional to the number of atoms of which the radiation is characteristic).

Decrepitation is the term used to describe the bursting of individual fluid inclusions with the violent expellation of their contained phases. This phenomena is observed when crystalline (fluid inclusion-bearing) material is heated. The decrepitation linked induction

coupled plasma technique (DICP) basically involves the analysis of fluid inclusion contents released by this mechanism.

Decrepitation of inclusions takes place when the internal pressure within an inclusion exceeds the confining strength of the host crystal, which for quartz is in the range 300-600 °C, (Thompson and Walsh, 1983). The dissolved material in an inclusion forms a fine aerosol as the water evaporates. Thus if decrepitation is carried out in a stream of argon and the efficiency of transfer to the carrier gas is high, a high proportion of fluid inclusion contents could be injected into the plasma.

The analysis of fluid inclusion contents by induction coupled plasma spectophotometry (ICP) has been utilized at Imperial College, London, England since 1979. The ICP has many advantageous analytical characteristics, which include (from Thompson and Walsh, 1983).

i) Rapid sample turn around.

ii) Simultaneous multi-element capability.

iii) Low detection limits for a large number of elements (>20).

iv) Linear calibration over several orders of concentration magnitude.

v) Low interference effects.

This chapter outlines the instrumentation, methodology of the applied technique and subsequently interprets the results gained at the Randsburg field site. Many of the evaluatory techniques detailed were developed during the study and are described to highlight the strength and weakness of DICP in the exploration environment.

Research objectives

The dual objectives of this research were:

a) to evaluate the application of decrepitation linked induction coupled emission plasma spectrographic analyses as an exploration tool for intrusive related gold mineralization.

b) To develop and refine the DICP technique for the geochemical analysis of fluid inclusions.

Previous work

DICP analyses have been performed at Imperial College, London, England since 1979, see Thompson and others (1980), Alderton and others (1982), Alderton and Rankin (1982), Chryssoulis (1983a,b) Hart (1984), and Jones, (1985). In these studies, fluid inclusions from a

variety of minerals have been analysed including quartz, topaz, apatite, barite, fluorite, galena, sphalerite, calcite and chalcopyrite. Since 1979 several thousand samples have been analyed using this technique and considerable developmental advances have been made (Alderton and others, 1982; Chryssoulis, 1983a,b; and Hart and Rankin, 1983). The results presented here were collected from research carried out at Imperial College, until August 1984.

Material studied

DICP studies were confined to whole rock quartz principally of two origins:

i) vein quartz and,

ii) igneous intrusive quartz.

Approximately one hundred analyses were carried out on Randsburg quartz. Previous studies evaluating the application of DICP to stream sediment quartz had met with varying success (Rankin and Alderton, 1982; Hart, 1984). The author rejected the stream sediment quartz approach based on the conclusions drawn from research at the gold mineralized margins of the Carsphain intrusive in southwestern Scotland (Hart, 1984). Here it was found that the complexity introduced due to the multiplicity of

origin for stream sediment quartz, outweighed the reduced turnaround period resulting from disaggregated samples.

Sample selection

The location and geological setting of samples was detailed in Chapter 2. The field sample usually consisted of approximately 0.5kg of intrusive or vein material. Approximately 80 samples were collected for DICP analyses.

Sample preparation

All samples were crushed using Amselco Exploration Inc. (Phoenix) equipment. The <4mm ⩾2mm and <2mm ⩾1mm size fractions were retained for petrographic examination. An attempt was made to prepare all samples for DICP analysis, however due to the lack of a suitable quartz fraction in some samples, only sixty were prepared.

About 0.5-1.0g of quartz was hand picked from the <2mm >1mm size fraction of each sample. This is usually the most arduous task in the preparation. An approximately 0.5g sample of hand picked quartz was accurately weighed out. The sample was then washed in concentrated HCl for three hours at 80 °C, to remove any

adhered contaminants. The samples were then rinsed repeatedly with 'double-deionized' water and dried thouroughly in a clean oven at 60-80 °C for at least 24 hours. Dry samples are essential, owing to the plasma's sensitivity to water. A flow diagram to illustrate the various preparation stages is shown in figure 3.1.

Instrumentation and methodology

The equipment used is shown schematically in figure 3.2 (from Chryssoulis, 1983a). Inclusion contents were analysed using an ARL 3400c vacuum emission spectrophotometer with an inductively coupled plasma source, analysing for 36 elements simultaneously (table 3.1).

The samples, in borosilicate test tubes, are attached to the plasma (figure 3.2). The tubes are heated by a variable resistance electrical furnace. A constant setting of 750 °C was used for the analyses. Typical heating rate curves for empty tubes are shown in figure 3.3.

In this study the tubes were preheated for fifteen seconds followed by a forty five second measurement of the decrepitational response. The selection of a '15-45' second preheat-measurement interval is explained by

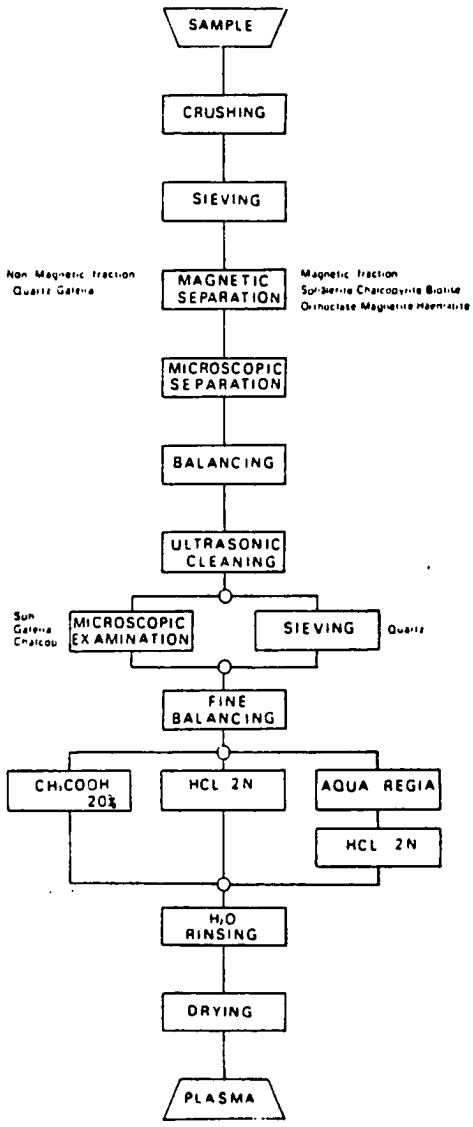

FIGURE 3-1 FLOW CHART FOR THE PREPARATION OF SAMPLES FOR FL. INCLUSION ANALYSIS BY THE D.-I.C.P. METHOD

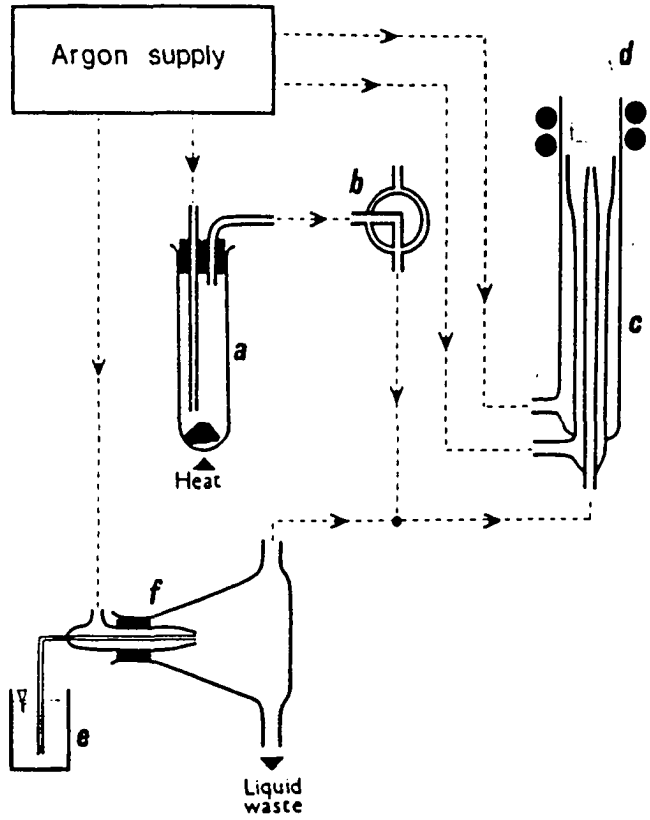

Figure 3-2 Schematic diagram of the D-ICP system. a = pyrex test tube (sample container); b = three port gas valve; c = silica plasma torch; d = plasma; e = calibration solution or blank solution and f = nebuliser system. (From Chryssoulis 1983a)

Table 3.1. Relative sensitivities and approximate detection limits for the elements determined by ICP.

Element	Wave-length, nm	Relative sensitivity, Na = 100	Absolute detection limit, ppb
Ag	328.1	40	2.8
Al	308.2	0.28	63
As	193.8	1.4	32
B	249.7	14	2.1
Ba	455.4	6.7	2.8
Be	313.0	350	0.2
Bi	223.1	1.0	35
Ca	317.9	0.21	56
Cd	226.5	22	3.2
Co	228.6	3.2	9.9
Cr	267.7	16	3.8
Cu	324.8	9.1	3.4
Fe	259.9	0.28	27
Hg	194.2	7.7	7.3
K	766.5	1.8	81
La	398.8	7.4	4.1
Li	670.8	12	2.3
Mg	279.1	0.25	94
Mn	257.6	1.0	15
Mo	281.6	38	5.4
Na	589.0	1.0	32
Ni	231.6	5.4	12
P	178.3	3.9	19
Pb	220.3	3.3	27
Rb	780.0	0.91	91
S	180.7	1.0	110
Sb	206.8	0.68	120
Se	196.1	0.36	110
Si	288.2	3.1	45
Sn	190.0	5.1	11
Sr	407.8	29	2.3
Te	214.3	1.9	32
Ti	337.3	0.3	52
V	311.1	15	2.4
Zn	202.5	5.0	11
Zr	349.6	50	2.7

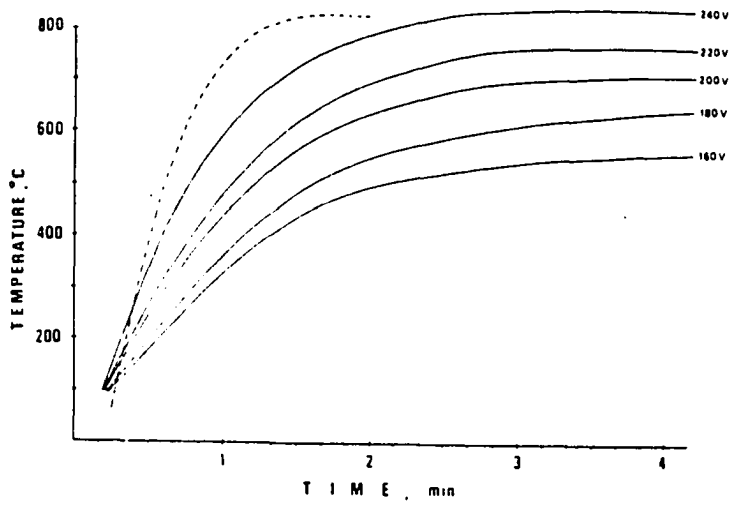

Figure 3-3 Typical heating rate curves used for various furnace voltage settings

from Chryssoulis(1983a)

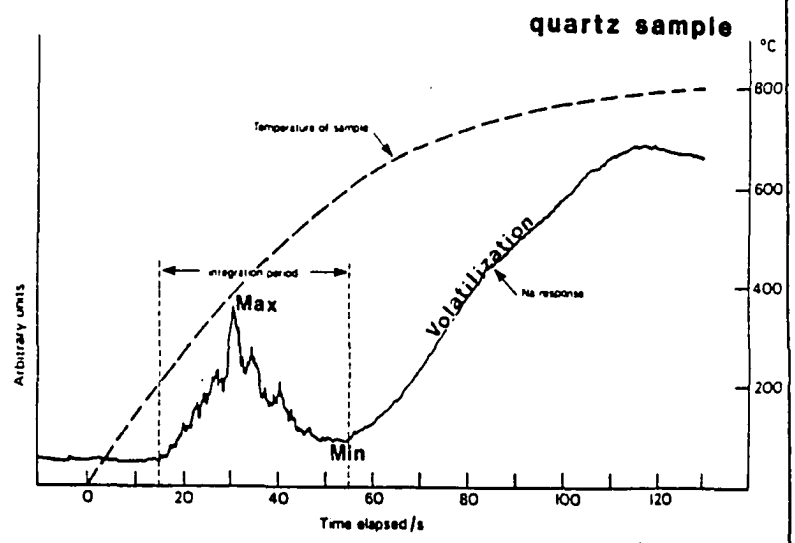

Figure 3-4Time resolved sodium response plot

(after Thompson and Walsh1983)

figure 3.4. This illustrates a typical time resolved response for the sodium channel during a decrepitation run on quartz. For approximately the first fifteen seconds after being placed in the furnace, there is little change in response. Response increases markedly with the onset of decrepitation (x), reaching a peak at thirty seconds (max) and fal ling to a minimum at approximately sixty seconds (min). The increase in response after fifty to sixty seconds is due to volatilization (and not decrepitation) of any salts not expelled during decrepitation, or from precipitates formed on the surface during decrepitation, (Chryssoulis, 1983a; Chryssoulis and Wilkins, 1983). The '15-45' second time interval ratio was chosen to effectively isolate the decrepitate response (figure 3.4).

Sequential integration of plasma response

The ARL 34000c allows complete time resolved plots for only one channel at a time. However, it was possible to monitor multi-element response temporally by utilizing sequential, short (1 sec) integrations of the plasma response. After each integration the results were written to floppy disc, a process taking four seconds for thirty six elements. Therefore it was possible to use this effective five second unit, to obtain a plot of

response level versus time. Using this technique it was possible to establish whether specific elements were being released during peak decrepitation, or were derived from some other source.

Routine analytical procedure

The term 'blank' is used for clean empty tubes analysed in exactly the same manner as sample tubes. Blank tubes were analysed 'en bloc' at the start of an analytical run, and then after every five sample tubes. The last sample is always followed by a blank, which allows the background (blank) response to be monitored as a function of time throughout an analytical run. After the decrepitation was completed the instrument was calibrated using standard solutions (Alderton et al, 1982).

Calibration of the DICP Technique

Calibration of the technique is problematical, primarily because the volume of the inclusion fluid presented to the plasma is unquantified, precluding the estimation of absolute metal ion concentrations. A further complication results from the unknown efficiency of decrepitation and transfer mechanisms.

Concentration ratios were established from the raw millivolt (mv) response by the use of sensitivity ratios obtained by nebulising the aqueous calibration standards. The term equivalent ppm (equ-ppm) from Chyrssoulis (1983a) is occassionaly used to indicate the sensitivity corrected values (see Table 3.1 for sensitivity ratios relative to sodium).

RESULTS EVALUATION AND INTERPRETATION

Quality control evaluation

The validity of geochemical analyses is a measure of the reliability of the results. This reliability is usually gaged in terms of accuracy and precision. In the indentification of anomalies for minerals exploration, precision is probably the most important (M.Thompson. person. comm.). Poor precision can disguise existing anomalies and create spurious ones.

Precision

Precision was estimated using the method described by Thompson and Howarth (1976 and 1978), involving the duplication of analyses. The standard deviation of eighteen duplicate pairs was plotted against concentration as shown in figure 3.5.

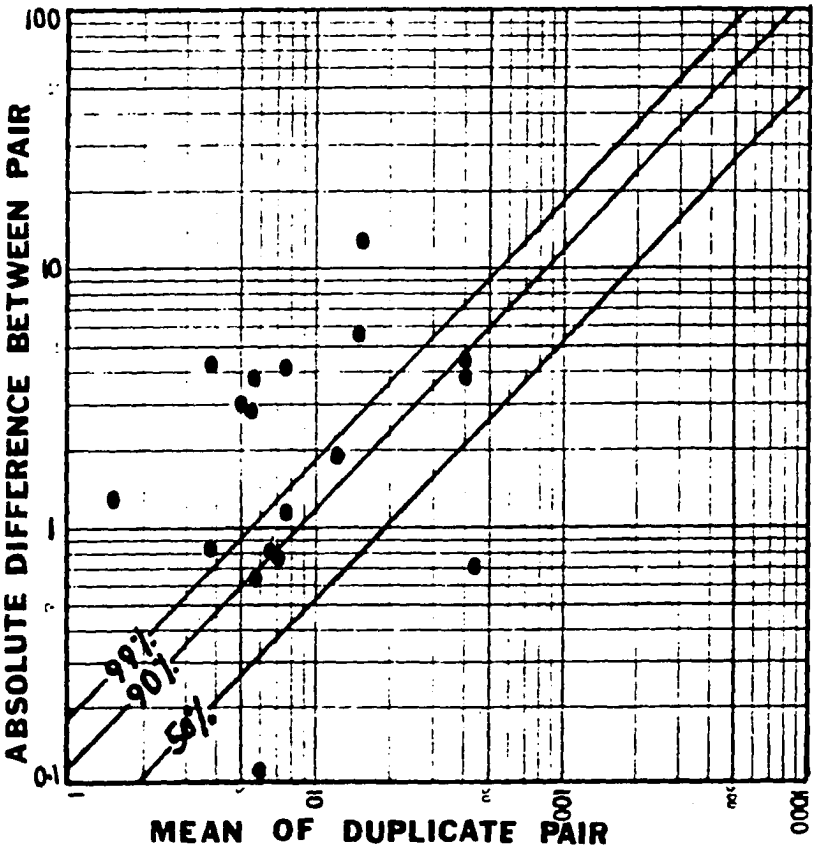

Figure 3.5 Precision plot for sodium values of duplicated samples (millivolts)

Thompson and Howarth (1978) illustrated that methods commonly used for the estimation of analytical precision either assume a constant relative error (by using the coefficient of variation) or a constant absolute error (using the standard deviation). If such an approach is utilized over a wide range of concentration, erroneous conclusions can be drawn. A plot relating standard deviation to concentration is appropriate.

The duplicate analyses for sodium (Table 3.2) are plotted on a 'ten percent precision chart' in figure 3.5. This illustrates the sodium precision is worse than ten percent. Nine analyses (of eighteen) exceeding the ninety-ninth percentile is anticipated to occur in an infinitely small number of cases at this precision level. Sodium precision, using this method, is estimated at approximately twenty percent, which is acceptable for exploration purposes.

Precision for all other elements tested is markedly worse than twenty percent. This supports the tenet that analytical precision is a function of concentration level, schematically illustrated in figure 3.6. In decrepitation studies, sodium response levels are used as indicators of decrepitation activity (based on the assumption that sodium is derived exclusively from

Table 3.2. Data for sodium precision plot (Figure 3.5).

ID	Na(mv)	Mean($\bar{x}$)	(X_1-X_2)	RSD(%)
YA10A	3.96	5.0	2.1	21.1
10B	6.08	5.4	2.9	26.8
10C	6.86	6.5	0.8	6.0
10D	6.10	5.0	2.1	21.3
		6.09	0.02	0.2
		6.5	0.8	5.9
YA1A	5.04	7.2	4.3	29.6
1B	9.30			
YA51A	42.2	41.9	0.7	0.8
51B	41.5	39.9	4.6	5.8
	37.6	39.6	3.9	4.9
YA55A	10.6	11.6	1.9	8.2
55B	12.5			
YA54A	13.8	16.6	5.5	16.6
54B	19.3			
YA27A	6.78	7.4	1.22	8.3
27B	19.3			
YA23A	22.52	15.8	13.5	42.7
23B	9.0			
YA14A	1.85	1.24	1.22	49.2
14B				
YA45A	2.44	2.86	0.84	15.0
45B	3.28			
YA33A	5.98	5.71	0.54	4.7
33B	5.44			
YA6A	0.45	2.7	4.5	85.0
6B	4.95			

Note: $RSD = \frac{\text{standard deviation}}{\text{mean}} \times 100$

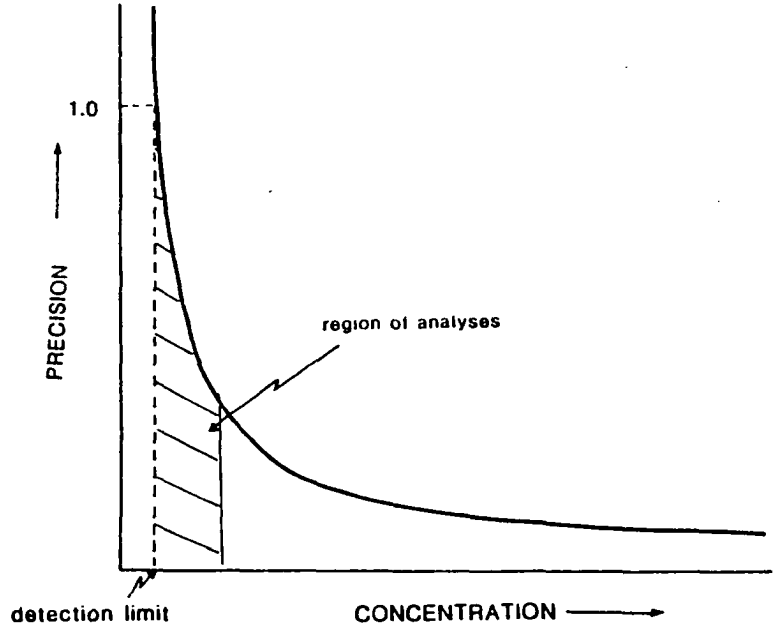

Figure 3-6 Diagram to illustrate effect of concentration on analytical precision

after Thompson and Howarth (1976)

inclusion contents). Alderton and others (1982) observed that the effect of ratioing both 'major' and 'minor' element responses to their sodium response was to reduce the relative standard deviation of duplicate pairs (i,e an improved estimate of analytical precision). They concluded that varying decrepitation levels between duplicate samples accounted for a pessimistic estimate of analytical precision. Alderton and others (1982) arrived at general figures of ten percent relative standard deviation (RSD) for 'major' elements and thirty percent relative standard deviation for the minor elements after ratioing to sodium. To test this concept some major and minor element millivolt responses in duplicate pairs were ratioed to their sodium response. Figure 3.7 illustrates the results (Table 3.3) for arsenic plotted on a ten percent precision chart. No improvement in analytical precision is percieved after ratioing to sodium, which is typical for the other elements tested. This observation conflicts with that of Alderton and others (1982) and is felt to indicate that the poor precision (>30%) cannot be explained exclusively in terms of varying decrepitation levels between duplicate pairs. Poor precision arises as the analytical detection limit is approached (figure 3.6) explaining the better precision for sodium than any other element. It was concluded that the absolute response

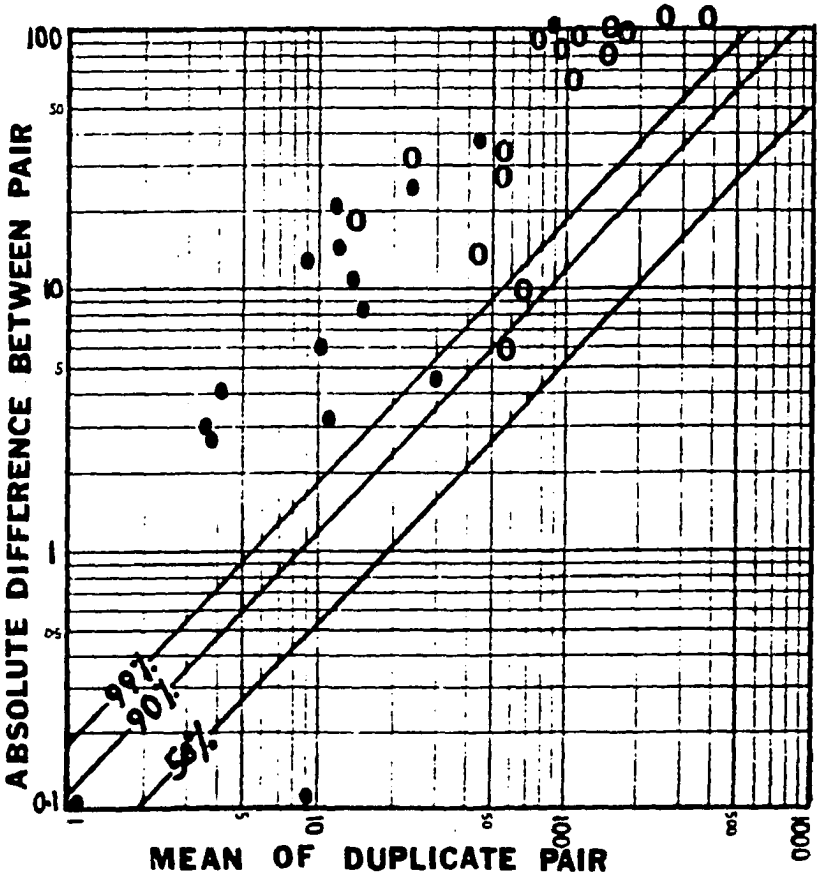

Figure 3.7 Precision plot for arsenic and arsenic/sodium values for duplicated samples(values in millivolts)

Table 3.3. Data for arsenic precision plot and arsenic/sodium precision plot (values in background stripped millivolts)

ID	Na	As	As/Na	$\bar{X}$=As	X_1-X_2 (As)	RSD% (As)	$\bar{X}$=As/Na	X_1-X_2 (As/Na)	RSD (As/Na)
YA 10A	3.96	0.36	0.09	0.54	0.36	33.3	0.11	0.03	14.3
10B	6.08	0.72	0.12	1.05	0.66	31.4	0.16	0.08	3.8
10C	6.86	1.38	0.20	0.95	0.86	45.3	0.145	0.11	37.9
10D	6.10	0.52	0.09	0.44	0.16	18.2	0.09	0	0
1A	5.04	0.23	0.05	0.14	0.18	64.3	0.28	0.045	82.0
1B	9.30	0.05	0.005						
51A	42.2	0.61	0.01	1.13	1.03	46.0	0.025	0.03	60
51B	41.5	0.55	0.01	0.58	0.06	5.2	0.01	0	0
51C	37.6	1.64	0.04	1.60	1.09	34.0	0.025	0.03	60
55A	10.6	0.27	0.03	1.6	2.66	83.1	0.13	0.20	76.9
55B	12.5	2.93	0.23						
54A	13.8	0.25	0.02	0.72	0.93	65.0	0.04	0.04	50.0
54B	19.3	1.18	0.06						
27A	6.78	3.97	0.59	2.88	2.19	38.1	0.41	0.37	45.7
27B	8.0	1.78	0.22						
23A	22.52	0.90	0.04	1.31	0.82	31.0	0.12	0.15	65.2
23B	9.0	1.72	0.19						

Table 3.3 (Continued)

ID	Na	As	As/Na	$\bar{X}$=As	X_1-X_2 (As)	RSD% (As)	$\bar{X}$=As/Na	X_1-X_2 (As/Na)	RSD (As/Na)
YA 14A	1.85	0.67	0.36	3.90	6.45	82.8	0.23	0.25	55.6
14B	0.63	7.12	0.09						
45A	2.44	0.39	0.16	0.23	0.33	73.3	0.09	0.14	77.8
45B	3.28	0.06	0.02						
33A	5.98	0.39	0.07	0.54	0.29	27.1	0.1	0.06	30.0
33B	5.44	0.68	0.13						
6A	0.45	0.71	1.58	0.66	0.1	7.6	0.85	1.46	85.9
6B	4.95	0.61	0.12						

level of the minor elements were probably highly influenced by instrumetal background fluctuation or contamination. Consequently the proximity of specific elements to their instrumental detection limit were assessed.

Further comparison of the Randsburg data with that of Alderton and others (1982) and Rankin and Alderton (1982) highlight the generally low level of sodium response gained for Randsburg DICP analyses (table 3.4).

Data handling and blank based detection limits

The large volume of data generated by DICP, i.e a thirty six element read out for each analysis, neccessitated a system of data 'significance testing' be established to evaluate whether individual element responses were above background (blank) levels.

A realistic evaluation of the DICP detection limit for each element was obtained by monitoring 'blank tube' millivolt responses. The millivolt response for a batch of blank tubes were monitored over a short time period, usually less than one hour. The percentage deviation of apparent analyte response around its mean blank value was generally small. The mean blank response value for an element corresponds to zero concentration, and twice the

Table 3.4. A comparison of the sodium DICP response levels (after background stripping) for quartz from various localities.

Location	Rock type/ intrusive	Quartz type	Sodium response (mV)	References
S.W. England	Granite (Cammenellis)	Whole rock	5-100	Rankin and Alderton, 1982
S.W. England	Granite (Bodmin)	Whole rock	20-120	Rankin and Alderton, 1982
S.W. England	Granite (Bodmin)	Whole rock	40-200	Rankin and Alderton, 1982
S.W. England	Granite (Bodmin)	Whole rock	40-150	Rankin and Alderton, 1982
S.W. Scotland	Granite-Tonalite (Carsphairn)	Stream sediment	20-40	Hart, 1984
S.W. Scotland	Granite-Tonalite (Loch Doon)	Stream sediment	15-25	Hart, 1984
S.W. USA Randsburg	(EW) Granodiorite (Yellow Aster)	Whole rock	0.8-41.8	Hart and Rankin, 1983
S.W. USA Randsburg	Microgranodiorite (Yellow Aster)	Whole rock	0.9-1.8	Hart and Rankin, 1983

Table 3.4 (Continued)

Location	Rock type/ intrusive	Quartz type	Sodium response (mV)	References
S.W. USA	Felsic breccia pipe (Colosseum)	Whole rock	70-85	Hart and Rankin, 1983

Note: Analyses are for 0.5 g of <2 mm >1 mm diameter quartz

positive standard deviation around this mean (zero concentration) is felt to be a realistic detection limit (herein termed, the blank-based detection limit). The blank-based detection limit could then be used to assess the magnitude of the sample responses for an element after the background value for that element had been 'stripped' from the sample.

Although data for thirty-six elements is aquired for each analysis, probably only ten or less elements are present at detectable levels in most decrepitates. A statistical technique was utilized to establish which elements were present at background levels only (i.e. the same as those levels exhibited by blank tubes).

If an element was not present in a sample, the plasma millivolt response would be close to the value gained for blank tubes. Thus, a set of samples with no response (or very small ones) for a specific element, would have approximately the same mean, standard deviation and therefore variance as the element in blank tubes.

A full explanation of the technique utilized is contained in Appendix IV. The F-test (Davis, 1973) was applied to test the equivalence of sample and blank variances (the F-test assumes two normal distributions

are being used). The method was found very useful in establishing the general response level of an element in the decrepitates. However the F-test alone cannot distinguish between contaminant or decrepitate derived response and therefore should never preclude a qualitative review of all responses.

The evaluation of the Randsburg DICP quartz analyses revealed only sodium to be present in all samples at 'significant' levels (table 3.5). This confirms the conclusions drawn from the earlier precision analysis.

Accuracy

The estimation of analytical accuracy is usually facilitated by the analysis of known reference materials (Rose, Hawkes and Webb, 1979). Such references did not exist for DICP analyses. An attempt was made by the author to establish a crude reference material by repeatedly analysing 0.5gram fractions of a crushed quartz vein over a period of several months (figure 3.8). A mean sodium value of 11.97 millivolts (background reduced) was obtained for the same quartz vein material during the Randsburg quartz analyses. This suggests the values obtained for the Randsburg quartz are slightly high. However between sample variation of the 'reference

Table 3.5. Sodium millivolt responses for Randsburg quartz.

ID	Na	K	As	Location	Rock Type
YA 1	5.0			GH	Quartz vein
2	0.2				Silicified intrusive
4	1.1		X		Highly altered intrusive
5	2.3		X		Highly altered intrusive
6D	2.7		X		Highly altered intrusive
7	4.3				EW granodiorite
8	2.8				Pegmatetic vein
9	7.3				Highly altered intrusive
10D	5.7				Quartz vein in Rand Schist
13	7.2				Xenolith phase of intrusive
14D	1.3		X		EW granodiorite
16	2.5				EW granodiorite
17	34.8	X			Quartz vein
19	10.0				Highly altered intrusive
21	2.1			UGH	Microgranodiorite (phyllic alt.)
22	3.8				EW granodiorite (minor phyllic)
23	22.5	X			EW granodiorite (minor phyllic)
24	4.2				Phyllic rock (EW?)
26	0.8				Microgranodiorite
27	6.8		X	See Map	Quartz vein
30	6.3				Quartz vein
32	6.0				EW granodiorite (phyllic)
33D	5.7				Quartz vein
36	0.3				Quartz vein

Table 3.5 (Continued)

ID	Na	K	As	Location	Rock Type
38	0.4			See Map	Highly altered intrusive
39	5.9	X	X		Highly altered intrusive
45D	2.9			See Map	GW granodiorite
47	0.7				GW granodiorite
48	4.7				GW granodiorite
49	8.9				GW granodiorite
51D	41.8	X			GW granodiorite
52	22.4				GW granodiorite
54	13.8				GW granodiorite
55	10.6				GW granodiorite
57	0.9			See Map	Microgranodiorite (unaltered)
58	1.2				Microgranodiorite (unaltered)
59	1.1				Microgranodiorite (unaltered)
61	1.8				EW granodiorite (phyllic)
62A	15.6	X	X		EW granodiorite (phyllic)
63	0.8				EW granodiorite (phyllic)
64	4.2				EW granodiorite (phyllic)
65	2.3				EW granodiorite (phyllic)
71	0.8				EW granodiorite (minor
72	-				alteration)
73	0.8				Xenolith phase of intrusive

Table 3.5 (Continued)

ID	Na	K	As	Location	Rock Type
YA 119	10.3			See Map	Gold bearing 'limonite rock'
123	8,6				Gold bearing 'limonite rock'
128	5.3				Gold bearing 'limonite rock'
131	2.1				Quartz vein-(Rand Schist)
142	3.4				Quartz vein-(Rand Schist)
(Atolia Quartz Monzonite Igneous Quartz)					
AT 1	0.13			See Map	Atolia Quartz Monozite intrusive
AT 2	12.6	X		See Map	Atolia Quartz Monozite intrusive
AT 3	0.9			See Map	Atolia Quartz Monozite intrusive
AT 4	1.7			See Map	Atolia Quartz Monozite intrusive
(Kelly Mine - gloryhole Dump - Quartz)					
KM 1	0.9			See Map	Kelly Mine Quartz
KM 2	1.8				Kelly Mine Quartz
KM 2B	1.8				Kelly Mine Quartz
KM 2C	4.2				Kelly Mine Quartz

Key: GH = glory hole at Yellow Aster
UGH = upper glory hole at Yellow Aster
X = above background based detection limit response

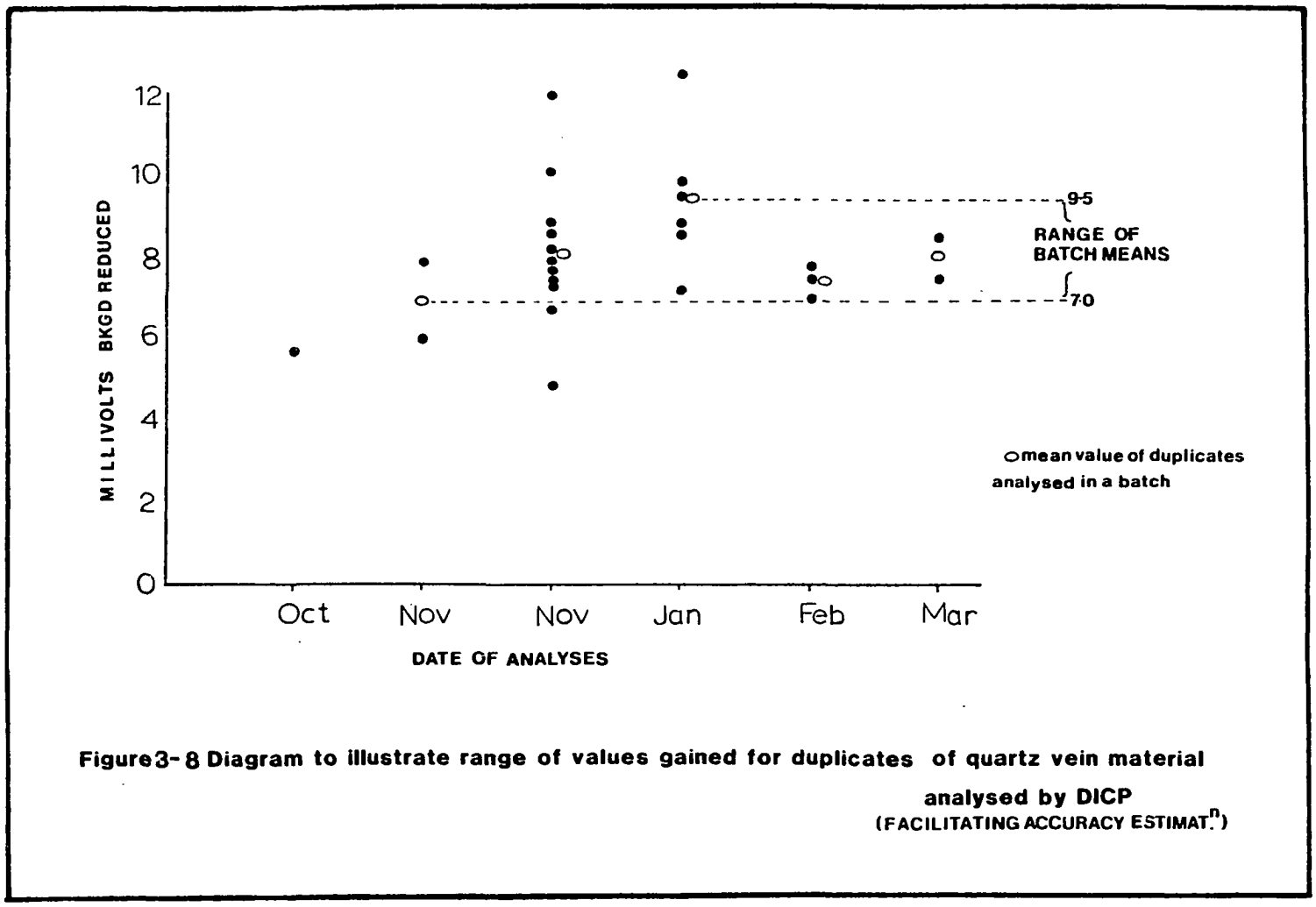

Figure 3-8 Diagram to illustrate range of values gained for duplicates of quartz vein material analysed by DICP (FACILITATING ACCURACY ESTIMAT^{n})

material' preclude quantification of such an error. The use of this reference material serves to highlight any order of magnitude error.

Contamination

Contamination was evaluated using the techniques outlined in Appendix IV. Contamination was found to be insignificant in most cases.

Discussion of results

The background stripped sodium millivolt values for Randsburg DICP analyses are presented in Table 3.5. The above background values for potassium, calcium and arsenic are also indicated.

Tables 3.4 and 3.5 illustrate that the overall sodium response (and by implication the decrepitation activity) for Randsburg quartz was very low.

A qualitative assessment of the results indicates that the various 'unaltered' intrusive lithogies might be distinguished on the basis of their sodium response. The EW granodiorite forming the ridge between the Yellow Aster pit and the Atolia-Randsburg road seems to contain an inclusion population that is characterized by a higher

sodium response than that of the Microgranodiorite adjacent to the Yellow Aster pit. The areal distribution of the sodium response values is shown in figure 3.9.

The sodium responses associated with the intensely fractured rocks of the Yellow Aster pit are lower than equivalent lithologies outside the pit e.g. EW granodiorite. This is probably a result of the destruction of a primary inclusion assemblage, and the response of a smaller diameter (smaller volume) secondary assemblage.

The sodium responses gained from both the Atolia quartz monzonite quartz and Kelly Mine quartz were also low. It appears that sodium responses could not effectively be used as a discriminant for quartz from the gold, silver or tungsten mineralized areas. A notable feature of the results is the unexpecetdly low sodium responses associated with quartz from the intensly altered rocks of the Yellow Aster pit. These rocks had previously been reported to contain a well developed fluid inclusion assemblage (Harris, 1980b). Figure 3.9 illustrates a discrete anomaly centered on sample YA51. This anomaly is real and reproducible, located approximately six hundred meters east of the Yellow Aster pit.

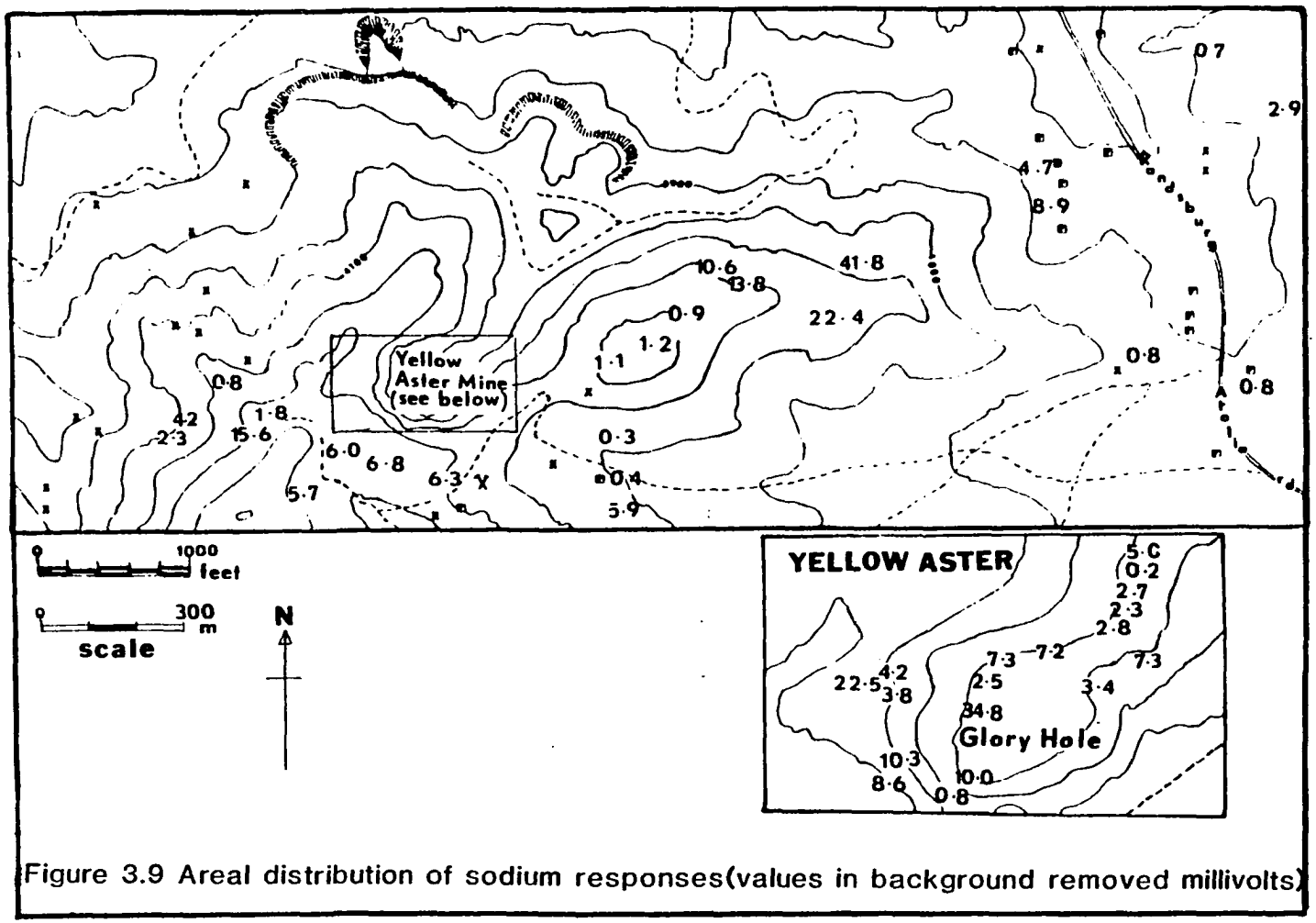

Figure 3.9 Areal distribution of sodium responses(values in background removed millivolts)

The overall low sodium values gained at Randsburg were surprisingly low and were interpretted as the result of low decrepitation activity and/or that a very low salinity inclusion population occured in most rocks.

Subsequent analyses using DICP

Because of the low sodium DICP results gained it was postulated that the Randsburg quartz might contain a fluid inclusion population that decrepitated within the fifteen second preheat period utilized in the initial analyses (figure 3.4). To investigate this, two approaches were adopted:

i) DICP analyses with a zero to sixty (0-60) second integration period, i.e no preheat period.

ii) 'Windowed' integrations of the plasma response over a sixty second period (see earlier section).

Using this window technique it is also possible to establish whether elements are derived from decrepitation or some other source (figure 3.10).

Table 3.6 illustrates that no systematic increase in sodium response value was observed on utilizing a zero to sixty second integration period. This suggested an inclusion population that decrepitated within the fifteen second pre-heat period was not present. "Window"

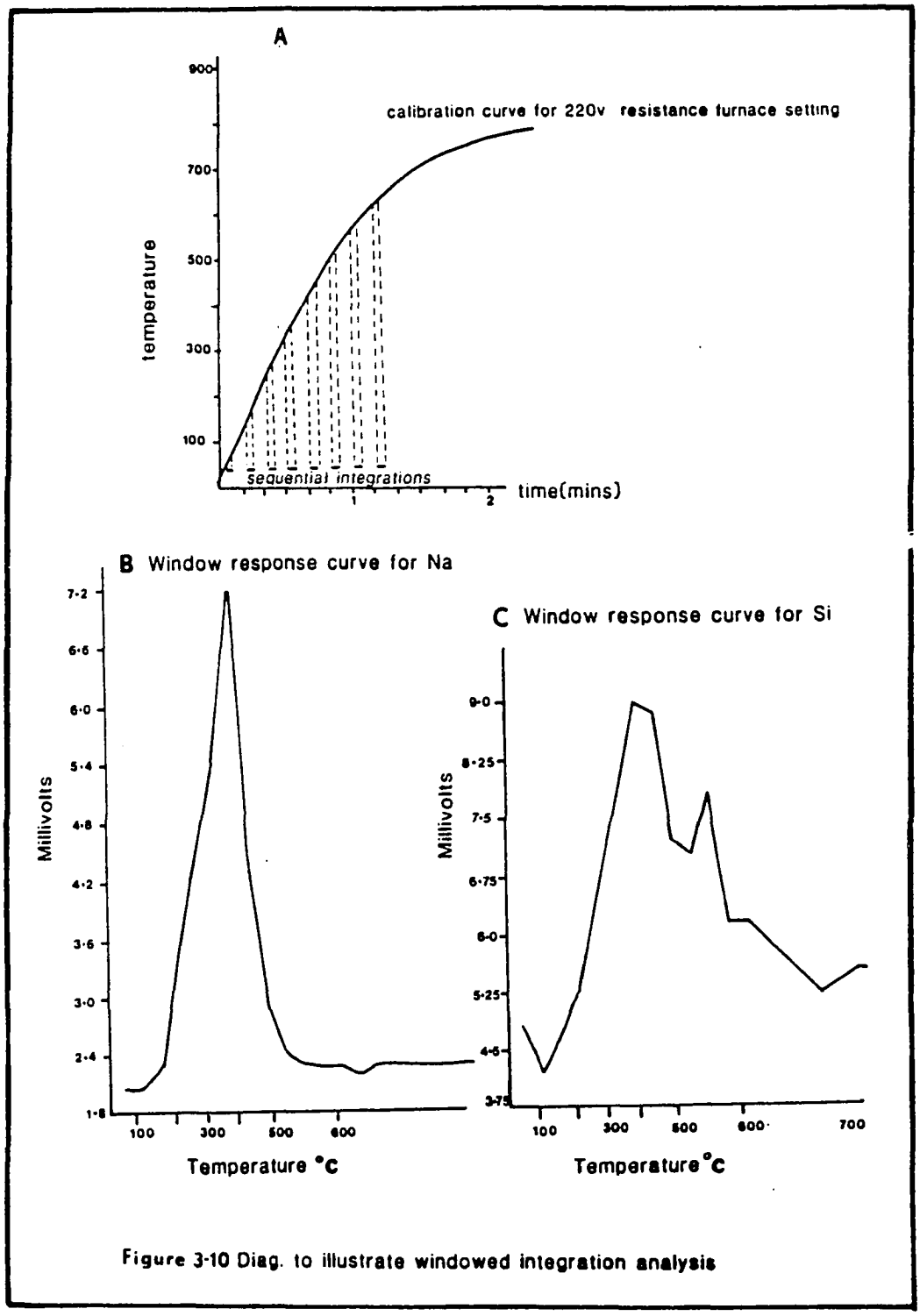

Figure 3-10 Diag. to illustrate windowed integration analysis

Table 3.6. Comparison of sodium response for 0-60 second and 15-60 second integration periods. Values are background reduced millivolts.

ID	Sodium response 0-60 seconds	Sodium response 15-60 seconds	$\frac{(15\rightarrow60-(0\rightarrow60)}{(0\rightarrow 60)} \times 100$
YA1	9.1	7.2	-20.9%
YA10	5.9	5.8	-1.69%
YA23	9.1	15.8	+73.6%
YA27	8.0	7.4	-7.5%
YA51	37.4	40.4	+8.0%
YA54	9.4	16.6	+76.6%
YA55	12.3	11.6	-5.7%

analyses (figure 3.10 and 3.11) support this conclusion. Figure 3.11 also illustrates that many elements (especially those very close to background values) are probably not derived from the decrepitation of inclusions and are contamination/sublimation derived.

Figure 3.10b illustrates the coincident decrepitation peaks for sodium and silicon. These peaks occur at thirty-four seconds equivalent to a temperature of 370 °C (±10 °C). These peaks represent the temperature of maximum decrepitation (Thompson and others, 1982: Thompson and Walsh, 1983).

Conclusions on the applicability of the DICP-Quartz Technique

The conclusions that can be drawn from the DICP analysis of Randsburg quartz are:

i) massive decrepitation of the inclusion population ensues at 350-370 °C, as indicated by the sodium response.

ii) Sodium is the most abundant cation in the inclusion fluids.

iii) Most other elements are not derived from inclusion fluids.

iv) Most quartz contains either:

a) a low salinity inclusion population, or

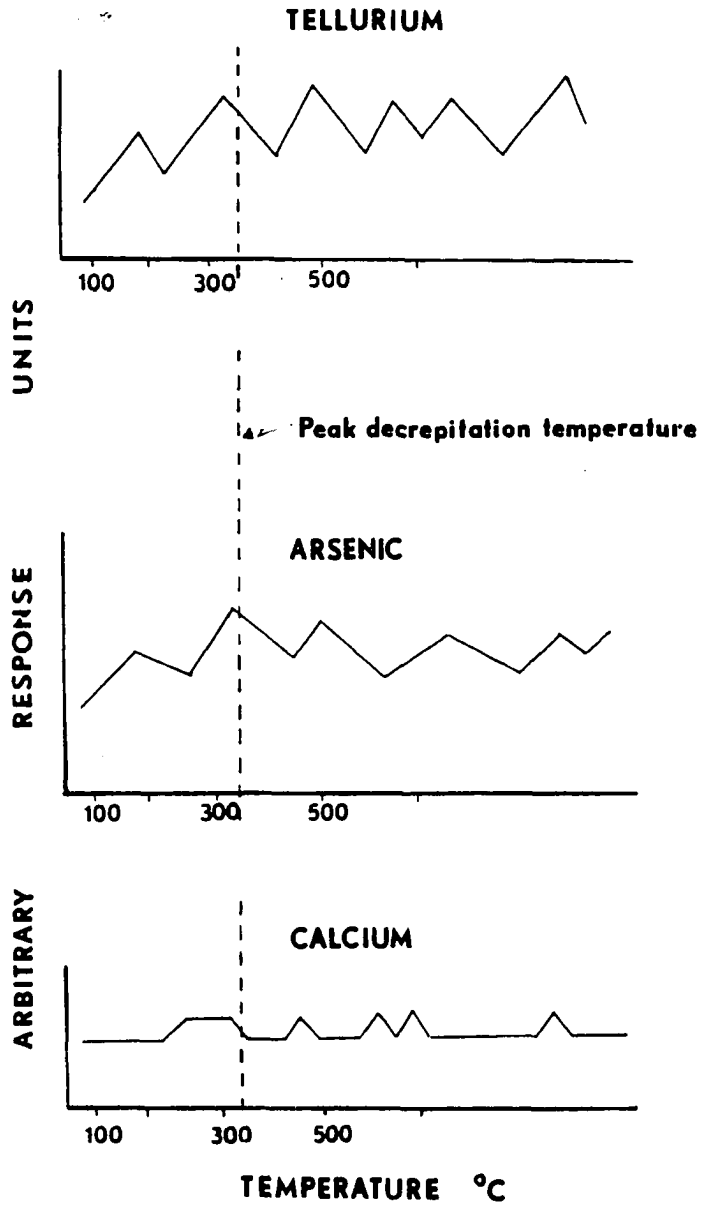

Figure 3.11 Window analyses for various elements

b) a low abundance of inclusions.

General conclusions on the technique as an exploration tool are deferred until the fluid inclusion petrography has been reported. However, the conclusions drawn at this juncture serve to illustrate the uncertainty involved in the interpretation without any petrographic data base. A qualitative review of the data suggests:

i) DICP could not be used to distinguish between the fluid inclusion populations at the gold, silver and tungsten mineralized areas.

ii) The presence of a well developed, abundant inclusion assemblage at Randsburg is not predicted by the DICP sodium response.

iii) Sodium response levels suggest distinct fluid inclusion populations are associated with the altered and unaltered varieties of the EW granodiorite.

The limitations of the DICP technique apparent from this present study are:

i) The multi-element data generated by DICP are not specific to a single generation of fluid inclusions present within the cyrstalline host. Thus any sodium response might be the aggregate response of several temporally distinct inclusion populations, whose

individual responses (and therefore fluid chemistry) cannot be simply isolated and evaluated. This has important implications for DICP application to mineralization, such as gold, commonly associated with episodic hydrothermal fluid activity.

ii) The volume of inclusion fluid presented to the plasma, and therefore the absolute concentration level (or average concentration level if more than one fluid inclusion population is involved) of an element in the inclusion fluid cannot be obtained.

iii) The results for minor (and some major) elements are difficult to validate at low decrepitation levels.

The concept of 'decrepitation level', as indicated by the magnitude of the sodium response, is questionable (see point two above). If the volume of the fluid causing an increase in sodium response is unquantified, several interpretations of the cause are plausible:

i) an increased total abundance of decrepitable inclusions,

ii) an increased average volume of decrepitable inclusions,

iii) an increased average salinty of decrepitable inclusions,

iv) Some combinations of i) through iii).

These points highlight the possible interpretative difficulties that might be encountered if a fluid inclusion halo or 'steam aureole' (figure 1.1) does accompany mineralization. The 'steam aureole' concept holds that an increased number (not neccessarily an increased volume or salinity of inclusion fluid) will be encountered on approaching mineralization. The concept, even if valid, does not predict an increased sodium response should be correlative with an increased abundance. Thus 'decrepitation level' evaluation should not preclude petrographic investigation of the fluid inclusion population in quartz, which is felt to be of fundamemtal importance to the interpretation of DICP data. Petrographic evidence only, can indicate the direction of increasing fluid inclusion abundance, and hence the palaeo - fluid focus.

Suggestions for improvement to the DICP Technique as applied to whole rock quartz

The general application of DICP techniques would be greatly improved by the following developments:

a) a method enabling the volume of inclusion fluid released during decrepitation to be quantified. This would allow absolute concentrations levels of metal ions to be established.

b) A technique to estimate the number of individual decrepitation events accoustically, to run contemporaneously with DICP analysis. This would allow rapid identification of areas subjected to higher levels of hydrothermal activity. This might also be used to crudely quantify the chemistry of primary and 'overprinting' generations of inclusions.

Chapter 4

FLUID INCLUSION PETROGRAPHY OF THE RANDSBURG MINING DISTRICT WHOLE ROCKS

Introduction

This chapter details observations made from ordinary petrographic thin sections. Microthermometric studies of fluid inclusions in quartz wafers are detailed in the following chapter. This artificial dichotomy allows the use of fluid inclusion mapping, utilizing thin section observations, to be evaluated on its own merits.

Sample collection

The thin section suite (approximately one hundred) detailed in Chapter 2 formed the basis of this study (figure 2.3). Mineralogy and alteration features of the suite were reported in Chapter 2.

Methodology

Standard (thirty microns thick) thin sections were used to study the size, morphology, abundance and contents of fluid inclusions present in quartz at room temperature (25°C) and at 15°C to test for the presence of carbon dioxide.

An empirical approach to a classification scheme was adopted, based on the gross composition and morphology of inclusions observed within the previously stated temperature range. A sixfold classification of fluid inclusions was developed (figure 4.1). The classification boundaries are somewhat arbitrary, and some overlap undoubtedly exists. However, the classification scheme was found to be effective. A genetic classification of inclusions was attempted where possible but due to the inherent subjectivity involved (Appendix I) this approach was less useful than the descriptive morphology method.

Fluid inclusion classification

Type 1 inclusions exhibit a round to equant shape are (figure 4.1) generally less than 10μm diameter and contain carbon dioxide phases only. This inclusion type includes both two phase (liquid and vapor) and single phase (liquid or vapor) inclusions, and any volumetric combination between the one phase and two phase end members. Positive identification of one phase carbon dioxide bearing inclusions (usually carbon dioxide gas) often required cooling the thin section to fifteen degrees centigrade. This is easily achieved at the University of Alaska, with the prevailing winter climate.

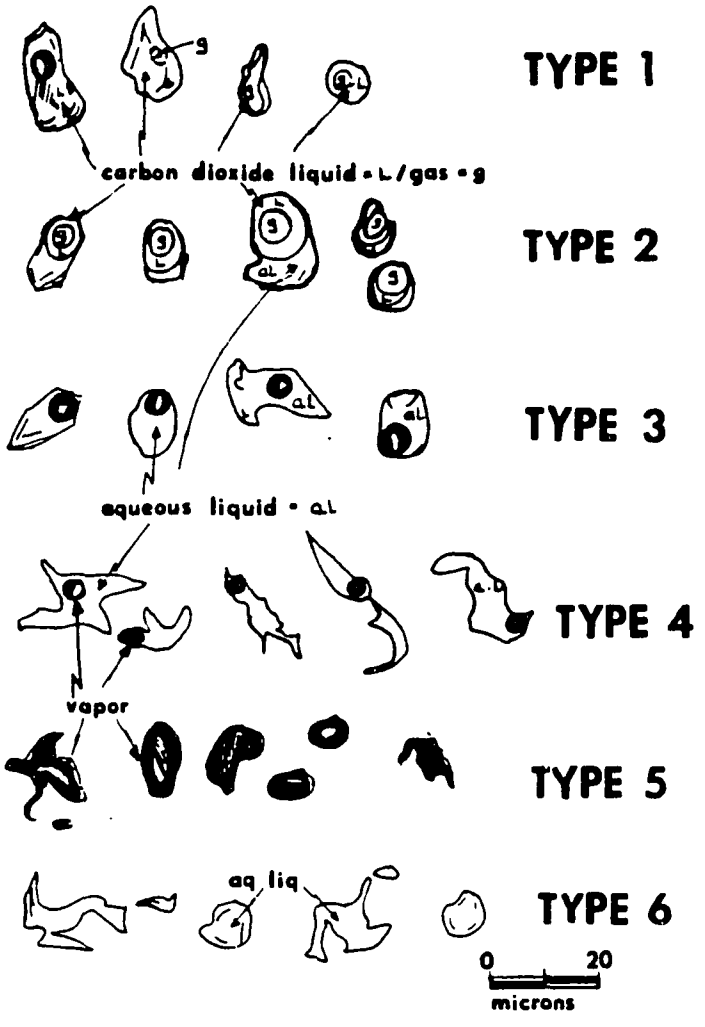

Figure 4.1 Inclusion type classification

Cooling of the sections, achieved by observation within a cooled room, often results in the condensation of a liquid rim of carbon dioxide. The difficulty associated with the positive identification of type 1 inclusions has probably resulted in an underestimation of their abundance. However, microthermometric study of polished wafers confirm that type 1 inclusions are relatively rare in the Randsburg Mining District.

Type 2 inclusions (figure 4.1) exhibit a round to occasionally irregular shape, ranging from less than 5µm to greater than 50µm diameter. Most inclusions are less than 15µm diameter. Type 2, describes three phase inclusions containing aqueous liquid (aq-liq), carbon dioxide liquid (CO2 liq) and carbon dioxide vapor (CO2 vap). The volumetric proportion of phases observed at room temperature (25 °C) varied through the range shown in figure 4.1. Rarely, type 2 inclusions were observed to contain a small highly birefringent daughter mineral, possibly a carbonate. Type 2 inclusions were observed as primary, or pseudosecondary inclusions at various localities.

Type 3 inclusions (figure 4.1) are two phase aqueous inclusions containing a liquid and high-relief vapor bubble (vapor usually constitutes less than twenty volume

percent). The inclusions exhibit a round to equant shape generally less than 15μm diameter, with most less than 10μm diameter. Type 3 inclusions were generally secondary or pseudosecondary occupying planar fractures in quartz.

Type 4 inclusions exhibit a ragged, irregular morphology and also contain two aqueous phases (liquid and vapor). A variable proportion of liquid to gas phases is an artifact of post entrapment modification of morphology knkown as 'necking down' processes (Roedder 1984a). Type 4 inclusions were observed as both primary and secondary inclusions (temperatures of homogenization subsequently obtained from such inclusions were often variable suggesting necking, post-evolution of a vapor bubble).

Type 5 inclusions are round to irregular morphology, monophase (gas rich) inclusions, generally less than 20um diameter. The composition of the vapor phase cannot be ascertained by observation only, but is assumed to be a carbon dioxide and water bearing fluid phase. Type 5 inclusions are dominantly secondary in origin commonly occuring in planar groups, corresponding to post - crystallization fractures within the host crystal.

Type 6 inclusions are ragged, irregular, monophase, aqueous liquid rich inclusions, commonly occuring with type 4 and type 5 inclusion, in planar groupings, indicating a secondary origin. Inclusion size is highly variable as illustrated in figure 4.1.

Estimation of fluid inclusion abundance in quartz

The abundance of inclusions in quartz in thin section was estimated using the charts illustrated in figure 4.2. The charts contain idealized microscope fields of view. The areal densities of inclusions are assigned scores (higher scores corresponding to higher areal densities of inclusions). The use of standard thickness petrographic thin sections allows a constant volume of quartz to be viewed at each count (providing the field of view is filled). The thin sections are observed at four hundred times magnification with a polarizing transmitted light microscope. Fifty to one hundred half fields of view were observed per thin section and the abundance scores estimated by visual comparison with figure 4.2. At approximately two microns diameter the inclusions are too small to be classified optically (being at the effective resolution limit of the microscopes used). Consequently, the abundance of inclusions above and below the two micron 'cut-off' are

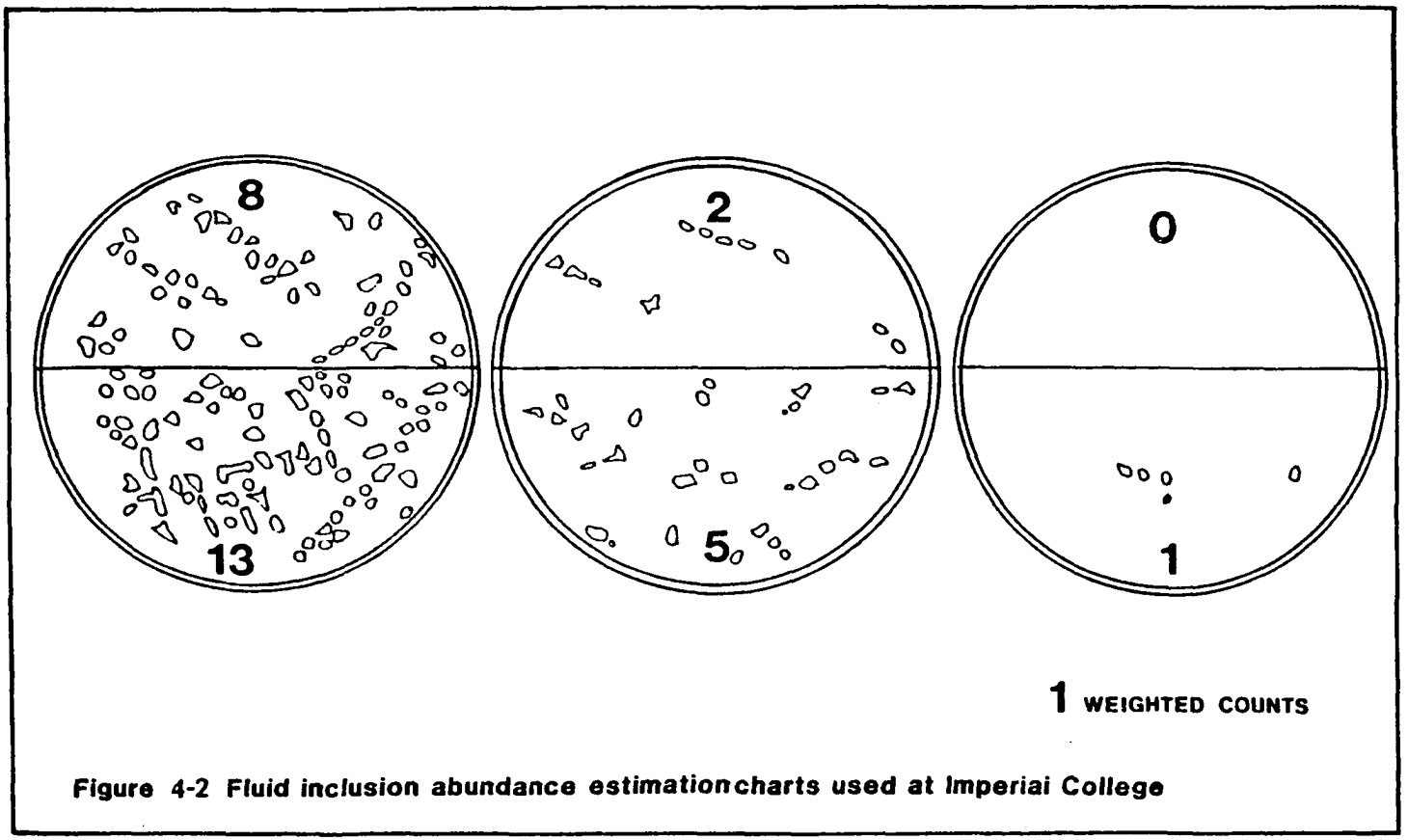

Figure 4-2 Fluid inclusion abundance estimation charts used at Imperial College

independently recorded (Table 4.1). The mean abundance score was estimated as indicated:

$$\frac{\Sigma A}{n} = A^* \qquad \text{where } {}^*A = \text{abundance mean}, \; n = \text{number of counts}, \; A = \text{individual count}$$

The subjectivity of the abundance estimation technique was investigated by repeatedly comparing the mean abundance scores obtained from one thin section by two persons. Reproducibility was surprisingly good with the difference between operatives generally less than ten percent, and commonly less than five percent.

Type estimation

After ten abundance estimations, a count of the various inclusion types was made. The results are expressed as an approximate percentage of the inclusions observed. The accuracy of the estimation was more difficult to assess. However, use of one operative was felt to minimize the imprecision.

Table 4.1. Abundance estimates for fluid inclusions quartz.

ID	Abundance 2µM	Abundance 2µM	% Estimate of Types 1	2	3	4	5	6	Comments on Quartz	Rock Type	Alteration	Mineral-ization	DICP (Na)
YA 2	2.5	13	-	10	10	30	30	20	Weakly deformed	EW granodiorite	Sc, Si	Py	0.2
4	2.8	>8	-	5	25	20	30	20	Moderately deformed	EW Granodiorite	Sc, Si	Py	1.1
6	1.8	>8	-	-	15	10	60	25	Planar fractures common	EW Granodiorite	Sc, Si, Hm	Py	2.7
10	5.7	13	-	2	8	15	60	15	Planar fractures common	Quartz vein	-	none	5.7
13	1.4	13	10	5	25	10	40	10	Moderate deformation	EW Granodiorite	Bi	none	7.2
14	1.4	≤5	<5	<5	25	15	30	20	Planar fractures common	EW Granodiorite	Bi	Py	1.3
15	1.8	<5	-	10	10	40	20	20	Inclusions in calcite	Carbonate cemented	Hm, Si, Sc	±Au	-
19	2.3	>8	-	<5	<5	10	60	25	Planar fractures common	--	Sc, Si, Hm	Py	10.0
21	≤0.5	13	-	-	*	*	*	*	Classification precluded	Microgranodiorite	Sc, Si	Py	2.1
22	1.7	13	-	<5	20	45	10	15	Planar fractures common	EW Granodiorite	Sc, Si	Py	3.8
23	≤0.5	>8	-	*	*	*	*	*	Size precludes classn.	EW Granodiorite	Sc, Si	Py	22.5
24	≤0.5	>8	-	*	*	*	*	*	Local recrystallizn.	EW Granodiorite (?)	Sc, Si	Py	4.2
25	≤0.5	>8	-	*	*	*	*	*	Local recrystallizn.	Microgranodiorite	Sc, Si	Py	-
26	≤0.5	>8	-	*	*	*	*	*	Local recrystallizn.	Microgranodiorite	Sc, Si	Py	0.8
27	5.5	9	-	10	35	20	15	25	Two ages of quartz	Quartz vein	-	-	6.8
28	2.5	-	-	-	15	15	40	30	Planar fractures common	EW Granodiorite	Sc, Si	Py	-
30	3.7	-	-	-	40	10	25	25	Planar fractures common	Quartz vein	-	-	6.3
31	<0.5	<5	-	-	*	*	*	*	Moderately fractured	Microgranodiorite	Sc, Si	Py	-
32	7.2	-	<5	<5	15	10	30	35	Highly fractured	EW Granodiorite	Sc, Si	Py	-
35A	<0.5	<5	-	-	*	*	*	*	Moderately fractured	Microgranodiorite	Sc, Si	Py	-
35B	<0.5	>8	-	-	*	*	*	*	Highly fractured	EW granodiorite	Sc, Si	Py	6.0
38	4.0	>8		<5	25	<15	15	40	Fractured	EW granodiorite	Si	-	5.9
39	5.0	>8	>5	<10	15	15	15	35	Fractured	EW granodiorite	Si	-	-
46	<1.0	≤2	-	>5	40	10	25	20	Fine grained	EW granodiroite	Si	-	-
48	<1.0	≤2		<10	20	40	10	20	Moderate deformation	EW granodiorite	Si	-	4.7
49	2.0	≤2		<10	30	30	15	15	Moderate deformation	EW granodiorite	Si	-	8.9
50	3.0	≤5	<5	35	15	10	20	15	Moderate deformation	EW granodiorite	Si, Bi	-	-
51	2.3	≤5	<5	30	20	10	25	10	Moderate deformation	EW granodiorite	Si, Bi	-	41.8

Table 4.1 (Continued)

ID	Abundance 2μM	Abundance 2μM	% Estimate of Types 1	2	3	4	5	6	Comments on Quartz	Rock Type	Alteration	Mineral-ization	DICP (Na)
YA 52	1.5	5	<5	30	10	15	30	10	Fractured quartz	EW granodiorite	Bi	none	22.4
54	2.0	≥5	<5	30	10	10	25	20	Fractured quartz	EW granodiorite	Bi	none	13.8
55	1.0	≥5	<5	25	30	10	20	25	Fractured quartz	EW granodiorite	Bi	none	10.6
57	<1.0	<5	-	-	*	*	*	*	Underformed-igneous	Microgranodiorite	none	none	0.9
59	<1.0	<5	-	-	*	*	*	*	Underformed-igneous	Microgranodiorite	none	none	1.1
60	<1.0	<5	-	-	*	*	*	*	Underformed-igneous	Microgranodiorite	none	none	-
61	<1.0	<5	-	-	*	*	*	*	Deformed-igneous	EW granodiorite	min. Sc	Py	1.8
62	<1.0	≥8	-	10	20	10	20	60	Deformed-igneous	EW granodiorite	Bi	none	-
62A	<1.0	≥5	-	-	*	*	*	*	Highly fractures	EW granodiorite	Sc, Si, Hm	Py	15.6
63	1.6	≥8	-	-	15	15	20	50	Planar fractures	EW granodiorite	Sc, Si, Hm	Py	0.8
64	3.1	≥8	-	10	30	15	20	25	Slight deformation	EW granodiorite	Sc, Si, Hm	Py	4.2
65	1.7	≥8	-	-	*	*	*	*	Slight deformation	EW granodiorite	Sc, Si, Hm	min. Py	2.3
66	<1.0	≥8	-	-	*	*	*	*	Fine grained veining	EW granodiorite	Hm, Si,	Py	-
67	<1.0	≥5	-	-	*	*	*	*	Minor quartz	Gov peak stock	Weath	none	-
71	<1.0	≥5	-	-	*	*	*	*	Slight deformation	EW granodiorite	Bi	none	0.8
74	<1.0	≥5	-	-	*	*	*	*	Slight deformation	EW granodiorite	Bi	none	-
75	<1.0	≥5	-	-	*	*	*	*	Slight deformation	EW granodiorite	Bi	none	-
84	5.9	13	-	<5	10	20	35	30	Deformed quartz clasts	Breccia pipe in EW grd	Bi, Si	none	-
86	<1.0	≤5	-	-	*	*	*	*	Very fine silicif.	Breccia pipe in EW grd	Bi, Si	none	-
101	2.2	13	-	<5	20	30	20	30	Deformed	Qtz vein-late calcite	-	Py, Hm	-
103	2.0	13	-	10	20	20	30	20	Highly deformed	Qtz vein-late calcite	-	Py, Hm	-
104	2.0	13	<5	<10	35	15	25	15	Highly deformed	Qtz vein (Rand-level)	-	none	-
106	2.4	≥8	<5	10	45	10	10	60	Complete rexystalln.	R. Schist (Rand-level)	-	Py, Hm	-
108	<1.0	13	-	-	*	*	*	*	Deformed coarse grains	Fe oxide rich rock	Si, Cc,	Au, Hm	-
110	9.8	13	<5	<10	10	15	20	35	Highly deformed	Qtz vein (first level)	-	-	-
112	<1.0	13	-	-	*	*	*	*	Highly deformed/rexn	Qtz vein (Jupiter adit)	-	-	-
113	2.0	13	-	-	*	*	*	*	Moderately deformed	Qtz vein (Jupiter adit)	-	-	-
116	13.8	13	<10	45	10	5	20	20	Moderately deformed	Qtz vein in Rd. Sch.	-	-	-
118	1.8	≥5	-	-	-	-	-	-	Graphic Intergrowth	EW granodiorite	Si, Sc, Cc	-	-

Table 4.1 (Continued)

ID	Abundance 2cM	Abundance 2µM	% Estimate of Types 1	2	3	4	5	6	Comments on Quartz	Rock Type	Alteration	Mineralization	DICP (Na)
YA119	<1.0	13	-	-	*	*	*	*	Deformed coarse grains	Fe oxide rich rock	Hm, Si, Cc	Au	10.3
121	<1.0	<1	-	-	-	-	-	-	V. v. fine grained	Kelly dike	-	Sb, Hg	-
123	2.6	13	-	<5	10	20	30	25	>2 ages of quartz	Fe oxide rich bxa	Hm, Si, Cc	Au	8.6
124	6.0	13	-	10	20	10	30	30	Highly deformed	EW granodiorite	Sc, Si	Py	-
128A	6.9	13	>5	15	10	15	35	20	>2 ages of quartz	Fe oxide rich bxa	Si, Cc	Au	5.3
128B	3.0	13	-	<5	<10	15	40	35	Highly deformed	Qtz vein (Stringer dis)	Si, Cc	none	-
131	3.1	13	10	35	10	10	25	10	Moderately deformed	Qtz vein in Rd. Sch.	-	non	2.1
132	2.9	13	<10	20	10	15	35	10	Highly deformed	Qtz vein in G.P.S.	Si, Sc, Hm	none	-
133A	2.0	<5	-	-	10	25	40	25	Moderately deformed	Gov. Pk. stock	Si, Sc	non	-
133B	<1.0	<5	-	-	*	*	*	*	Very fine grained	Gov. Pk. stock	Si, Sc	Py	-
136	<1.0	<2	-	<5	50	15	15	15	Weakly deformed	Qtz Pod in EW grd	none	none	-
139	1.7	<13	-	<5	20	15	30	30	Weakly deformed	Silic (graphic intergth)	Si, Sc	none	-
140	1.5	<2	<10	15	30	5	35	10	Highly deformed clast	'Romeo' breccia pipe	Si, Sc	none	-
141	<1.0	13	-	*	*	*	*	*	Moderately deformed	Quartz vein	Si	none	-
143	-	-	15	35	10	10	20	10	Graphic intergrowth	Pegmatite dike	none	none	-
Kelly Silver Mine													
YA120A	<1.0	<2	-	-	*	*	*	*	V. fine grained	Siliceous vein	Si (1 ages)	Ag, Sb	0.9
120B	<1.0	<2	-	-	*	*	*	*	V. fine grained	Siliceous vein	Si (1 ages)	Ag, Sb	0.9
120C	<1.0	<2	-	-	*	*	*	*	V. fine grained	Siliceous vein	Si (1 ages)	Ag, Sb	0.9

Table 4.1 (Continued)

ID	Abundance 2µM	Abundance ≥2µM	% Estimate of Types 1	2	3	4	5	6	Comments on Quartz	Rock Type	Alteration	Mineral-ization	DICP (Na)
Atolia Quartz Monzonite													
AT84A	2.0	≥2	-	<5	50	10	20	15	Weak deformation	Atolia quartz monzonite	Chl, Si	Sch	1.7
84B	2.1	≥2	-	<5	45	10	25	15	Weak deformation	Atolia quartz monzonite	Chl, Si	Sch	1.7
84C	2.0	≥2	-	<5	45	10	20	20	Weak deformation	Atolia quartz monzonite	Chl, Si	Sch	1.7
EAT1	1.5	≥5	-	-	30	20	30	20	Moderately deformed	Atolia quartz monzonite	Chl, Si, Sc	Py	0.13
2	1.0	≥8	-	<5	20	15	30	30	Moderately deformed	Atolia quartz monzonite	Si, Hm	Py	12.6
3	2.0	≥8	-	<5	15	15	40	25	Undeformed	Quartz and Cc vein	none	Sch	0.9

Key: Hm = hematite; Si = silica; Cc = calcite; Sc = sericite; Py = pyrite; Au = gold; Ag = silver; Hg = mercury; Sch = scheelite; Sb = stibnite

Discussion

Table 4.1 contains the abundance and type estimates for all samples. Figure 4.3 highlights the areal distribution of the inclusion abundances, and illustrates several important features, namely:

i) the high abundance of less than 2μm diameter inclusions observed in quartz from samples within the Yellow Aster glory hole and those taken from the Rand and First levels of the underground workings.

ii) A high abundance of compositionally similar (to those above) inclusions associated with gold mineralization at the western extreme of the Government Peak Stock.

iii) The low abundance of fluid inclusions associated with the microgranodiorite body located at the southeast of the Yellow Aster glory hole. The sparse inclusion population is felt to represent the primary inclusion assemblage of this intrusive phase. Hydrothermally altered varieties of this igneous lithology (e.g. YA21, 24 and 25) contain a much larger abundance of fracture-introduced secondary inclusions.

iv) The generally higher abundance figures for greater than 2um diameter inclusions observed within EW granodiorite to the east of the Yellow Aster mine. Table 4.1 also illustrates that the inclusions observed within this intrusive phase have an important carbon dioxide

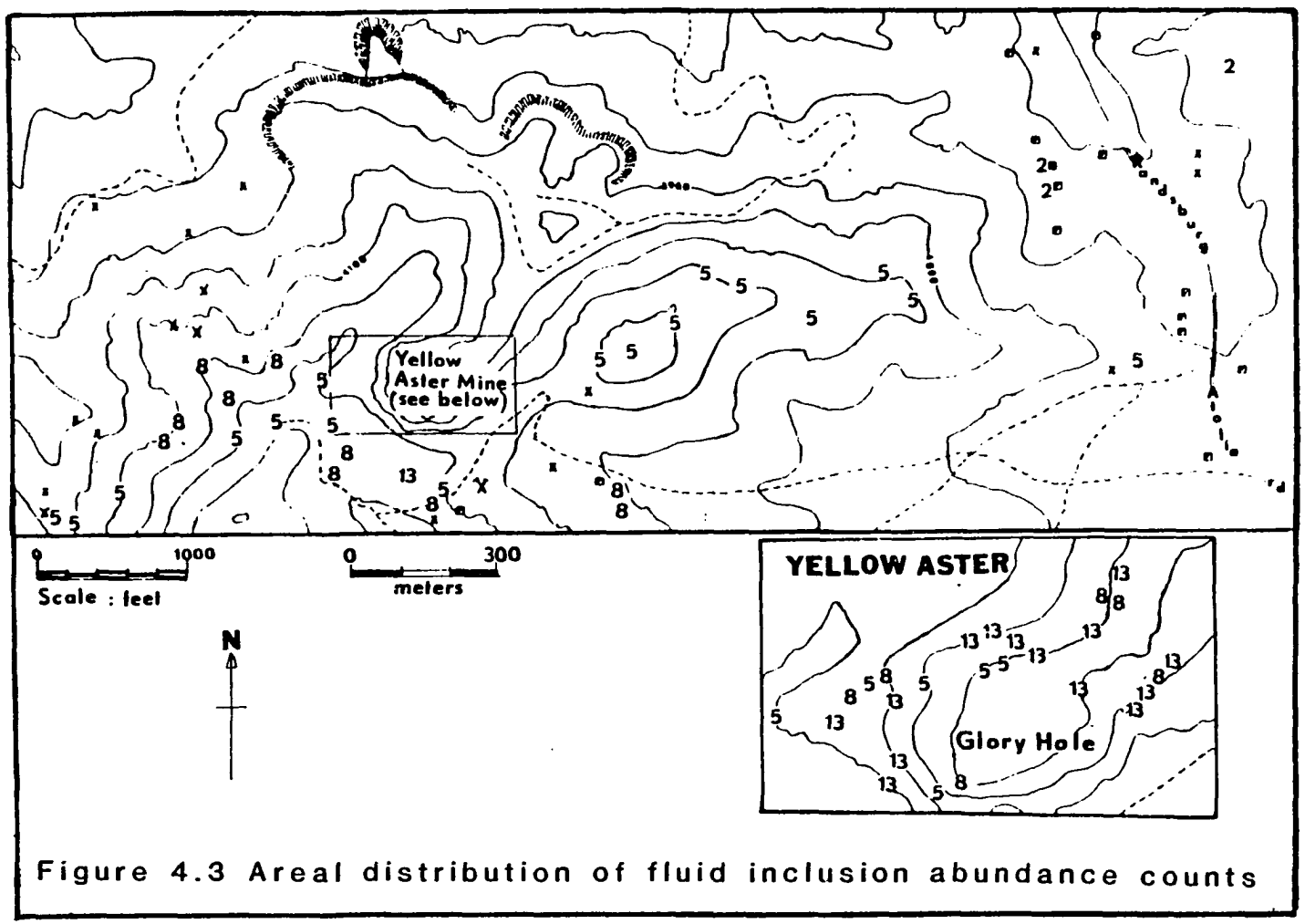

Figure 4.3 Areal distribution of fluid inclusion abundance counts

component.

v) Quartz veins, segregations and coarser grained silica-rich rocks from the Yellow Aster glory hole, and Government Peak Stock exhibit a higher average inclusion abundance than most igneous quartz (mean abundance $\geqslant 5$). Many quartz veins were observed to contain a significant population of carbon dioxide-bearing inclusions e.g. (YA 131, 132, 104, 116) as both primary and secondary inclusions.

vi) The fine grained silica accompanying silver mineralization at the Kelly Mine contains a very low abundance of fluid inclusions. Classification of inclusion types was precluded by the very small size of these inclusions.

vii) The quartz veins and silicification accompanying scheelite mineralization within the Atolia quartz monzonite contained a moderate to low inclusion abundance lacking a major carbon dioxide component.

This study suggests that the gold mineralized areas are characterized by a higher abundance of fluid inclusions in quartz. Mineralization at the Yellow Aster mine was intimately associated with intense brittle fracturing of the Rand Schist and intrusive lithogies observed in the 'glory hole'. Consequently, a very high proportion of fracture-related small secondary inclusions

was observed in quartz from this locality. The quartz is typically moderate to highly deformed (Table 4.1) and contains many cross cutting planes of secondary inclusions, suggesting temporally distinct periods of fracturing and fluid introduction. On the basis of cross cutting fluid inclusion relationships, at least two (and often more than three) periods of fluid inclusion formation can be discerned in the Yellow Aster mine region. The later generations of secondary inclusions distinguished by this criterion appear to contain a significantly decreased proportion of carbon dioxide (validation of this observation was confirmed by microthermometric investigation) and are dominantly type 4-6 inclusions. Similarly, primary inclusions in quartz veins and irregular lenses within the Rand Schist marginal to the Yellow Aster glory hole contain a higher proportion of carbon dioxide than cross cutting secondary inclusion trains. Primary inclusions in quartz veins and lenses outside the zones of intense deformation proximal to the Yellow Aster mine were also observed to contain a greater proportion of carbon dioxide than cross cutting secondary inclusions. Late stage post-deformation euhedral quartz (YA123) contains large primary type 3 and type 4, two phase aqueous inclusions with no discernible carbon dioxide content at either fifteen or twenty five

degrees centigrade, confirming the observed loss of carbon dioxide.

These observations suggest that during the fracturing episodes the carbon dioxide component of the prevailing fluid was progressively depleted. The mechanism for the loss of carbon dioxide is further discussed in the following chapter. However, the potential usefulness of petrographic observation is highlighted. Petrographic observation strongly suggests gold - pyrite - arsenopyrite mineralization at the Yellow Aster mine could be related to the loss of the carbon dioxide volatile from the hydrothermal fluid. This fact could crudely be used to investigate a possible metal depositional mechanism prior to microthermometric investigation.

Figure 4.3 also illustrates some of the potential drawbacks associated with fluid inclusion mapping. If the abundance of larger than 2μm fluid inclusions in quartz were selected as a measure of hydrothermal activity, then the Yellow Aster mine area is (on this basis only) similar to background, and would not merit further study. However, if the total abundance of all inclusions in quartz is a measure of hydrothermal activity then the Yellow Aster mine area is distinctly

anomalous. This also serves to illustrate the importance of describing all inclusions observed, whether primary or secondary.

Total inclusion abundance in quartz would appear to be a useful tool in the delineation of potential gold mineralized areas at Yellow Aster. However, the presence or absence of carbon dioxide within inclusions would appear to be an inadequate criterion to delineate potentially mineralized areas (the positive identification of a carbon dioxide component to the prevailing fluid would nevertheless be a very important observation in the development of any genetic model subsequently used in exploration). Fluid inclusion mapping could not be used to infer anything about the grade of the potential mineralization, and will never preclude a thorough geochemical evaluation. A concise discussion of the potential uses of fluid inclusions in minerals exploration can be found in Roedder 1984a.

This study suggests that fluid inclusions can also be used to crudely distinguish between the spatially distinct areas of gold, tungsten and silver mineralizations in the Rand Mining District. To a large extent this is a function of the quartz grain size accompanying the specific mineralization considered.

Silver mineralization at the Kelly Mine is associated with a very fine grained quartz which does not favor the formation of large primary inclusions, and is consequently characterized by a very low abundance of fluid inclusions (Table 4.1). However, a low abundance of observed inclusions does not imply reduced hydrothermal activity accompanied mineralization. The composition of the fluid inclusions could not be evaluated due to their small size. Multiple episodes of brittle fracturing does not appear to characterize the silver mineralization events and thus the abundance of planar groups of secondary inclusions is also low.

Scheelite mineralization occurs in approximately east-west trending quartz - calcite veins within the Atolia quartz monzonite (figure 2.3). The veins have relatively narrow alteration selvages which range up to a maximum thickness of several meters. The vein quartz contains a low abundance of type 3 - type 4 primary two phase aqueous inclusions. The proximal igneous wall rock is characterized by a low abundance of type 3-6 inclusions occupying planar fractures. A possible carbon dioxide component was noted in all rocks. Fluid inclusions suggest the mineralization was a discrete single event, which contrasts with the style of mineralization at Yellow Aster.

Conclusions

The results suggest that fluid inclusion mapping is a useful ancillary tool in the identification of potentially gold mineralized areas proximal to the Yellow Aster mine. Fluid inclusions observed in petrographic thin sections could be used to distinguish between gold, silver and tungsten mineralized regions (based on the relative paucity of inclusions in the latter two mineralization types) within the Rand Mining District.

The temporal evolution of the fluid accompanying the fracturing episodes in the Yellow Aster glory hole suggest that gold mineralization might be associated with the loss of carbon dioxide from the fluid regime.

This study strongly suggests that fluid inclusions should be routinely described as part of any petrographic investigation which constitutes part of a precious metal exploration program. The potential to characterize the ore fluid and even the ore depositional mechanism might be realized at an early stage and might lead to confirmation or re evaluation of any genetic model used in exploration.

Chapter 5

FLUID INCLUSION MICROTHERMOMETRY

Introduction

This chapter summarizes over 1000 microthermometric analyses for samples collected at the Yellow Aster Mine and surrounding area. The instrumentation and theory underlying the techniques utilized to quantify fluid inclusion compositions is also reviewed.

Fluid inclusion microthermometry

Fluid inclusion microthermometry describes the non-destructive method of investigation used to quantify fluid inclusion compositions. By carefully controlling the heating and cooling of fluid-filled inclusions in mineral slices the investigator is able to observe a variety of phase transitions which are characteristic of the components contained in the inclusion. The various phase transitions utilized in these studies are summarized in Table 5.1. Roedder (1984b), Hollister (1981), Holloway (1981), Burruss (1981), Crawford (1981) and Shepherd, Rankin and Alderton (1985) cover much of the theory and development of the techniques.

Table 5.1. Summary of phase transitions, and their significance, used in heating and freezing studies.

Phase Transition	Abbrev. Symbol	Significance
1) Total homogenisation of aqueous liquid and vapor phase. Vapor phase can be H_2O or CO_2+H_2O.	THaq or $THCO_2$-H_2O	Defines a minimum trapping temperature (and pressure).
2) Partial homogenisation of the CO_2 liquid and gas phase within a three phase (+ aqueous liquid) inclusion.	$THCO_2L$ or $THCO_2G$	L and G postscripts indicates homogenisation by disappearance of either gas or liquid phase. Temperature defines density of CO_2 phase.
3) Last melting point clathrate hydrate.	TM Clath	Clathrate formation confirms presence of CO_2. Salinity of the coexisting aqueous phase estimated by depression of the pure clathrate freezing point.
4) Last metling point of ice cyrstals.	TM ice	Defines salinity using the depression of freezing point from that of pure ice at 0°C.
5) Melting point of solid CO_2.	TM CO_2	Deviation from the pure melting point at -56.6°C indicates presence of another component.

Table 5.1 (Continued)

Phase Transition	Abbrev. Symbol	Significance
6) Decrepitation	TD	Temperature at which inclusions were observed to explode. Indicates a high internal pressure.

Instrumentation

Microthermometric analyses were carried out using a LINKHAM TH600 combined heating and freezing stage (Roedder, 1984b: Shepherd, 1981) in conjunction with a Leitz Ortholux polarizing light microscope capable of 400x magnification. The temperature range of the Linkham TH600 is -180 °C to +600 °C. Roedder (1984b) states the uncertainty to be ±2 °C between -95 °C and +200 °C. However, with careful calibration, the author believes an uncertainty of ±0.5 °C is possible between -48 °C and +50 °C.

At this juncture it is expedient to note that the presence of some minor components (e.g methane) is often inferred in many studies by observing small (<0.5 °C) variations in the temperature of specific phase transitions for documented experimental systems such as carbon dioxide - water (Roedder, 1984b). The author feels that positive identification of minor phases, in light of attainable temperature precision, requires another independent method.

The instrumentation used at both Imperial College, London and the University of Alaska at Fairbanks, is essentially identical. Careful temperature calibration using pure organic standards and reference samples, to

evaluate the magnitude of any corrections, allow results to be directly compared.

Sample preparation

Heating and freezing studies require 0.5 to 1.0mm thick wafers of the rock or mineral to be studied. Good optical resolution is facilitated by polishing both sides of the mineral or rock slice. Several methods of obtaining 'polished wafers' were utilized throughout the study but do not warrant detailed description. Roedder (1984b, P154-156) covers the important steps in the preparatory procedure. However, it should be noted that slow rates of sawing, lapping and polishing are essential to avoid straining or overheating the sample. Ordinary petrographic thin sections should not be used for microthermometric study because of the oxidation/alteration of the mounting media during heating cycles.

The selection of samples suitable for polished wafer preparation was made subsequent to the thin section petrographic investigation. This method was found to be the most time/cost efficient because only samples observed to contain 'useable' fluid inclusions in thin section were selected to be cut into wafers. The author

highly recommends this sequence of investigation with the qualitative descriptive element preceeding, and allowing a fuller interpretation of, the microthermometric study.

Fluid inclusion classification

The classification scheme adopted in the study was that outlined in Chapter 4. Positive identification of the phases tentatively identified at the descriptive stage was provided by microthermometry. Important compositional measurements pertinent to the classification are discussed below.

Type 1 inclusions (figure 4.1)

Positive identification of a carbon dioxide component was obtained on cooling the type 1 inclusions to approximately -100 °C. Around this temperature, small crystals of solid carbon dioxide were observed to form. Controlled heating of the inclusion resulted in the melting of the pure carbon dioxide crystals at temperatures around -56 °C. The triple point of the pure carbon dioxide system is -56.6 °C (Burruss, 1981). Thus, type 1 inclusions appear to contain one component only.

Carbon dioxide crystals were occasionally observed to finish melting at temperatures as low as -58.1 °C. This might suggest the presence of a minor methane component (Burruss, 1981).

Type 2 inclusions

Identification of a carbon dioxide rich phase was confirmed by the formation of clathrate hydrate (CO2 5.75 H2O) on cooling through -40 °C. Though often difficult to observe, the formation of clathrate provides a sensitive test for the occurrence of carbon dioxide in an inclusion (Hollister and Burruss, 1976). Furthermore, the formation of clathrate has a considerable effect on the salinity of the residual solution (Collins, 1979).

Collins (1979) describes a method wherein the observed clathrate hydrate melting temperature can be used to estimate the equivalent weight percent sodium chloride (salinity) of the aqueous liquid phase, provided no other gas phase is present (Hollister and Burruss, 1976).

In the binary system carbon dioxide - water, the TM clathrate (Table 5.1) would occur at the invariant point x (figure 5.1), at +10 °C. With an increased concentration of solute (expressed as sodium chloride

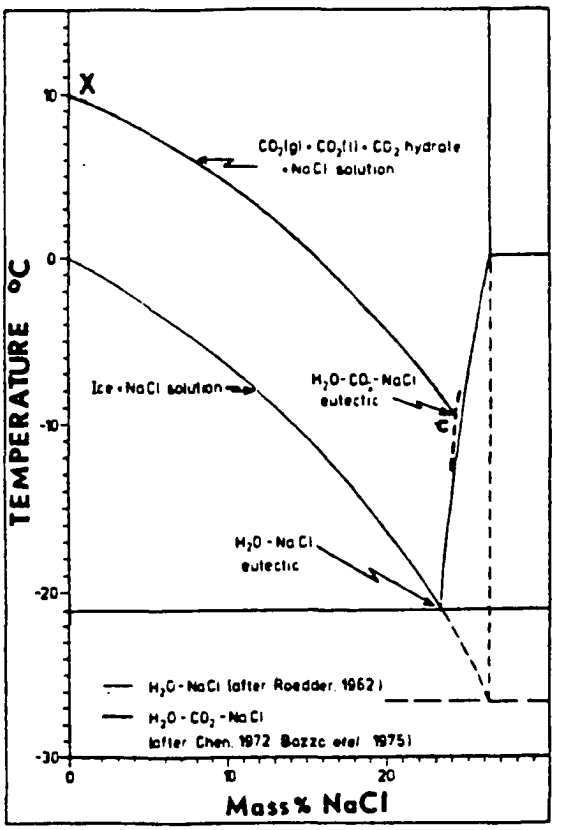

Figure 5.1 Depression of clathrate hydrate freezing point by NaCl (from Collins,1979)

equivalent) the invariant point is depressed along the line XC. Using this technique a range of salinities from 0 to ⩽3 equivalent weight percent sodium chloride was obtained during this study for type 2 inclusions. Figure 5.1 illustrates that the carbon dioxide-water system is relatively pure when TM clathrate is approximately 10°C. It should be noted that the term 'equivalent weight percent sodium chloride', is used to express the total concentration of dissolved solute species (decrepitate induction coupled plasma analysis revealed sodium to be the major cation in most inclusion fluids (see Chapter 3) and thus the dominant solute is inferred to be sodium chloride). Henley and Hedenquist (1985) illustrate that for some aqueous inclusions this assumption might not be valid, this subject is addressed further in the discussion of type 3 inclusions.

Type 2 inclusions also permit estimation of the density of the carbon dioxide component, and the overall 'bulk' inclusion density. Carbon dioxide density can be estimated using the observed homogenisation of the liquid and vapor phases to a single fluid phase at temperatures ⩽31.1°C as ilustrated in figure 5.2.

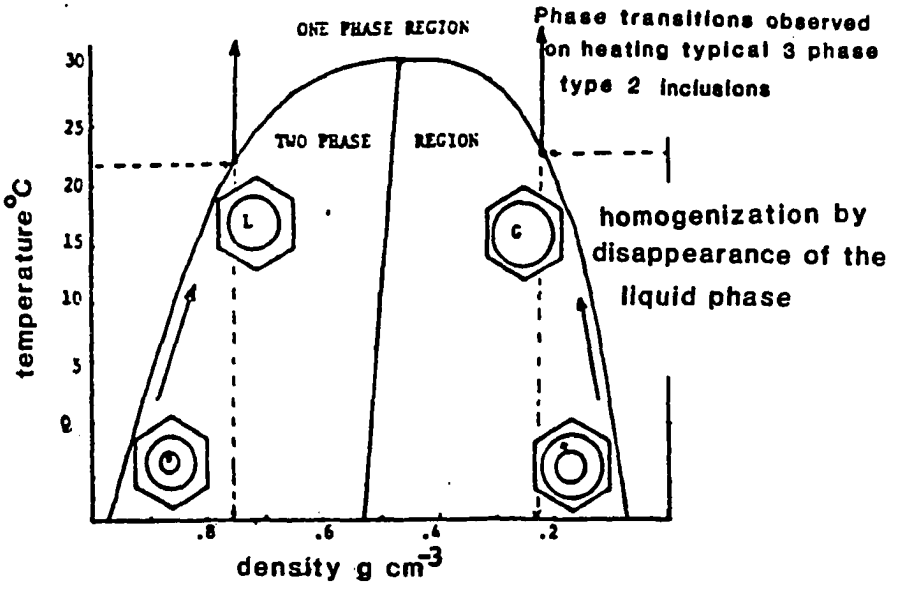

Figure 5.2 Temperature-density plot for pure CO2 (after Higgins,1980)

Carbon dioxide density allied with an estimation of the volumetric proportion (degree of fill) of the carbon dioxide relative to aqueous liquid phase can be used to calculate the molar proportion of the components (Bodnar, 1983; Rankin, 1978). The time consuming and repetitive nature of this calculation led to the development of the set of curves (with fellow student Roger Burleigh) illustrated in figure 5.3. This figure allows a rapid estimation of the molar proportion of carbon dioxide providing the TH CO2 has been recorded and volumetric ratio of phases estimated at 40 °C. An explanation of theory underlying the calculations, and the computer program developed to draw the curves is contained in Appendix V.

The accuracy of the mole proportion value obtained using figure 5.3 (or by calculation) is very dependent on the accuracy of the initial volume estimate of the phases, a point stressed by Roedder (1984b). Other possible errors are much less significant in comparison. This figure allows the rapid investigation of the spatial distribution and temporal evolution of carbon dioxide contents of the fluid inclusions.

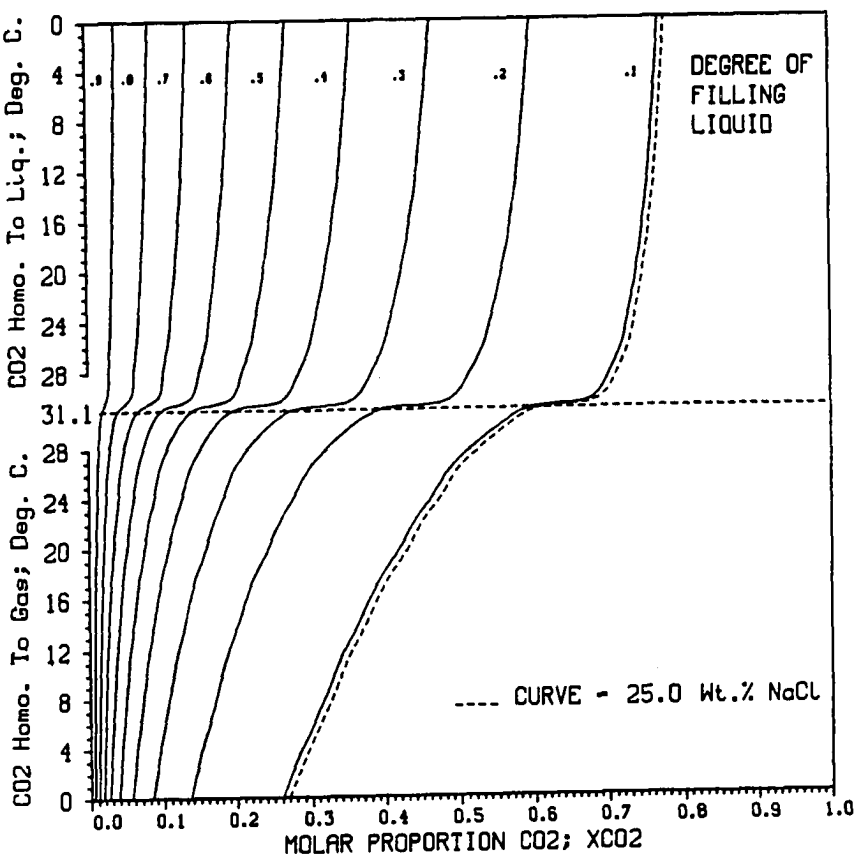

FIGURE 5.3 GRAPH FOR THE ESTIMATION OF XCO2
BASED ON HOMOGENISATION TEMPERATURE
OF CO2 IN CO2-H2O INCLUSIONS

The total homogenization temperature of type 2 inclusions was often difficult to obtain. Decrepitation was observed to take place at <300°C coinciding with the temperature of the onset of decrepitation observed using the windowed decrepitate induction coupled plasma technique (Chapter 3).

Estimation of the trapping pressure within type 2 inclusions was achieved using the technique outlined by Roedder and Bodnar (1980). Using this technique a range of minimum internal pressures from 400 to >1000 bars was obtained. This estimate assumes the inclusions are composed of pure carbon dioxide and water. The effect of a sodium chloride component is to lower the pressure required for homogenization at a given temperature (Takenouchi and Kennedy, 1964).

Type 3 inclusions

Apparent salinity of two phase aqueous inclusions expressed as equivalent weight percent sodium chloride was estimated using the depression of freezing point technique (Roedder, 1984b). Hedenquist and Henley (1985) have pointed out that estimates of salinity (total dissolved salts) are frequently in error when based on fluid inclusion ice melting measurements in the absence of an independent determination of the dissolved carbon dioxide content of the inclusion fluid. The authors emphasize that in the absence of carbon dioxide analyses, inclusion fluids containing 0.2 weight percent sodium chloride and up to 4.4 weight percent carbon dioxide may be interpreted to have apparent salinities of 0.85 equivalent weight percent sodium chloride. This could result in relatively large errors in the reconstruction of the P-T regime, pH, metals solubility and depth of formation estimates. These observations are felt to be very pertinent to the study of type 3 and 4 inclusions which generally have a low apparent salinity and lack an independent estimate of dissolved carbon dioxide content. It seems very likely that some fraction of the freezing point depression measured for type 3 or 4 inclusions (figure 5.4) is due to the presence of dissolved gas species. However, quantification of the dissolved gas

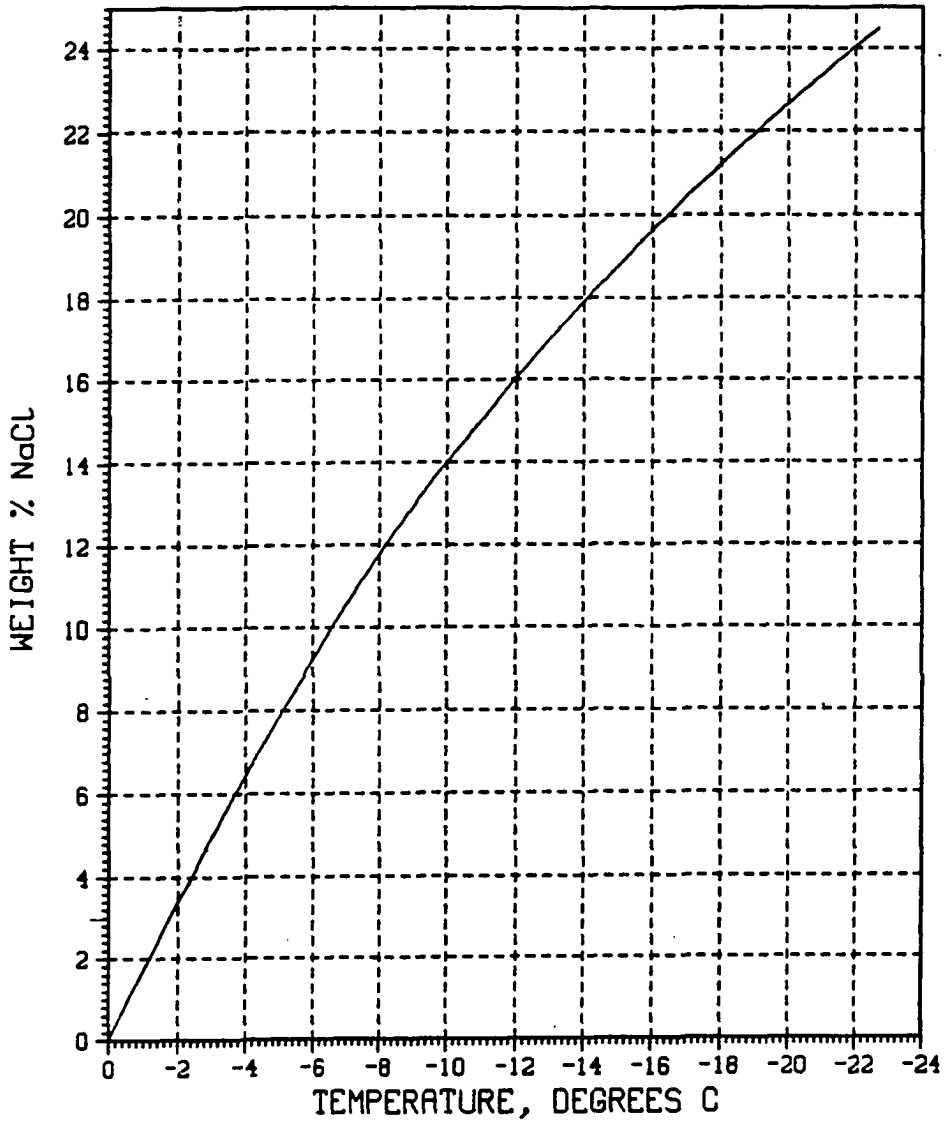

FIGURE 5.4 GRAPH FOR THE DETERMINATION OF WEIGHT PERCENT NaCl FROM FREEZING POINT DEPRESSION OF H2O IN PURE H2O-NaCl SYSTEMS FROM POTTER, et. al. ,1978

species was not undertaken in this study.

A minimum temperature of trapping corresponds to the observed TH for type 3 inclusions. A minimum trapping pressure is obtained from the measured TH using a temperature - density diagram, figure 5.5 or figure 5.6, for the pure water system. The contours in figure 5.6 represent lines of constant volume (and density for inclusions) in P-T space. Minimum trapping pressures upwards of 200 bars are obtained by this method (assuming a pure water system) for fluid inclusion from Yellow Aster.

Sample selection

The samples selected for microthermometric analysis were chosen based on the observations made from petrographic thin sections. Figure 2.3 previously illustrated the location of the samples used. Microt for microthermometric analysis were chosen based on the observations made from petrographic thin sections. Figure 2.3 previously illustrated the location of the sample used. Microthermometric data on inclusions in quartz from the various igneous intrusive phases and veins was collected.

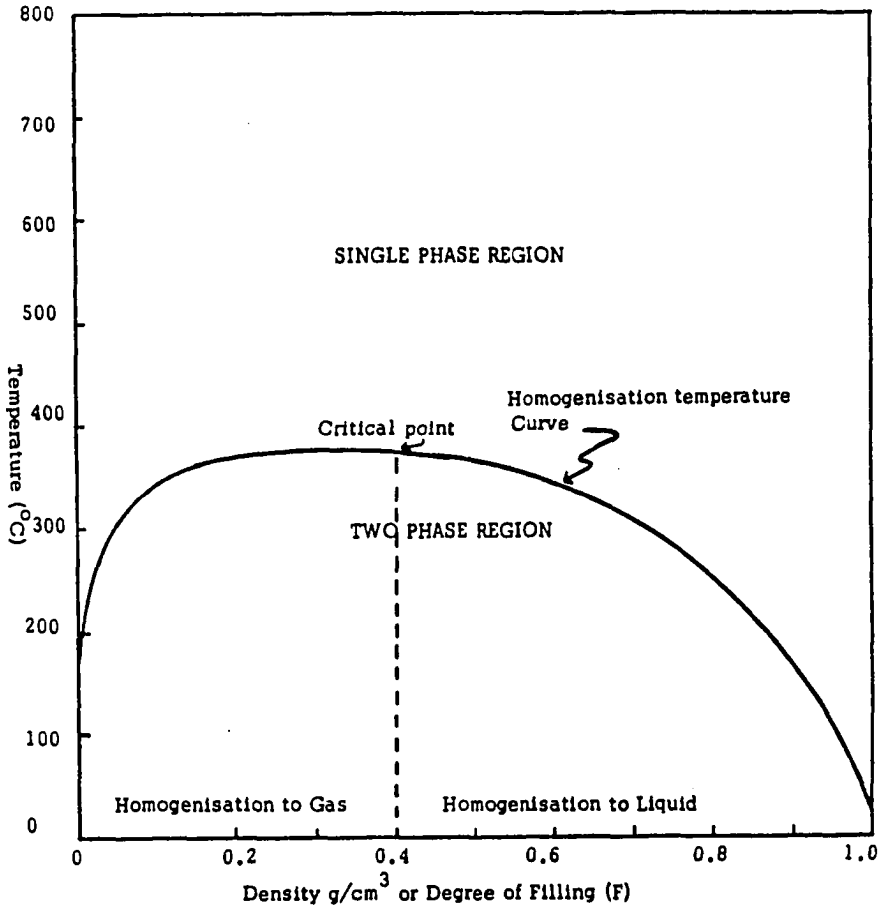

Figure 5.5 Temperature-density plot for pure water (from Fisher,1976)

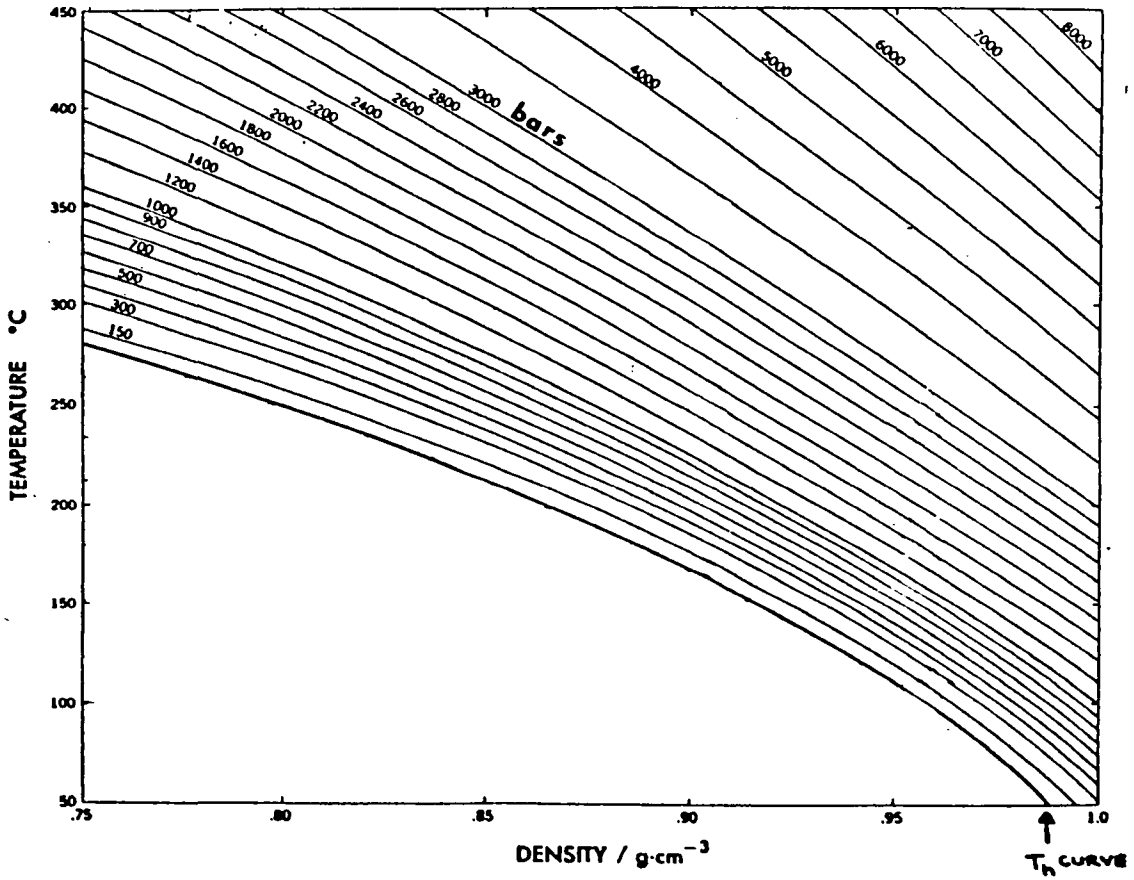

Figure 5.6 Temperature-density-pressure diagram for pure water (from Rankin, 1978)

MICROTHERMOMETRIC DATA

Data for samples that clearly illustrate important features are contained in this section. Additional data felt to be duplicative are contained within Appendix VI.

Quartz veins-segregations at the Yellow Aster Glory Hole (Samples YA27, 142, 10, 104, 123, 110 and 17)

Quartz veins within the glory hole, or the accessible parts of the Yellow Aster mine workings contained a variable proportion of carbon dioxide-bearing inclusions. Petrographic examination (Chapter 4) of quartz veins - segregations revealed most to have been subjected to at least one period of brittle deformation. Carbon dioxide-bearing, primary, type 2 inclusions, were most commonly preserved in weakly deformed quartz.

Figure 5.7, the TH frequency histogram for YA27, illustrates typical total TH values obtained for type 2 and type 3 inclusions for quartz veins. Type 3 inclusions appear to form two discrete populations and are felt to represent temporally distinct periods of fracture and fluid introduction. Overprinting secondary type 3 inclusions represent a fluid with a much lower carbon dioxide content (5.45 weight percent maximum - Roedder 1984b) than those type 2 inclusions interpretted

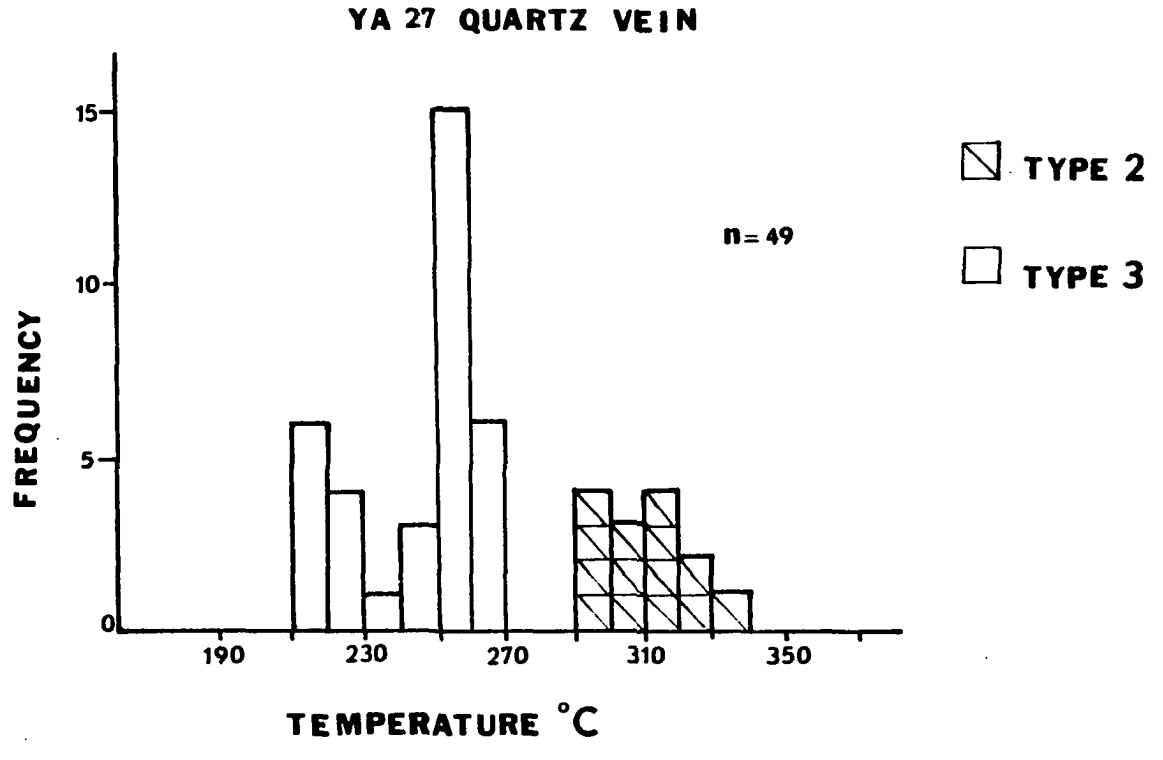

Figure 5.7 Histogram of TH data for YA27

to be primary.

Figures 5.8 and 5.9 illustrate the TH frequency histograms for spatially separate samples taken from a large quartz lens within the glory hole. Sample YA141 (figure 5.8) exhibited a moderately deformed texture in thin section. Sample YA142 (figure 5.9) exhibited areas of local recrystallization and grain boundary migration. The TH frequency histograms support a secondary origin for the type 3 inclusions. Isolated type 2, primary inclusions in sample YA141 (figure 5.8) are relatively rare and homogenize, by shrinking of the carbon dioxide rich phase, to a single fluid phase over the range 300 to 330 °C. A similar range of TH was observed for type 2 inclusions in figure 5.7 (YA27). The author feels the broad range of TH is probably a result of minor modification of some inclusions concomitant with the brittle formation and introduction of secondary type 3 inclusions. Figure 5.8 possibly exhibits two populations of secondary type 3 inclusions.

The effects of partial recrystallization on the inclusion population within the quartz lens is well illustrated by figure 5.9 where type 2 inclusion measurements are absent. Type 2 inclusions exist only as highly irregular large, coalesced, inclusions that

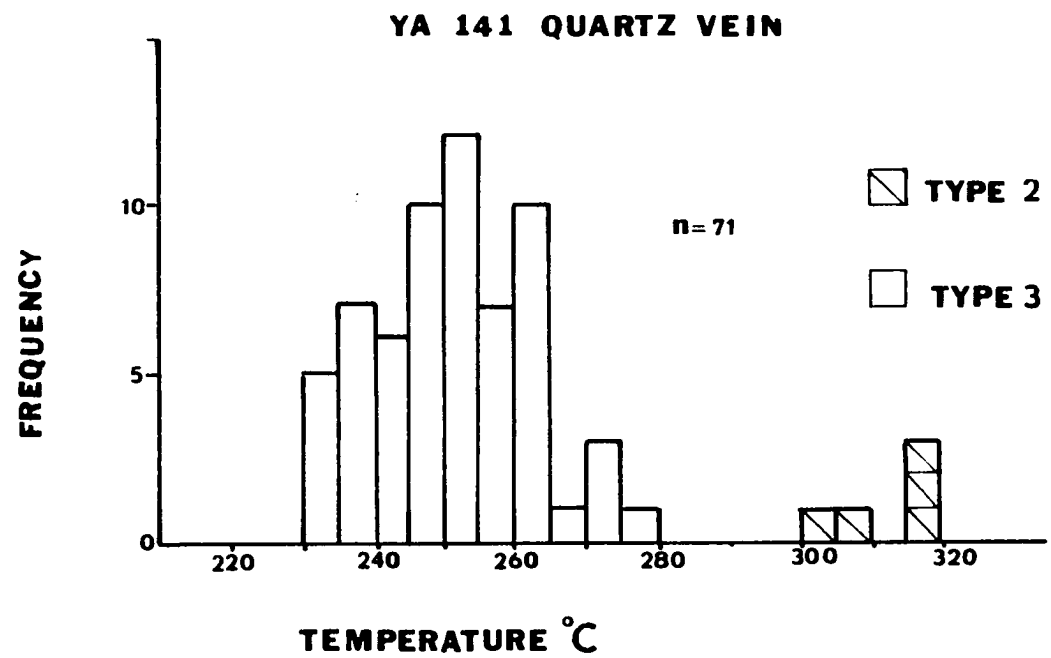

Figure 5.8 Histogram of TH data for YA141

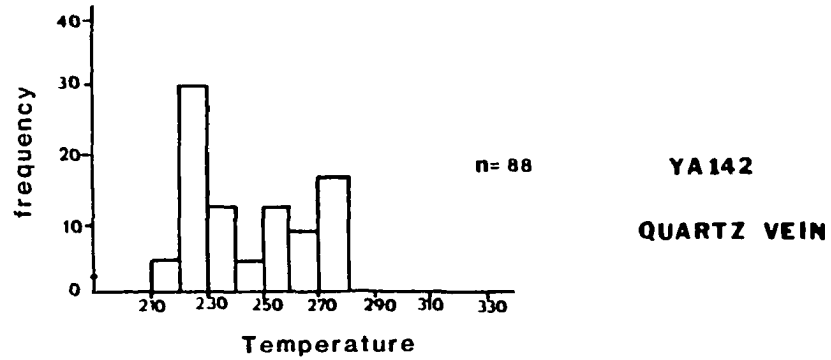

Figure 5.9 Histogram of TH data for YA142

decrepitate prior to homogenization. Figure 5.9 (YA142) contains two discrete type 3 populations and the lower temperature population may correspond to that detected in sample YA27 (figure 5.7).

The TH data for samples YA27, 141 and 142 strongly suggest two periods of fracturing and secondary type 3 inclusion formation. Frequency histograms indicate the type 3 inclusions have temperature means centered on 240 and 260 °C. The lower temperature type 3 inclusions post date the higher temperature inclusions. Similar trends were observed for samples YA110 and YA17 (Appendix VI).

Sample YA104(figure 5.10), a strongly deformed gold bearing quartz veinlet approximately five centimeters wide, taken from the Rand level of the Yellow Aster mine contained abundant small (≤2μm,) secondary planar inclusion groups. Minor flecks of gold were observed to occupy planar fractures and thus post date initial quartz vein formation. Figure 5.10 illustrates the TH values obtained for two phase aqueous, type 3, inclusions observed in recrystallized quartz proximal to a gold bearing planar fracture. The author feels that these inclusions probably are the best available samples of the fluid accompanying gold deposition. The single population has a mean TH of approximately 240 °C.

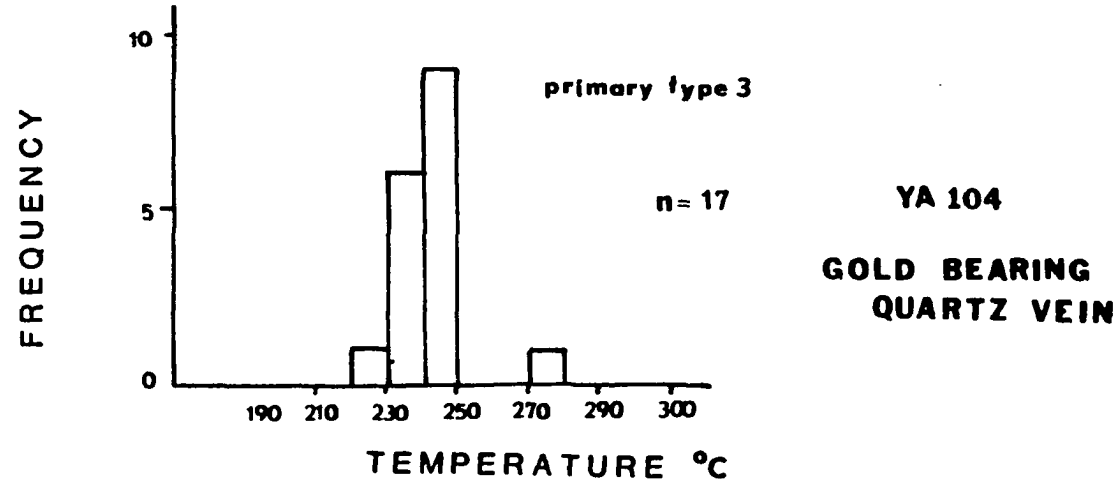

Figure 5.10 Histogram of TH data for YA104

Depression of freezing point estimates of apparent salinity for the same inclusions suggest a total dissolved solute concentration equivalent to the range 2 to 3 weight percent sodium chloride (figure 5.11). The aqueous fluid possibly contains a dissolved carbon dioxide component in the range 2-3 weight percent. This amount of dissolved carbon dioxide could account for a - 0.86 °C to - 1.3 °C depression of the freezing point, calculated using the expression:

$$-TM = Kf.M$$

:where Kf is the constant of proportionality for freezing point depression (Kf=1.86) and were M is the molality of the solute (Higgins, 1985; Hedenquist and Henley, 1985). This possibility could be examined by performing crushing stage analyses to evaluate the partial pressure of carbon dioxide, but was not carried out in this study.

Summary of Yellow Aster quartz vein data

Figure 5.11 illustrates the narrow range of apparent salinities measured for inclusions in quartz veins. Apparent salinity data points are plotted against their corresponding total TH values. Sample YA142 exhibits three distinct populations and a wide range of apparent salinity from 0.1 to 6.9 equivalent weight percent sodium

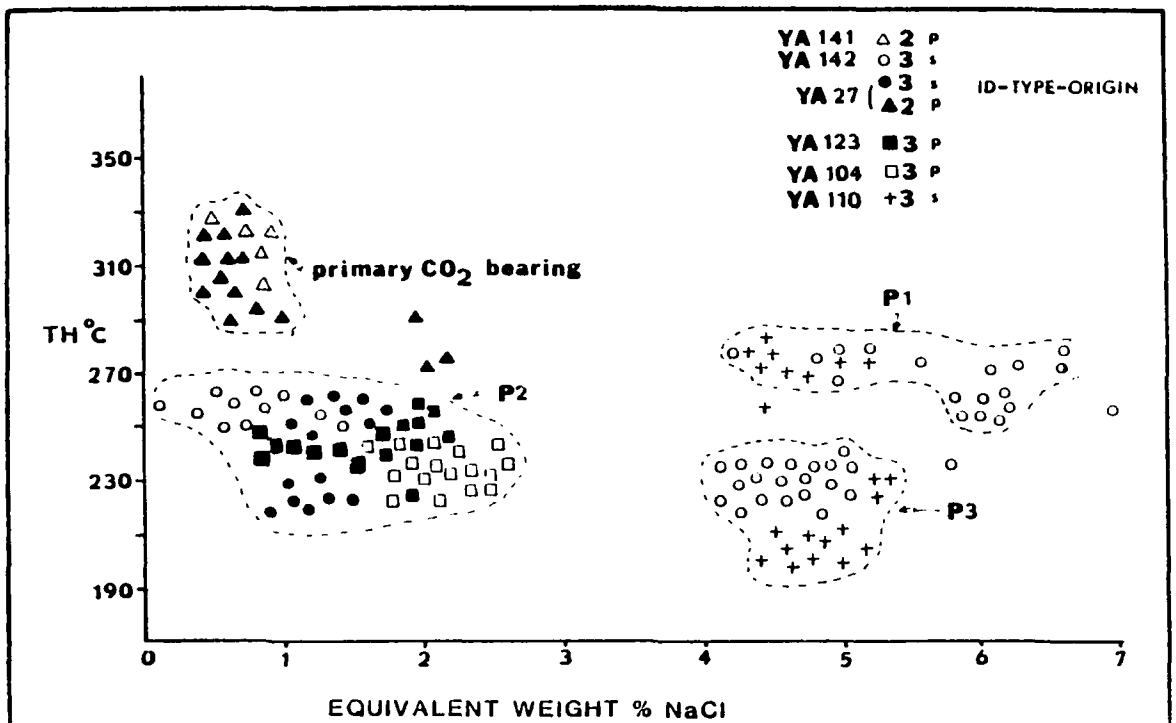

Figure 5.11 TH versus salinity for quartz veins from the Yellow Aster mine area

chloride. The irregularity of the points labelled P1 suggest eroneous measurement of inclusions probably subject to post entrapment modification. In contrast P3 exhibit a relatively tight cluster and are probably the latest of the secondary inclusions, and have been subject to little or no post entrapment modification. The constancy of phase proportions observed for most type 3 inclusions in YA142 suggest the fracturing was accompanied by a homogeneous fluid phase.

Sample YA27 contains inclusions with a much lower apparent salinity than YA142 or YA110 (the dominant solute species possibly being carbon dioxide) containing less than 2 equivalent weight percent sodium chloride. The range of salinities observed for secondary type 3 aqueous inclusions in YA27, and one secondary population from YA142 (P2) broadly overlap the inclusions of YA104 thought to possibly represent a gold mineralizing fluid. Thus, the mechanism involved in the deposition of gold from solution could have involved fluid cooling and loss of the carbon dioxide component from the homogeneous fluid phase.

Figure 5.11 also contains data for euhedral inclusions observed in unstrained quartz-calcite veinlets post-dating deformation. These discrete narrow (<2cm)

veinlets (YA123) post-date a pervasive hypogene hematization observed at some localities. Some specimens contained small flecks of gold visible on broken surfaces. A spatial correlation between gold and quartz veining at the location of sample YA123 was not discerned either in outcrop, hand specimen or thin section. A fine grained pervasive silicification was observed to both predate and occasionally be contemporaneous with the quartz-calcite veining.

Euhedral quartz from these late stage veins contained a relatively low abundance of large, primary type 3 (to type 4) inclusions, with a mean TH of 243 °C and apparent salinity range of 0.8 to 2.2 equivalent weight percent sodium chloride. The TH frequency histogram for YA123 is contained within Appendix VI. The primary inclusions observed in YA123 have a similar TH and composition as those inclusions believed to be samples of the gold mineralizing fluid in YA 104 (figure 5.11). Data for YA123 also plot in the same region of figure 5.11 as some of the secondary inclusions observed in planar arrays in samples YA27 and YA142 (barren quartz veins). Thus, the presence of type 3 inclusions plotting in this region of the TH-X diagram cannot be utilized to predict the specific distribution of significant gold mineralization. However the absence of type 3

inclusions, with either primary or fracture related origins could possibly be used to preclude areas of low gold mineralization potential.

Quartz veins and lenses outside the Yellow Aster Glory Hole (Samples YA131, 51 and 136)

Samples YA131, YA51, and YA136 were taken from quartz veins or pods within the Rand Schist or various phases of the igneous intrusions, outside the areas of known gold mineralization.

Sample YA131

Figure 5.12, the TH frequency histogram for sample YA131, a quartz vein parallel to Rand schistosity, illustrates the abundance of 3 phase carbon dioxide-bearing type 2 inclusions. Figure 5.13 highlights a typical inclusion assemblage observed in YA131.

Two populations of type 2 inclusions are suggested by figure 5.12, with means centered at 318 °C ±1.8 and 306 °C ±7 °C. On this basis the lower temperature population is felt to be of secondary origin (or possibly pseudosecondary?), a distinction also made during petrographic observation.

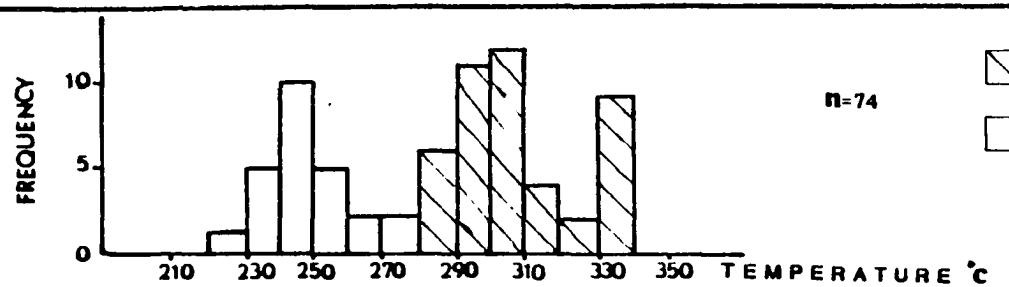

Figure 5.12 Histogram of TH data for YA131

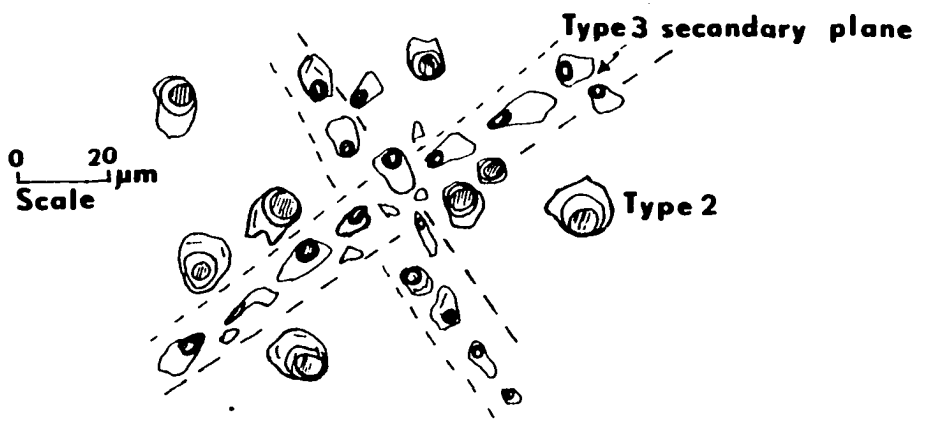

Figure 5.13 Typical inclusion assemblage observed for YA131

Figures 5.14 and 5.15 further support separating type 2 inclusions into distinct populations. Primary type 2 inclusions contain a higher mole fraction of carbon dioxide (.19 to .26) than those observed in planar arrays (0.08 to 0.2). Constancy of phase proportions in both primary and pseudosecondary/secondary type 2 inclusions, suggests trapping of an originally homogeneous fluid phase at both stages. Primary type 2 inclusions typically have a DF 0.5 with TH CO2 to the liquid phase at temperatures of 16 to 20°C. Secondary or pseudosecondary type 2 inclusions exhibit a wider range of DF (0.5 to 0.9) and higher TH CO2 to the liquid phase typically above (>20°C).

Figure 5.12 also illustrates the presence of lower temperature (mean 242°C) population of secondary type 3 two phase aqueous inclusions. These inclusions were typically $\leqslant$10μm and formed planar arrays defining intercrystalline fractures. Type 3 inclusions were much rarer than their relative volume of data would suggest. This results from the common decrepitation of type 2 inclusions on attempting to establish total TH. This also illustrates that the inclusion 'type estimate' for sample YA131 outlined in the previous chapter (Table 4.1) significantly deviates from that observed during microthermometric study. This undoubtedly is due to the

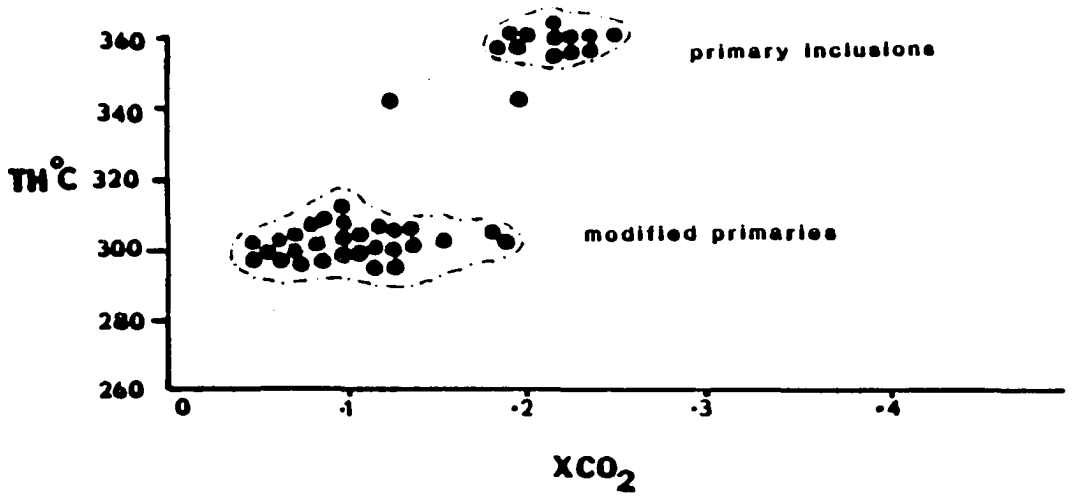

Figure 5.14 TH versus molar proportion CO2 for YA131

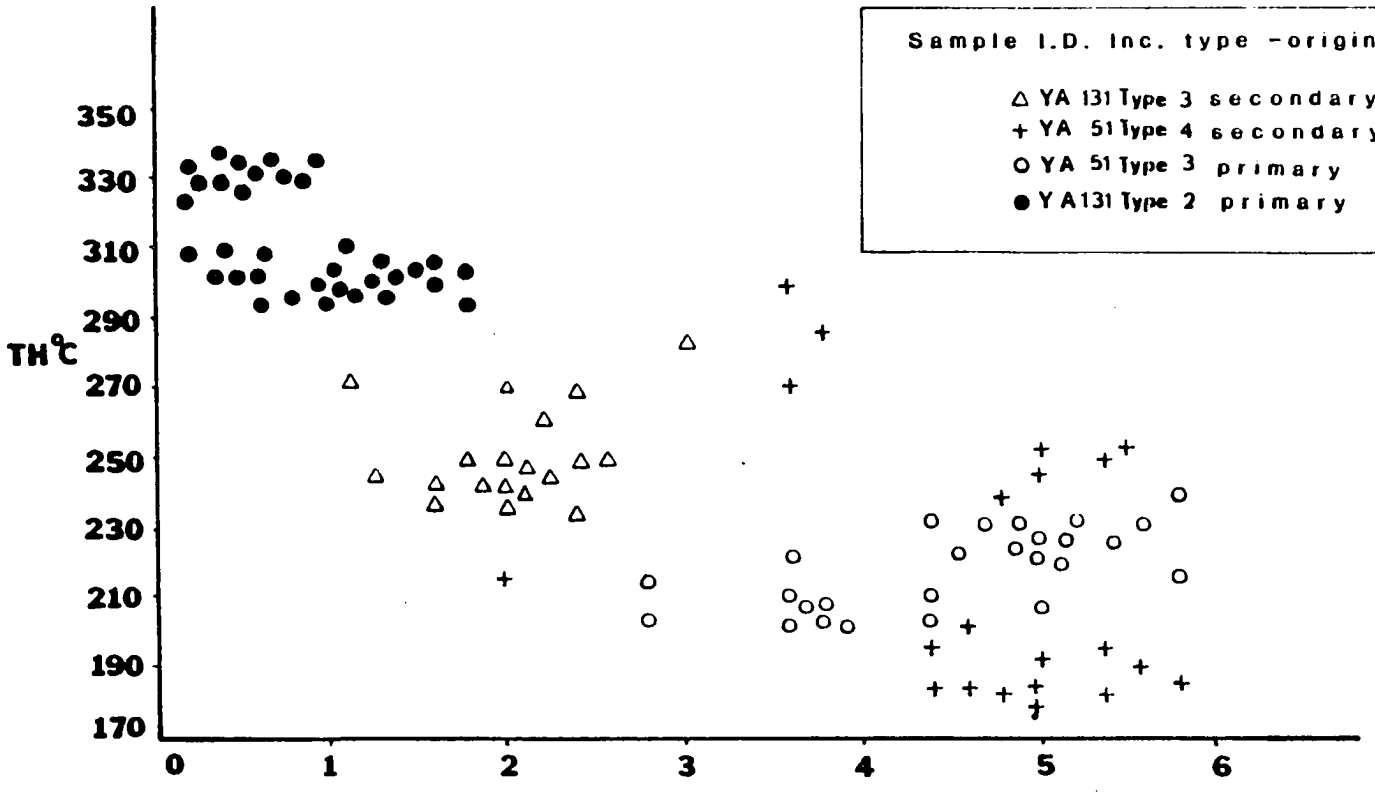

Figure 5.15 TH versus salinity for quartz veins from unmineralized areas

fact that most three phase carbon dioxide-bearing inclusions homogenized to a two phase assemblage i.e, single carbon dioxide phase plus aqueous phase at temperatures below 25 °C. The high proportion of vapor filled type 5 inclusions observed in thin section (Table 4.1) probably resulted from decrepitation of type 1 and 2 inclusions, induced at temperatures attained during thin section preparation.

Figure 5.15, the total TH against apparent salinity plot for YA131 and YA51 illustrates several important features. Salinity of type 3 inclusions was established using the depression of freezing point technique(Roedder 1984b), and that of type 2 inclusions using the depression of clathrate hydrate melting temperature (Collins, 1979). Type 2 inclusions from YA131 plot in two well defined clusters. The primary type inclusions have a narrow salinity range 0.2 to 0.9 equivalent weight percent sodium chloride with a mean value of 0.55. The lower temperature type 2 inclusions of probable pseudosecondary origin are also very low salinity but exhibit a slightly broader range, 0.2 to 1.8 equivalent weight percent sodium chloride with a mean value of 1.0. Secondary type 3, two phase aqueous inclusions have a slightly higher dissolved solute content than earlier type 2 inclusions, with a mean apparent salinity of 2.0

equivalent weight percent sodium chloride. Type 3 inclusions also exhibited a relatively constant volumetric proportion of phases suggesting the inclusions were trapped as an originally homogenous fluid. The apparent salinity of type 3 inclusions probably reflects the combined effect of dissolved carbon dioxide gas and sodium chloride on the freezing/last melting point of ice. The presence of a sodium chloride component was confirmed during DICP analyses (Chapter 3). However, the 2.1,mv sodium response was the lowest obtained for any of the quartz veins analyses during that study, supporting the low salinity microthermometric data.

The microthermometric data for YA131 indicate that the evolution of fluids in the Rand Schist at the margins of the Government Peak stock (figure 2.3)was similar to that described for quartz veins within the Yellow Aster glory hole. A noteable difference is the lower abundance of fracture related type 3 secondary inclusions streaming through the quartz. Thus, gold mineralization is demonstrably related to the intense fracturing events that took place at Yellow Aster.

Sample YA51

Sample YA51, a narrow (<1.0cm) milky quartz-vein cutting the EW granodiorite west of the Atolia - Randsburg road (figure 2.3) contains abundant two phase aqueous inclusions. Figure 5.16 illustrates the TH frequency distribution for two phase aqueous inclusions. Although they are generally not measured, type 4 inclusions (commonly necked) were studied to elucidate the source of the high sodium response, 41.8mv, obtained for sample YA51 during the DICP study (Table 3.5). The primary type 3 inclusions observed exhibited a broad range of TH from 210°C to 243°C, with a mean of 221°C and could possibly represent two overlapping populations, not distinguished at the chosen temperature interval.

Figure 5.15 illustrates the TH-apparent salinity data for sample YA51. The data for the irregular morphology, commonly necked type 4 inclusions, exhibit a range of apparent salinity, from 3.6 to 5.8 equivalent weight percent sodium chloride. Type 3 inclusions can be crudely separated into two groups (figure 5.15). Type 3 inclusions have an 'overall' average salinity of 4.4 equivalent weight percent sodium chloride. The microthermometric data for YA51 explain the high sodium response obtained during DICP analysis. The data also

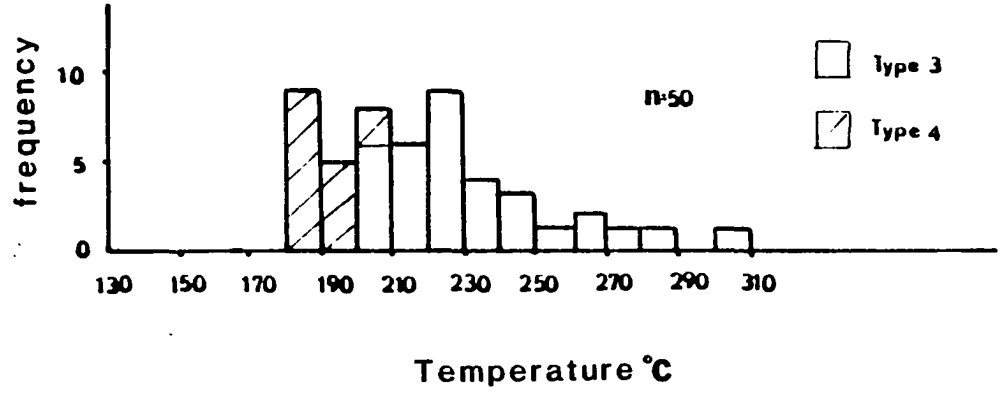

Figure 5.16 Histogram of TH data for YA51

suggest the P-T-X conditions at YA51 (figure 2.3) were significantly different to those prevailing at YA31 or within the Yellow Aster glory hole. The age of the veining at YA51 relative to the temporal evolution of fluids discerned from microthermometric studies of other quartz veins is unclear.

Sample YA136

Sample YA136 was taken from a 1 meter by 0.3 meter wide igneous quartz segregation, within a dioritic phase of the EW granodiorite (figure 2.3). Thin section observation revealed abundant needles of rutile and other unidentified, colored, micron sized mineral phases. Undulatory extinction of quartz suggested a weak, post solidification deformation event. The TH data for the exclusively secondary type 3 and type 4 inclusions are illustrated in figure 5.17. The low temperature population detected has a mean TH of 154°C, significantly lower than any previously described. The inclusions also have a very low and narrow apparent salinity range, from 0.2 to 0.8 equivalent weight percent sodium chloride. Thus data for YA136 plot outside the TH salinity field of figure 5.15. The significance of this population is unclear.

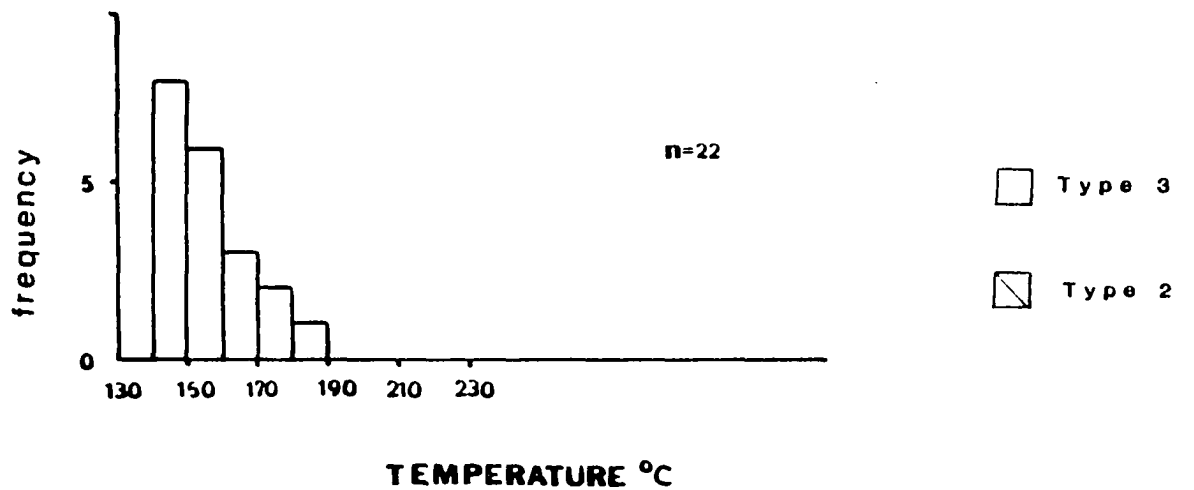

Figure 5.17 Histogram of TH data for YA136

Igneous Quartz sampled within the Yellow Aster Glory Hole

Many of the intrusive rocks within the Yellow Aster glory hole contained relatively coarse quartz suitable for microthermometric preparation (Chapter 2).Early production records (Hess, 1910: Hulin, 1925) indicate much gold was produced from 'crushed zones' within the intrusive phases or Rand Schist at the Yellow Aster mine, rather than from discrete quartz gold veins. Thus it was felt that the inclusion populations observed in undeformed quartz, and their comparison with deformed-shear zone igneous quartz would be informative. Furthermore, microthermometric data for all inclusions, regardless of origins, was necessary to fully interpret the previously reported DICP results (Table 4.1).

Sample YA9

The TH frequency histogram for sample YA9 (figure 2.3) is illustrated in figure 5.18. Sample YA9 was taken from a trench in the floor at the eastern wall of the entrance to the glory hole (figure 3.9). At this locality a 15 meter wide body of medium grained granodiorite exhibits a lensoid outcrop within the Rand Schist. Shearing was locally intense, and the intrusive exhibits a well developed red coloration due to the

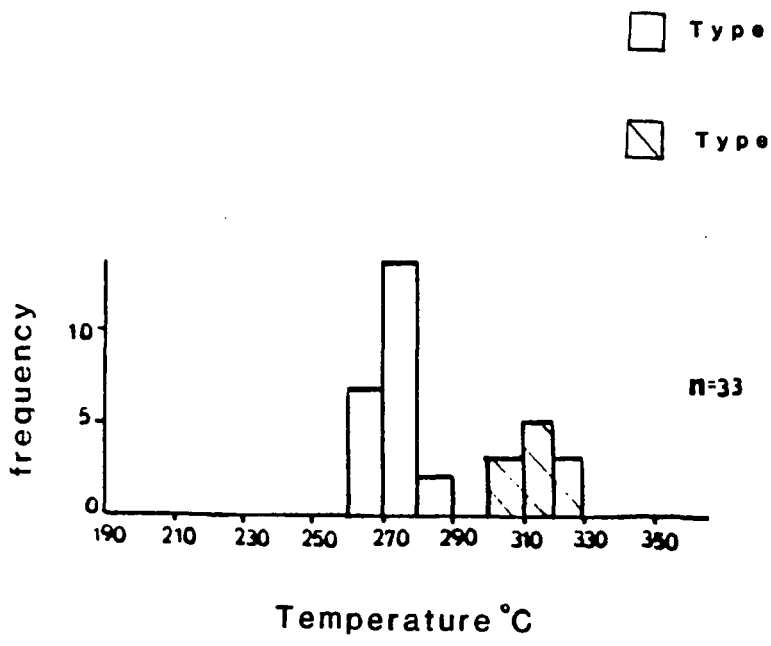

Figure 5.18 Histogram of TH data for YA9

breakdown of narrow, (0.5cm) pyrite veinlets.

Igneous quartz from YA9 contains a significant population of three phase carbon dioxide bearing type 2 inclusions (figure 5.18). The small size of most inclusions (≤5μm) prevented more comprehensive data acquisition. Type 2 inclusions were commonly arranged in linear groups and are probably pseudosecondary. The small number of type 2 inclusions measured have a mean TH value of 314 °C. Type 2 inclusions are post-dated by sharp well defined planar arrays of type 3, two phase aqueous inclusions. Type 3 inclusions exhibit a narrow range of TH with a mean at 272 °C. The limited salinity data are illustrated in figure 5.19 (a composite TH against salinity plot for several samples). Clathrate hydrate melting temperatures indicate a low salinity, <1.0 equivalent weight percent sodium chloride, aqueous fluid is contained in type 2 inclusions. Type 3 inclusions have a slightly higher salinity range from 0.6 to 3.8 equivalent weight percent sodium chloride.

YA9 type 2 inclusions also exhibit a small range of mole proportion carbon dioxide, type 2 inclusions partially homogenizing (THCO2) by disappearance of the gas or liquid phase (figure 5.2). Type 5 vapor rich inclusions were also observed in sample YA9to form solid

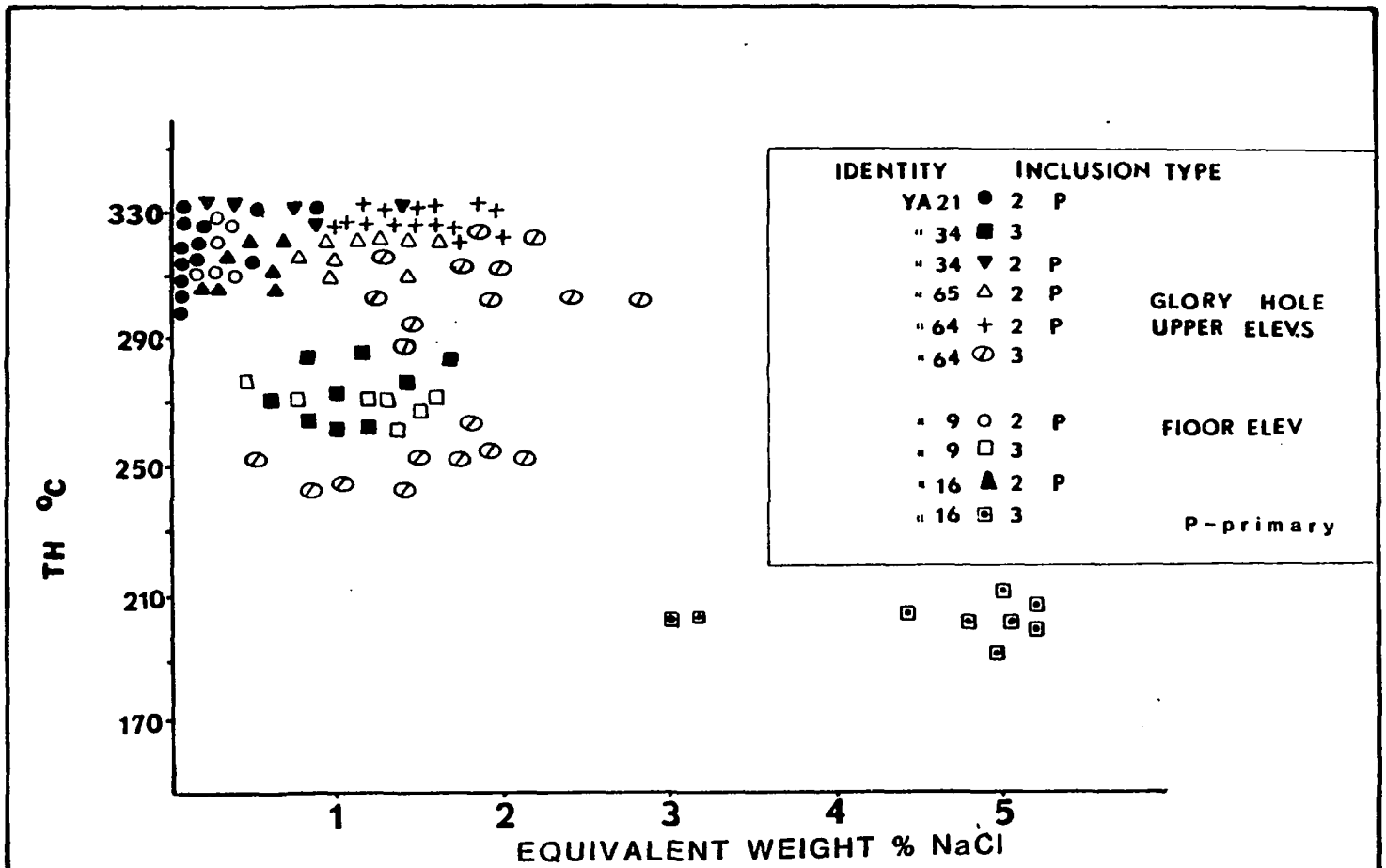

Figure 5.19 TH versus salinity for igneous quartz from the Yellow Aster mine area

carbon dioxide on cooling through -100 °C. However, further microthermometric quantification was negated by their small size (<5μm). Thus, YA9 contains a variable proportion of carbon dioxide within inclusions (figure 5.20). If these inclusions were trapped simultaneously, as observation suggests, the fluid may have been boiling or effervescing. The lack of TH data for type 5 inclusions place restrictions on this interpretation. A possible alternative explanation is post entrapment necking of an originally homogenous carbon dioxide - water bearing fluid after separation of two immiscible phases on cooling.

Sample YA16

Sample YA16 was taken from a relatively unaltered outcrop of EW granodiorite within the Yellow Aster glory hole. In hand specimen a gneissic texture is caused by the recrystallization and minor remobilization of dark green biotite.

Figure 5.21 contains the TH frequency data for YA16 igneous quartz. YA16 contains a small population of primary type 2 inclusions, with a mean TH 329.5 °C, and an average 0.14 mole proportion carbon dioxide (figure 5.21). THCO2 was to the liquid phase at ⩾27 °C. YA16

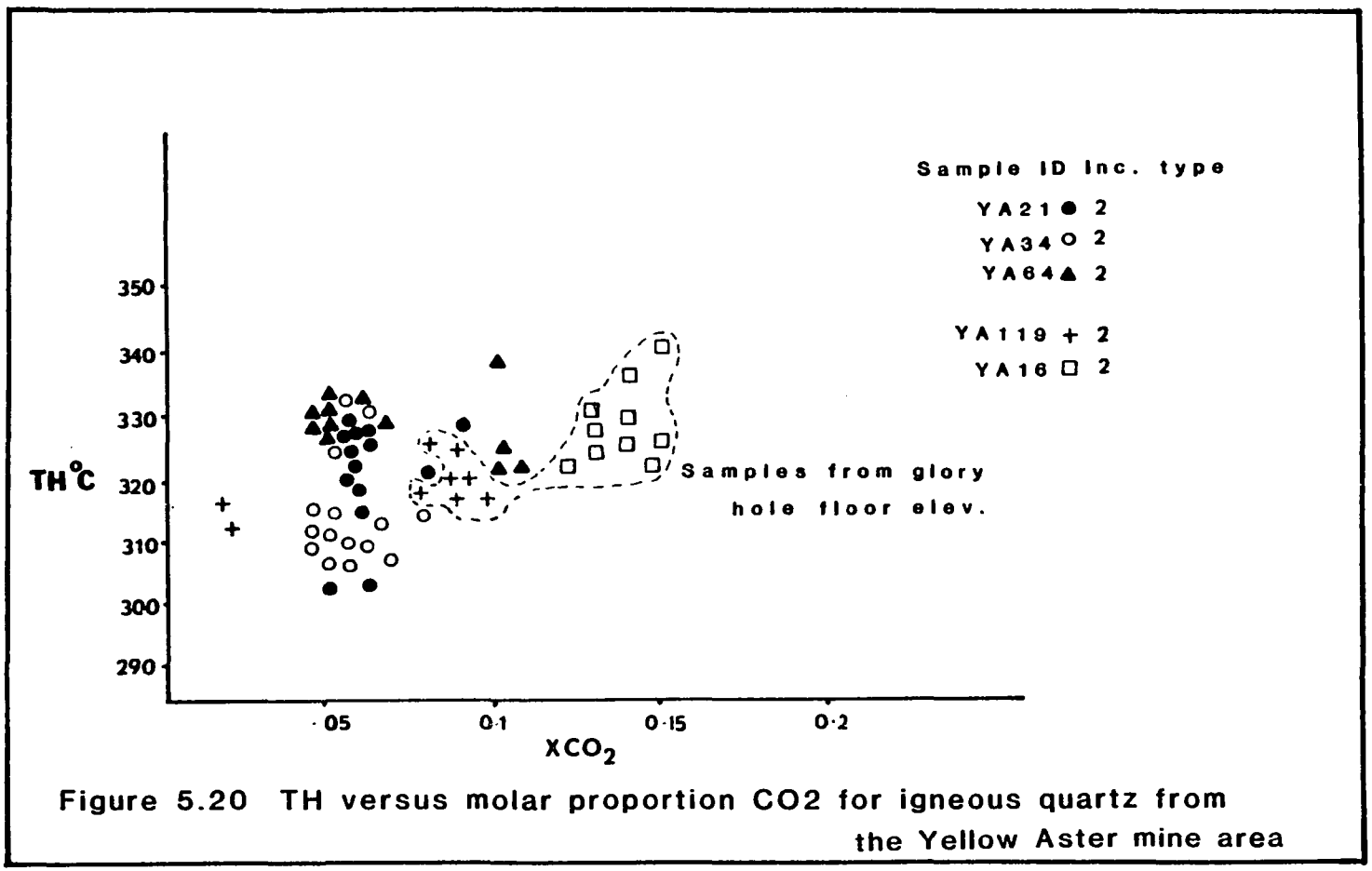

Figure 5.20 TH versus molar proportion CO2 for igneous quartz from the Yellow Aster mine area

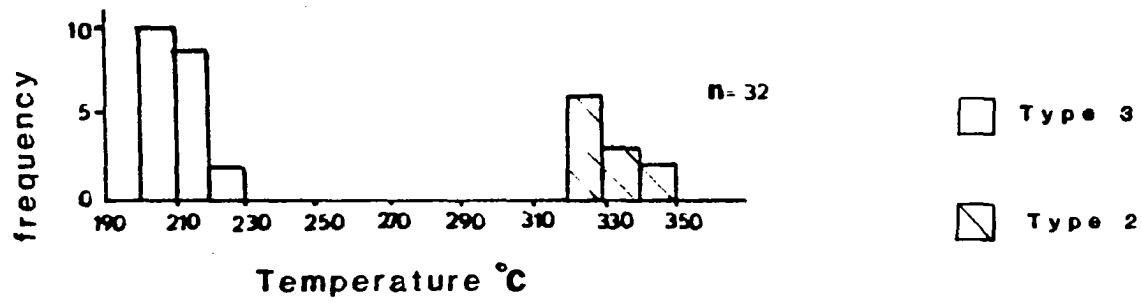

Figure 5.21 Histogram of TH data for YA16

also contains a later, lower temperature (mean TH=208°C population of secondary, type 3 inclusions. Salinity data for type 2 and 3 inclusions are shown in figure 5.19. Clathrate hydrate melting temperatures for type 2 inclusions indicate the aqueous phase contains ≤1.1 equivalent weight percent sodium chloride. Figure 5.19 highlights the higher proportion of solute in the type 3 aqueous phase. Data for samples YA5 and YA19 are contained in Appendix VI.

Data summary for YA9 and YA16

Microthermometric study of igneous quartz from the Yellow Aster glory hole indicate fluid compositions, temperatures and a temporal fluid evolution very similar to that obtained for inclusions in quartz veins/segregations. The effects of igneous quartz remobilization were commonly observed during fieldwork (and petrography) and probably explain the primary origin of type 2 inclusions observed in sample YA16, when compared to the pseudosecondary origin of type 2 inclusions in YA9 (figure 5.18). Thus, if quartz is unstable, secondary inclusions might be trapped at corrosion fronts, whereas primary inclusions could be trapped during new crystal growth a few cm/meters away.

Igneous quartz samples from the upper elevations of the Yellow Aster mine

YA21, 34, 64 and 65 are samples of various intrusive phases outcropping at surface or within small adits on the western rim of the Yellow Aster glory hole (figure 2.3). YA21 (Table 4.1) is a highly altered, hematite stained, intrusive exhibiting characteristics associated with the Microgranodiorite. Coarse patches and micoveinlets of quartz (1mm) suggest silica addition. Field observation revealed a stockwork-like system of narrow quartz veinlets containing relict pyrite cutting the intrusive. Quartz from a microveinlet was observed to contain a population of primary type 2 carbon dioxide bearing inclusions (figures 5.20 and 5.22). Total homogenization by disappearance of the carbon dioxide-rich fluid phase was observed around a mean temperature of 317 °C. Partial homogenization of carbon dioxide to the gas phase was noted for all type 2 inclusions over the temperature range 24.0 to 29.2 °C.

Using figure 5.3 the average mole proportion of carbon dioxide is estimated at 0.08 ±.02 (variation results from the anticipated errors in the initial phase volume estimates. Thus, it appears the type 2 inclusions within sample YA21 contain a decreased component of

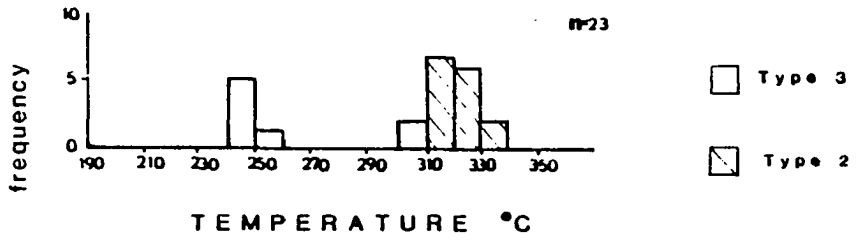

Figure 5.22 Histogram of TH data for YA21

carbon dioxide compared to type 2 inclusions previously described (figure 5.14). Type 2 salinities estimated using the Collins (1979) technique indicate a total dissolved solute concentration of ≤1 equivalent weight percent sodium chloride (figure 5.19).

YA21 also contains a population of small (<5μm) type 3 secondary inclusions. TH data for this population are presented in figure 5.22. The small size of most type 3 inclusions precluded determination of salinity.

Minimum trapping pressure estimates for type 2 inclusions were gained using the data of Takenouchi and Kennedy (1964) assuming zero weight percent sodium chloride. Using this data in conjunction with the mean TH (317°C) and mean mole percent carbon dioxide (8 mole%) gives a value of >250 bars.

Figure 5.20 illustrates that type 2 inclusions from igneous quartz samples taken at the floor elevation of the glory hole (3950 feet) occupy a separate area of T-X space compared to those type 2 inclusions from samples at the rim of the glory hole (4250-4300 feet). A minimum trapping pressure, for the averaged type 2 inclusions from the floor elevation of the glory hole (assuming pure H20-CO2 inclusions) indicate a minimum trapping value 370-400 bars. The effect of a sodium chloride component

is to raise the minimum pressure at a fixed temperature.

Comparison of data for igneous quartz from the Yellow Aster glory hole

Figure 5.19 illustrates the apparent salinities of type 2 (primary) and type 3 (secondary) inclusions for samples from both the floor and higher elevations of the glory hole. Type 2 inclusions for both localities plot in the same region of the diagram, suggesting no significant difference in salinity as estimated using the method of Collins (1979). At all locations considered there is little evidence for the simultaneous trapping of two immiscible phases (i.e carbon dioxide rich and water rich) and thus the prevailing fluid resulting in type 2 inclusions, lies above a solvus. The relative position of type 2 inclusions to the 300 bar solvus suggests type 2 inclusions from igneous quartz at the pit floor would plot in the two phase field (Higgins, 1985) of the 0% sodium chloride system. This suggests that inclusions trapped at the floor elevation experienced higher minimum pressures.

Pressure estimates based on the estimated total inclusion densities and TH of type 3 inclusions for YA34, YA64 give a minimum trapping pressure of approximately

300 bars. However, the accuracy of this estimate is questionable in light of the work by Hedenquist and Henley (1985), but is felt to be a reasonable accurate figure.

Further data i.e individual TH frequency histograms, for igneous quartz fluid inclusion populations are contained in Appendix VI (YA64, YA65 and YA34). Salinity and mole proportion carbon dioxide for these samples are contained in figures 5.19 and 5.20 respectively.

Igneous quartz samples from EW Granodiorite
(outside the Yellow Aster glory hole)

Samples of igneous rock taken from the east-west ridge between the Yellow Aster glory hole and the Randsburg-Atolia road (figure 2.3) contained quartz suitable for microthermometric study. Three phase carbon dioxide type 2 inclusions were observed during petrographic examination of the EW granodiorite quartz (Table 4.1, samples YA50, YA52, and YA54). Data for a quartz veinlet cutting the EW granodiorite has previously been reported (figures 5.15 and 5.16). Inclusions observed in samples YA54, 52 and 50 tended to be small, and the limited data presented are for the rarer $\geqslant$10μm, relatively equant inclusions.

Figure 5.23 illustrates the total TH frequency data for sample YA54 (Table 4.1) type 2 and type 3 inclusions. YA54 was also observed to contain abundant type 5, vapor rich inclusions. Cooling of equant,5μm size, type 5 inclusions resulted in the formation of a solid phase at -98 to -105°C. Carefully controlled heating (1°C/min) of these inclusions revealed the solid phases completed melting at approximately -57 ±1 °C indicating the presence of an almost pure carbon dioxide phase.

Sample YA54 also contains type 2 inclusions with a relatively narrow range of mole proportion carbon dioxide considering THCO2 by disappearance of liquid (Type 2A) or gas (Type 2B) was observed in various inclusions (figure 5.24). Figure 5.24 illustrates that YA54, type 2 inclusions occupy the 0.06 to 0.1xCO2 range of THX space. Careful observation suggests some carbon dioxide bearing inclusions are probably pseudo - secondary. A more definite secondary origin can be assigned to the lower temperature (mean 253°C) type 3 inclusions, observed to occupy distinct planar fractures, or be aligned at grain boundaries. Irregular type 4 and type 6 inclusions (figure 4.1) were also relatively common as secondary inclusions but were rarely measured.

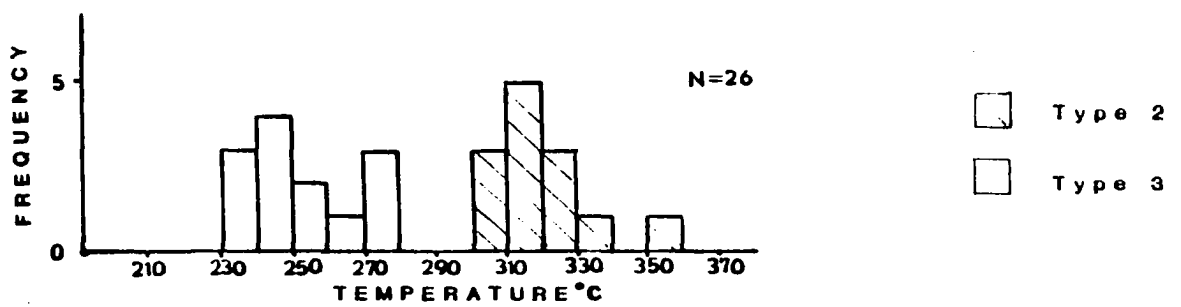

Figure 5.23 Histogram of TH data for YA54

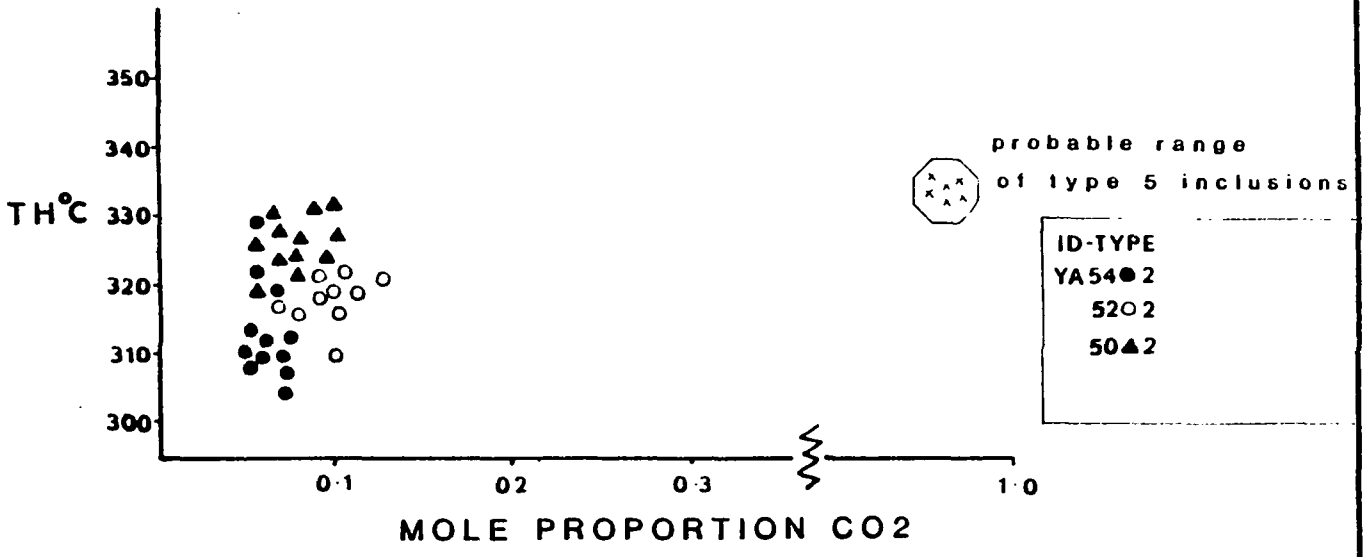

Figure 5.24 TH versus molar proportion CO2 for igneous quartz from the EW granodiorite

Observation suggests type 5 and type 2 inclusions are contemporaneous. Thus it appears that the prevailing fluid had separated into vapor-rich and liquid rich-phases (boiling?) at this location. However, conclusive proof of a boiling mechanism is prevented due to the absence of TH data for the carbon dioxide - vapor rich type 5 inclusions. Assuming that type 5 inclusions did homogenize at temperatures approaching 310 to 330 °C they could be used to define the position of the solvus at this location.

Secondary type 3 inclusions post dating the type 2 inclusions in YA54, YA52 and YA50 homogenize to the liquid phase over the range 210 - 270 °C. Individual TH histograms for YA52 and YA50 are contained in Appendix VI, and are very similar to figure 5.23 suggesting relatively constant fluid conditions over the area represented by these samples (figure 2.3). Figure 5.25 illustrates the TH versus apparent salinity data for YA54, YA52 and YA50. This plot suggests that the fluid inclusions contained in quartz at each location represent trapping of a widespread, compositionally consistent fluid phase. It also illustrates that the type 3 secondary inclusions at each location have an higher apparent salinity relative to the earlier type 2 inclusions.

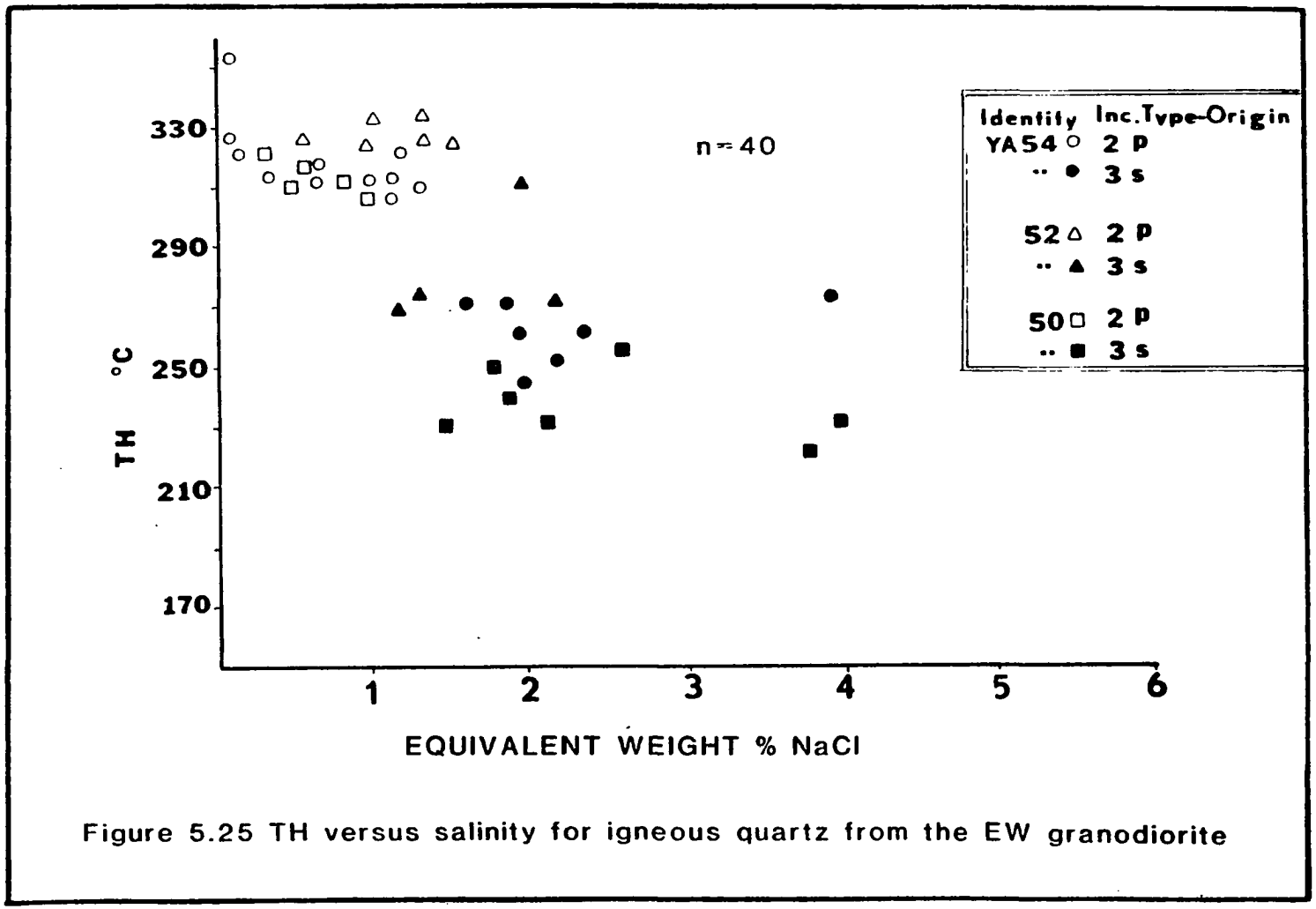

Figure 5.25 TH versus salinity for igneous quartz from the EW granodiorite

The type 2 and type 5 carbon dioxide inclusions observed within YA50, 52 and 54 probably represent a boiling assemblage. However, this assumption could not be verified due to the poor optical resolution possible with the dark type 5 inclusions, preventing any accurate or even approximate estimate of total TH. This constraint should be kept in mind during the discussion of the overall fluid regime at Yellow Aster.

Further discussion of thermometric data

Table 5.2 summarizes the data obtained for the various samples taken at Yellow Aster. Fluid inclusion studies indicate the chronological evolution of the fluid regime as summarized below:

1) silicification of the Rand Schist and quartz remobilization within the various intrusive lithologies is accompanied by a 300-330 °C, carbon dioxide-water ($xCO2=0.05$ to ≥ 0.2) low sodium chloride (<2 equivalent weight percent) fluid phase.

This fluid has a relatively wide distribution and is observed as primary type 2 inclusions in quartz veins (e.g.YA131, YA141 and YA21). Constancy of phase proportions (i.e.carbon dioxide to aqueous liquid) suggest trapping of a single homogenous fluid phase.

Table 5.2. Summary of microthermometric data.

Location	Quartz type	Inclusion type	TH °C	XCO_2	E. Wt % NaCL	pH
Yellow Aster glory hole	Quartz veins	Type 2	300-330	0.05→0.2	<1.5	4.5 (min)
		Type 3	210-230	<0.03	<1 to <6	
			250-270	<0.03	<1 to <6	
Yellow Aster glory hole	Quartz vein post dating deformation	Type 3	220-260	<0.03	0.8→2.2	≥4.9→5.5(?)
Various locations outside Yellow Aster glory hole	Quartz veins exhibiting variable deformation characteristics	Type 2	320-335	>.15	<1	≥4.5-5.5(?)
			295-310	0.05-0.2	<2	
		Type 3	235-270	<0.03	1.5-2.5	≥4.9-5.5
			210-250	<0.03	2.5-<6	
Yellow Aster glory hole floor	Igneous quartz/silicifications	Type 2	300-330	0.08 0.15	<1	
		Type 3	260-280	<0.03	<1.3	>5.5
			200-230	<0.03	3-5	
Yellow Aster glory hole upper elevation	Igneous quartz/silicifications	Type 2	300-330	0.05-0.09	0.0→2.0	
		Type 3	260-280	<0.03	0.05→2.0	
			250-270	<0.03	0.05→2.0	
EW Granodiorite near road	Igneous quartz	Type 2	300-330	0.02-0.1	<1.2	
		Type 3	230-270	<0.03	1 to 2.2	

However, at specific localities, e.g.YA54, observation indicates the simultaneous trapping of carbon dioxide vapor-rich and carbon dioxide/aqueous liquid-rich inclusion. This assemblage records the exsolution (boiling?) of a vapor-rich phase from a homogenous fluid.

2) Later pseudosecondary type 2 carbon dioxide-bearing inclusions have a slightly lower molar percent of carbon dioxide, suggesting the acid volatile is being depleted (lost to the vapor phase) as a function of time.

3) The intense fracturing (at all scales) observed within the Yellow Aster mine area was accompanied by a lower temperature (<270 °C) relatively carbon dioxide poor (≤.05 mole%) low apparent salinity, aqueous fluid phase.

4) Microthermometric data strongly suggest temporally restricted fracturing and fluid introduction events, with a general cooling trend.

5) Gold deposition was probably associated with the evolution of a low temperature (240 °C) low salinity (<3 equivalent weight percent sodium chloride) fluid. The passage of this fluid was recorded as primary type 3 inclusions observed within unfractured euhedral quartz forming late stage quartz and quartz-calcite veins quartz-calcite veins were observed to post date hypogene hematization preserved as occasional isolated clasts within the veins.

6) Primary inclusions in recrystallized quartz adjacent to a gold bearing microfracture, contain a fluid composition very similar to that outlined in 5.

Thus, an inspection of the data suggests gold deposition at the Yellow Aster mine could be a function of several variables, or combination of variables. These are:

i) the overall cooling of the hydrothermal solution from +330 C to $\leqslant 240\,^{\circ}C$.

ii) The loss of 5 to 20 mole percent carbon dioxide over the above stated temperature range. This is probably accompanied by the loss of H2S, an important gold complexing species (Seward, 1982: Seward 1973: Henley and others 1984: Krauskopf, 1954). The loss of these species will affect the pH of the solution and hence metal solubility (Henley and others, 1984: Hedenquist and Henley, 1985).

iii) The effect of oxygen fugacity on gold solubility. Petrographic observation suggests the widespread development of pyrite and arsenopyrite was followed by hypogene hematization. Furthermore, previous production records (Hess, 1910: Allen, 1923, and Hulin 1925) indicates gold grades were economic only in the oxidized zones of the Yellow Aster mine.

Gold transportation and deposition: a consideration of the plausible mechanisms

An important consideration during this discussion is the nature of the fluid regime, i.e.whether open or closed. Drummond (1981) modelled closed and open boiling hydrothermal systems as end members, in a very thorough study of the effect of such parameters as oxygen fugacity, temperature and pH on metals solubility. Drummond's data strongly suggests that all available geologic criteria be used to assess where a fluid regime lies relative to the open-closed end members. The intensity and large scale of the faulting and fracturing at Yellow Aster would facilitate the upward migration of a fluid phase (or evolved vapor phase). Hence, the Yellow Aster system is felt to closely approximate the open system of Drummond (1981). Minimum depth estimates based on fluid inclusion derived pressure data indicates depths 1km and support the above reasoning.

The partition of carbon dioxide to an escaping vapor phase might be an isothermal or isoenthalpic process (Drummond and Ohmoto, 1985). Fluid inclusion evidence suggests an isoenthalpic process is probably more realistic, as a definite difference in total TH is discerned for primary type 2 (300-330°C) relative to

later primary type 3 (240-250°C) inclusions.

The loss of carbon dioxide from the fluid phase will markedly affect pH. If we assume that the loss of carbon dioxide will effectively control the protolytic equilibrium in the hydrothermal solution, we can utilize the reaction:

$$H2CO3 \rightleftharpoons HCO3^{-}+H^{+} \qquad (A)$$

$$HCO3^{-} \rightleftharpoons CO3^{=}+H^{+} \qquad (B)$$

The second dissociation of aqueous carbon dioxide can be ignored for solutions within two pH units of neutral, at a specified temperature (Drummond and Ohmoto, 1985). To accurately evaluate the pH of the system we need to quantify many other variables such as the activities of at least 14 chemical species (H, CO2, H2S, H^{+}, Cl^{-}, Na^{+}, K^{+}, Ca^{+2}, Mg^{+2}, OH^{-}, $HCO3^{-}$, HS^{-}, $HSO4^{-}$ and SO4) involved in pertinent equilibrium reactions. However these data are not available, and a simplistic manipulation of equation A is used to approximately quantify the change in the pH with the loss of carbon dioxide. These calculations indicate that a change of at least 0.5pH units would be realized during the loss of $\leqslant$20 mole% carbon dioxide from the hydrothermal solution at Yellow Aster (Table 5.2). The pH of the early carbon dioxide rich, 300 to 330 °C hydrothermal fluid is

estimated to be 4.5 to 4.6, which makes the fluid slightly acid at these temperatures (neutral pH=5.8 at 300°C, Krauskopf, 1969).

The effect of this predicted pH change on gold solubility must be considered in tandem with the behavior of the most likely gold complexing species at these temperatures and pH conditions. Seward (1982) indicates that $Au(HS)^-_2$ is the most stable complex over the temperature range 0 to 300 °C and near neutral pH. Drummond (1981) and Drummond and Ohmoto (1985) indicate the H2S gas species also tends to partition strongly to the vapor phase, paralleling the behaviour of carbon dioxide. Drummond and Ohmoto (1985) point out that when a metal is stabilized by bisulfide complexes, solubility increases with increasing pH (within the pH range where H2S dominates over HS^-) according to a reaction approximated by:

$$Au^\circ + 15/8H2S + 1/8\ SO4 \rightleftharpoons Au(HS)^-_2 + 1/2\ H20 + 6/8\ H+$$

Thus, if the solution is boiling there are simultaneous and competing effects of diminishing proton and H2S concentrations on gold solubility. Consequently the ratio of log [H+]/ log [H2S] is important. Accurate quantification of this ratio is precluded due to the lack of complete fluid inclusion composition analyses.

Drummond and Ohmoto (1985) illustrate that this ratio tends to be highest in open systems at low (200°C) temperature, and when <2.5 (i.e.15/6) gold tends to precipitate from boiling solutions. At Yellow Aster the log [H+] >-0.5, but [H2S] remains unquantified. However with efficient removal of 20 mole percent carbon dioxide, it seems reasonable to assume a relatively efficient partitioning of H2S to the escaping vapor. Hence gold solubility is anticipated to decrease, because of the loss of H2S but the magnitude of the effect is counterbalanced by the approximately quantified increased in pH.

Another consideration is the temperature dependence of the reaction constants. Reaction (A) tends to increase with decreasing temperature (Henley and others, 1984: Helgeson, 1969: Higgins, 1985, and Read, 1975) and thus the effect of cooling is to increase the proton concentration (lower pH).

Figure 5.26 illustrates the relationships between pH and oxygen fugacity in the Fe-sulphide system at 250°C upon which Henley and others (1984) have superimposed solubility contours for gold as bisulfide complexes. Another tenable gold depositional mechanism at Yellow Aster is due to an increased oxygen fugacity following

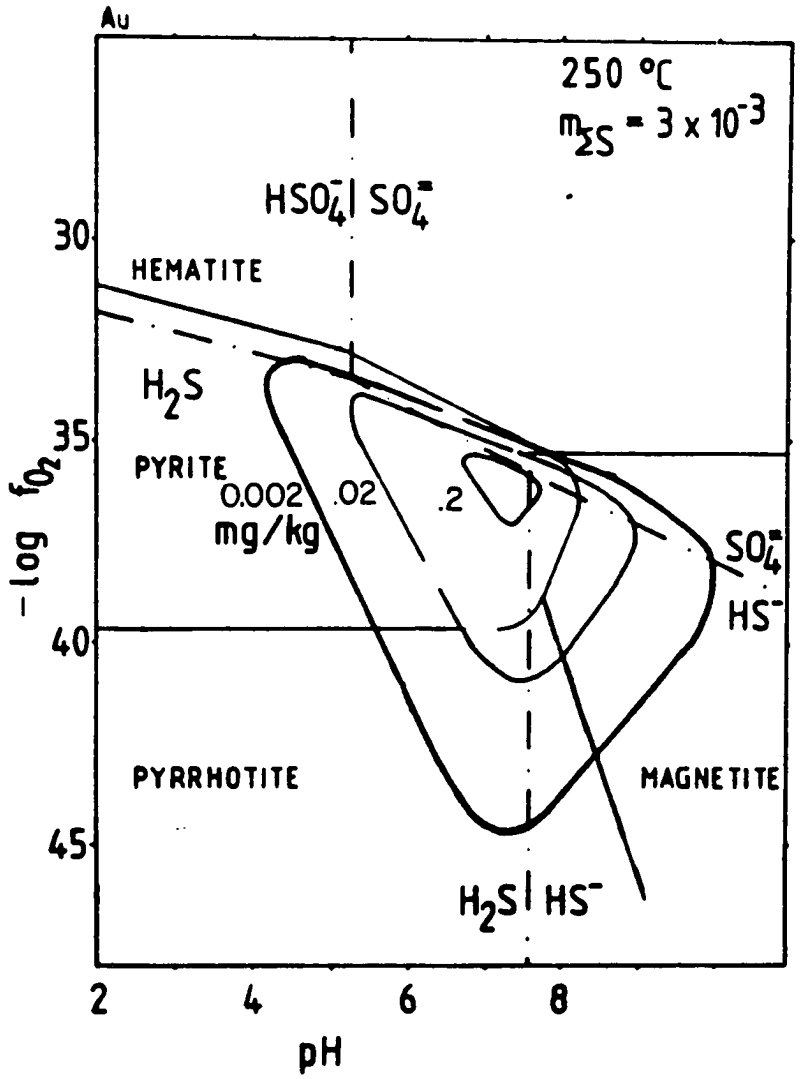

Figure 5.26 fO2-pH diagram at 250 C showing the stability fields of the principal sulphide species and solubility contours for gold in mg/kg as $Au(HS)_2^-$

(from Henley and others, 1984)

the development of the major fracture systems accompanying sulfide gold mineralization. The author feels that some fraction of the iron oxides at Yellow Aster are of hypogene hydrothermal origin (Chapter two, figure 2.10) post dating the longer interval of pyrite/arsneopyrite stability. This suggests that the upper portions of the fluid regime at Yellow Aster plot close to the pyrite-hematite stability boundary of figure 5.26 where gold solubility is significantly decreased. It is interesting to note Hulins (1925) observation that "practically all of the gold ores which have been mined in the Randsburg quadrangle have been oxidized ores. In only a few mines have primary sulphides been encountered and in practically every case they have been too low grade to work". Furthermore Hess (1910) and Hulin (1925) both report that at the Yellow Aster mine 'oxidized' ores were mined to a depth of 300 feet below the current floor of the glory hole. At this depth primary pyrite and arsenopyrite were encountered and the gold grades became uneconomic. A supergene enrichment origin for the oxidized ores is discounted based on the complete absence of manganiferous minerals. Thus the empirical observation made by Hulin (1925) based on the 25 year continuous production of the Yellow Aster mine are essentially in agreement with the conclusions based on

laboratory investigation.

In summary it appears that an increasing oxygen fugacity as the hydrothermal fluid approaches the surface is a very plausible mechanism to explain gold deposition at the Yellow Aster mine. However, this mechanism does not preclude gold mineralization accompanying primary sulphides, which has been observed at several mines e.g.Sunshine Mine (Hulin, 1925) but indicates higher grades should be located in zones containing hydrothermal iron oxides (rather than sulphide weathering products). This distinction constitutes a significant problem in the field.

The loss of the acid volatiles, carbon dioxide and hydrogen bisulfide, over the temperature range 330°C to 250°C probably resulted in a weak pyrite + arsenopyrite + gold mineralization at the Yellow Aster mine. An isoenthalpic boiling mechanism is felt to explain cooling and loss of volatile species observed during microthermometric study. This mineralization style (pyrite - arsenopyrite + gold) occured over a vertical extent of greater than 500m. This style of mineralization predates the gold deposition related to increasing oxygen fugacity (which probably extended to a depth of 200 - 300 m from the palaeosurface).

Conclusions

Microthermometric investigation at Yellow Aster has tentatively identified plausible gold depositional mechanisms and partially quantified the relevant PTFX conditions. These data have important implications for any genetic model used in a district wide exploration program or site specific exploratory program.

Chapter 6

GENERAL CONCLUSIONS

Introduction

This chapter briefly reviews the successes and failures of the fluid inclusion techniques applied at Yellow Aster. A more detailed account of the application of DICP, fluid inclusion mapping, and fluid inclusion microthermometry can be found in chapters three, four and five respectively.

DICP

The application of DICP analysis to quartz (igneous or vein) from the Yellow Aster mine area as a guide to gold mineralization was found to be relatively unsuccessful. The main reasons for this were:

a) fluid inclusion compositions at the Yellow Aster mine were found to be low salinity with an important volumetric component of carbon dioxide. The analytical technique utilized (DICP linked to an emission spectrophotometer) did not have the capacity to detect elemental carbon or oxygen.

b) The concentration level of most elements in fluid inclusions approaches, or is below the detection limit of

the analytical technique (10 to 100 ppb range).

c) The DICP technique produces results which are the aggregate response of the various generations of fluid inclusions contained in the analyte. Thus, the composition of a specific generation of inclusions associated with gold mineralization, in a sample exhibiting multiple overprinting cannot be simply isolated and evaluated.

d) The interpretation of DICP generated results is very difficult in the absence of petrographic studies of fluid inclusions in the decrepitate (analyte) material.

e) The rationale underlying the steam halo model (Ermakov, 1965) outlined in Chapter 1 suggests an increased DICP sodium response should correlate with areas subjected to increased hydrothermal fluid activity associated with a mineralizing event. The reverse situation was observed at Yellow Aster where quartz from the mine area exhibited relatively lower sodium responses. The interpretation of the magnitude of the sodium response in terms of 'hydrothermal activity' is erroneous (see chapter 3).

f) The volume of liquid released from fluid inclusions during decrepitation is unquantified and consequently the absolute metal concentrations are not available.

Fluid inclusion mapping

Fluid inclusion mapping, i.e. the petrographic observation of fluid inclusions in thin sections, was found to be a useful technique at Yellow Aster. Semi-quantitative data on fluid inclusion compositions, abundance and spatial distribution was gained from the study.

The data obtain from thin section observation is relatively cheap, compared to the cost of that produced by either fluid inclusion microthermometry or DICP analysis. The author suggests that a preliminary attempt to observe fluid inclusions should form part of any petrographic study of mineralized rocks particularly during the exploratory phase of a program . The data so generated could possibly be used to confirm or re-evaluate the genetic model used at the exploration stage.

A limitation to the widespread application of fluid inclusion mapping is imposed by the character of the country rock in a mineralized area. Hart (1984) reports that attempts to investigate the spatial distribution of inclusion types within and around the Cairnsmore of Carsphairn acidic intrusive in Scotland were unsuccessful. At Carsphairn, a compositionally zoned

felsic magma body intrudes into a sedimentary sequence composed of fine grained shales, siltstones, greywackes and conglomerates (Leake and others, 1978). The finer grained sedimentary lithologies did not contain quartz (or any mineral) coarse enough to be investigated for their inclusion content, using ordinary petrographic microscopes. Thus, at Cairsphairn fluid inclusion mapping could only be used within the boundaries of the intrusive body.

Fluid inclusion microthermometry

Fluid inclusion microthermometry provided meaningful data on the temperature, composition and temporal evolution of fluids that accompanied gold mineralization at Yellow Aster. Careful observation and measurement of many quartz samples revealed a relatively consistent picture of the hydrothermal regime.

The microthermometric data are extremely useful because they allow some quantification of the physico-chemical environment. The approximate quantification of P-T-X conditions can be used to predict stable mineralogy, which can be compared to that actually observed.

At Yellow Aster, microthermometric data can be used to predict a mechanism for gold deposition which seems to satisfy most of the available field and mineral stability criteria. An isoenthalpic boiling mechanism is used to explain to the loss of <20 molar% carbon dioxide from the earliest fluids discerned. Isoenthalpic boiling results in a lower temperature liquid phase (240-270°C). Carbon dioxide and hydrogen sulphide partition to the vapor phase and result in a decreased proton concentration (increased pH). The vertical extent of gold-sulphide mineralization at Yellow Aster (>1000') is probably a function of continued boiling of an ascendant hydrothermal fluid. However the more erratic and often spectacular gold grades associated with the surface oxidized zones (Hess, 1910) probably reflect the sharp decrease in gold solubility resulting from an increased oxygen fugacity encountered near surface (figure 5.26, after Henley and others, 1984).

Final comments

Fluid inclusion mapping and microthermometry applied at the Yellow Aster mine in California provided useful data to aid in the evaluation of potential ore depositional mechanisms. Such data could be used to establish or refine any genetic model used in a gold

exploration program within the Rand Mining District.

References cited

Alderton, D.H.M., Thompson, M., Rankin, A.H., and Chryssoulis, S.L., 1982. Developments of the ICP linked decrepitation technique for the analysis of fluid inclusions in quartz. Chemical Geology, V.37, pp.203-213.

Allen, A.W., 1923. The future of low-grade gold mine (the Yellow Aster at Randsburg, California - Amalgamation - Bulk Leaching-Time element in cyanidation). Eng. and Min. Jour. Vol.115, No.12 pp.539-541.

Berger, B.R., and Eimon, P.I., 1982. Comparitive models of epithermal silver-gold deposits: Soc. Mining Engineers AIME Reprint 82-13, 14pp.

Blake, D.W., Theodore, T.G., and Kretschmer, A.L., 1978. Alteration and distribution of sulphide mineralization at Copper Canyon, Lander County, Nevada: Ariz. Geol. Soc. Digest V.11, pp.67-78.

Bodnar, R.J., 1983. A method of calculating fluid inclusion volumes based on vapour bubble diameters and P-V-T-X properties of inclusion fluids: Econ. Geol. V.78, pp535-542.

Boyle, R.W., 1979. The geochemistry of gold and its deposits: Canada Geol. Surv. Bull. 280, 584pp.

Boyle, R.W., Alexenader, W.M., and Aslin, G.E.M., 1975. Some observations on the solubility of gold. Geol. Surv. Can. Pap.No.75, 24pp.

Boyle, R.W., 1954. A decrepitation study of quartz from the Campbell and Negus-Rycon shear zone systems, Yellowknife, Northwest Territories. Geol. Surv. Can. Bull. V.30, 20pp.

Buchanan, L.J., 1981. Precious metal deposits associated with volcanic environments in the southwest. Ariz. Geol. Soc. Digest. Vol.14, pp.237-262.

Burleigh, R.E., (in prep). Mineralization in the Willow Creek Mining District, Alaska. M.S. thesis, Univ. of Alaska.

Burruss, R.C., 1981. Analysis of phase equilibrium in C-O-H-S fluid inclusions: Chap.3 in Handbook to Mineralogical Association of Canada Short Course in Fluid Inclusions.

Chryssoulis, S.L., 1983a. Development of fluid inclusion techniques and their application to mineral exploration with reference to selected Mexican deposits: Unpub. Ph.D. thesis Univ.of London (Imp. Coll.).

Chryssoulis, S.L., 1983b. Study of the effects of feldspar and mica upon the analyses of fluid inclusions by decrepitation ICP method. Chemical Geology, V.40, pp.323-335.

Chryssoulis, S., and Wilkinson, N., 1983. High silver content of fluid inclusions in quartz from Guadalacazar granite. San Luis Potosi, Mexico: a contribution to ore genesis theory. Econ. Geol. v.78, pp.302-318.

Clark, W.B., 1970. Gold districts of California: Calif. Div. Mines and Geol. Bull. 193, pp.153-168.

Collins, P.L.F., 1979. Gas hydrates in CO2 bearing fluid inclusions and the use of freezing data for estimation of salinity. Econ. Geol., V.75, pp.1435-1444.

Cox, D.P., Gonzalez, J.P., and Nash, J.T., 1975. Geology, geochemistry and fluid inclusion petrography of the Sapo Alegre porphyry copper prospect and its metavolcanic wall rocks, West-Central Puerto Rico. U.S. Geol. Survey Jour. Research, 3, pp.313-327.

Crawford, M.L., 1981. Phase equilibria in aqueous fluid inclusions; Chap 4 in handbook to Mineralogical Assoc. Canada Short Course in Fluid Inclusions.

Davis, J.C., 1973. Statistics and data analysis in Geology John Wiley and Sons Inc., New York, 550pp.

Drummond, S.E., 1981. Boiling and mixing of hydrothermal fluids: chemical effects on mineral precipitation. Unpub. Ph.D. thesis, the Pennsylvania State Univ., 380pp.

Drummond, S.E., and Ohmoto, H. 1985. Chemical evolution and mineral deposition in boiling hydrothermal systems. Econ. Geol. Vol. 80, pp126-147.

Eimon, P. 1981. Exploration for epithermal gold and silver deposits. The Epithermal Model Paper presented at 'The First International Symposium on Small Mine Economics and Expansion', Taxco, Mexico, May 17-21 1981.

Ermakov, N.P., 1965. Use of gas liquid inclusions in prospecting and exploration for post magmatic ore deposits and blind ore bodies. Int. Geol. Review, 9, pp.947-956.

Fisher, J.R., 1976. The volumetric properties of H2O - a graphical portrayal. Jour. Research U.S. Geol. Surv. V.4, pp.189-193.

Fyon, J.A., and Crocket, J.H., 1980. Volcanic environment of carbonate and stratiform gold mineralization, Timmins area, in, Genesis of Archean, volcanic-hosted gold deposits. Ontario Geol. Sur. Open File Report 5293, pp.44-65.

Harris, M., 1980a. Gold mineralization at the Salave gold prospect northwest Spain. Inst. Min. Met. Trans. V.89, pp.1-4.

Harris, M., 1980b. Internal report to B.P. Minerals International, on alteration and fluid inclusions at Yellow Aster, 10pp.

Harris, M., 1979. Alteration and mineralization at the Salave gold prospect, Asturias, W.Spain. Unpub. Ph.D. thesis, Univ. of London.

Hart, D., 1984. The evaluation of fluid inclusion decrepitate analyses as prospecting guides to intrusive hosted mineralizations. Unpub. Diploma of Imperial College thesis, Imperial College, London.

Hart, D., and Rankin, A.H., 1983. 'Application of the ICP to the evaluation of steam aureoles as prospecting guides to intrusive hosted mineralization'. Final Report for Britsih Petroleum Minerals International sponsored research contract. Imperial College, London, England.

Hayba, D.O., 1983. A compilation of fluid inclusion and stable isotope data on selected precious-and base-metal epithermal deposits. US. Geol. Surv. Open file report 83-450.

Hedenquist, J.W., and Henley, R.W., 1985. The importance of CO2 on freezing point measurement of fluid inclusions: evidence from active geothermal systems and implications for epithermal ore deposition. Econ. Geol., V.80, pp.1379-1406.

Helgeson, H.G., 1969. Thermodynamics of hydrothermal systems at elevated temperatures and pressures. American Jour. Sci., V.267 pp.729-804.

Hendel, B., and Hollister, L.S., 1981. An empirical solvus for the CO2-H2O system. Geochem. et Cosmochim. Acta. V.45, pp.225.

Henley. R.W., Truesdell, A.H., and Barton, P.B., 1984. Fluid Mineral Equilibria in Hydrothermal Systems. Reviews in Economic Geology, V.1. Soc. Econ. Geol.

Henley. R.W., 1973. Solubility of gold in hydrothermal chloride solutions. Chemical Geology, V.11, pp.73-87.

Hess, F.L., 1910. gold mining in the Randsburg Quadrangle, California. US. Geol. Surv. Bull.430.

Higgins, N.C., 1985. Wolframite deposition in a hydrothermal vein system: the Grey River tungsten prospect, Newfoundland, Canada. Econ. Geol., V.80, pp.1297-1327.

Higgins, N.C., 1980. Fluid Inclusion evidence for the transport of tungsten by carbonate complexes in hydrothermal solutions. Can.J. Earth Sci., V.17,pp.823-830.

Hollister, L.S., 1981. Information intrinsically available from fluid inclusions. Chap. 1 in Handbook to Mineralogical Association of Canada Short Course in Fluid Inclusions. Calgary, 1981 (Hollister, L.S., and and Crawford, M.L., eds.).

Hollister, L.S., and Burruss, R.C., 1976. Phase equilibria in fluid inclusions from the Khtada Lake metamorphic complex. Geochem. et Cosmochim. Acta. V.40, pp.163-175.

Hollister, L.S., and others 1981. Practical aspects of microthermometry. Chap. 12 in Handbook to Mineralogical Assoc. Canada Short Course in Fluid Inclusions.

Holloway, J.R., 1981. Compositions and volumes of supercritical fluids in the earths crust. Chapter 2 in Handbook to Mineralogical Association of Canada Short Course in Fluid Inclusions.

Hulin, C.D., 1925. Geology and ore deposits of the Randsburg Quadrangle of California. Calif. State Mining Bureau, Bull. 95.

Hutchinson, C.S., 1985. Economic deposits and their tectonic setting. Wiley-Interscience, New York pp.365.

Jackson, S.E., and Strong, D.F., 1985a. Chemical and mineraological characteristics of alteration in porphyry gold environments, and geochronology of porphyry gold deposition. Unpublished report to Amselco Exploration Inc. (Dept. of Earth Sciences, Memorial University of Newfoundland, Canada). 82pp.

Jackson, S.E., and Strong, D.F., 1985b. Unpublished report to Amselco Exploration Inc. (Dept. of Earth Sciences, Memorial University of Newfoundland, Canada).

Jacobson, C.E., 1983. Structural geology of the Pelona Schist and thrust, San Gabriel Mountains, California. Geol. Soc. Am. Bull., V.94, pp.753-763

Jones, E., 1985. An evaluation of DICP at selected mineral deposits. Unpub. Ph.D. thesis, Univ. of London.

Kay, A., and Strong, D.F., 1983. Geologic and fluid controls on As-Sb-Au mineralization in the Moretons Harbour area, Newfoundland. Econ. Geol. v.78, pp.1590-1604.

Kerrich, R., 1980. Archaean gold-bearing chemical sedimentary rocks and veins: a synthesis of stable isotope and geochemical relations. In: Genesis of Archaean, Volcanic-Hosted Gold Deposits: Pye, E.G., Roberts, R.G., (ed) Ontario. Geol. Surv. Miscel. Paper 97 1-15 (1981).

Kerrich, R., and Fyfe, W.S., 1981. The gold-carbonate association. Source of CO2 and CO2 fixation reactions in Archaean lode deposits. Chemical Geology, V.33 pp.265-294.

Krauskopf, K.B., 1954. The solubility of gold. Econ. Geol., V.46, pp.858-870.

Krauskopf, K.B., 1969. An introduction to geochemistry. McGraw-Hill Book Comp., 721pp.

Leake, R.C., and others 1979. Gold mineralization at the southern margin of the Loch Doon granitoid complex, south west Scotland. Mineral Reconnaissance program. Report British Geol. Surv. No.46.

Lemmon, D.W., and Dorr, J.V.N., 1940. Tungsten deposits of the Atolia District, San Bernadino and Kern Counties, California. U.S.Geol.Surv. Bull. 922-H. pp.205-254.

Masterman, J.S., (in prep). Geologic investigation of gold mineralized areas, Circle Mining District, Alaska. M.S. thesis, Univ. of Alaska.

Metz, P.A., 1983. Ore petrology and geology of the Fairbanks Mining District, Alaska: abstract in Proc. northwest Mining Assoc. 88th Annual Meeting, Spokane, Washington.

Moore, W.J., and Nash, J.T., 1976. Alteration and fluid inclusion studies of the porphyry copper orebody at Bingham, Utah. Econ. Geol., V.69, pp.31-45.

Morehouse, J., 1984. The evolution of structural control on alteration and mineralization in the Randsburg Mining District, Mojave Desert, California. Rough Draft M.S. thesis: Univ. of Arizona, Tucson.

Nash, J.T., 1976, Fluid inclusion petrology-Data from porphyry copper deposits and application to exploration. U.S.Geol.Surv. Prof.Paper, V.907-D, 16pp.

Nash, J.T., (1973). fluid inclusion studies of some gold deposits in Nevada: U.S.Geol.Surv. Prof.Paper, V.800-C, pp.C15-C19.

Potter, R., 1977. Pressure corrections for fluid inclusion homogenisation temperatures based on the properties of the system NaCl - H2O. U.S. Geol. Surv. Journ. Research. No.5, pp.603-607.

Radtke, A.S., Rye, R.O., and Dickson, F.W., 1980. Geology and stable isotope studies of the Carlin gold deposit, Nevada. Econ. Geol., V.75, pp.641-672.

Rankin, A.H., 1978. Handbook to 'User School on Fluid Inclusion Equipment and Methods'. Applied Mineralogy Group short course at Imperial College of Science, London, England.

Rankin, A.H., and Alderton, D.H.M., 1982. Fluid inclusion studies on mineralized granites of the British Isles: an assessment of their use in the exploration for mineral deposits associated with granitic rocks. Final Report, Contract 041 MPP UK 168p. EEC. R and D program on 'Primary Raw Materials, Imperial College, London, England.

Rankin, A.H., and Alderton, D.H.M., 1983. Fluid inclusion petrography of SW. England granites and its potential in mineral exploration. Mineral. Deposita V.18, pp.335-347.

Rankin, A.H., and Hart, D., 1985. Final report on B.P. Minerals International Ltd., contract 'Fluid inclusions in gold deposits'. Imperial College of Science, London, England.

Rankin, A.H., and Alderton, D.H.M., Thompson, M., and Goulter, J.E., 1982. Determination of uranium-carbon ratios in fluid inclusion decrepitates by inductively coupled plasma emisssion spectroscopy. Min. Mag. V.46, pp.178-186.

Read, A.J., 1975. The first ionization constant of carbonic acid from 25 to 250 C and to 2000 bars: Journal of Solution Chemistry, V.4, pp.53-70.

Roedder, E., 1984a. Fluid inclusion evidence bearing on the environment of gold deposition. In: "Gold'82", Geol. Surv. Zimbabwe Spec. Pub. No.1 (R.P. Foster, ed.), A.A. Balkema, Rotherdam.

Roedder, E., 1984b. Fluid Inclusions. Reviews in Mineralogy. Vol. 12. Mineralogical Society of America.

Roedder, E., 1981. Origin of fluid inclusions and changes that occur after trapping: Chap.5 in Handbook to Mineralogical Assoc. Canada Short Course in Fluid Inclusions.

Roedder, E., 1977. Fluid inclusions as tools for mineral exploration. Econ. Geol. V.72, pp.503-525.

Roedder, E., 1976. Fluid Inclusion evidence in the genesis of ores in sedimentary and volcanic rocks. Handbook of stratabound and stratiform Ore Deposits, V.2 pp.67-110. Ed. K.H. Wolf. Amsterdam. Elsevier.

Roedder, E., 1972. The composition of fluid inclusions. Chapter 22 in Data of Geochemistry, 6th Edition, M. Fleischer ed., USGS., Prof. Paper 440.

Roedder, E., 1971. Fluid inclusion studies on the porphyry type ore deposits at Bingham, Utah, Butte, Montana and Climax, Colorado. Econ. Geol. V.66, pp.98-120.

Roedder, E., 1967. Environment of deposition of stratiform (Mississippi Valley-type) ore deposits, from studies of fluid inclusions. Econ. Geol. V.62, pp.349-62.

Roedder, E., 1963. Studies of fluid inclusions II. Freezing data and their interpretation. Econ. Geol. V.58., pp.167-210.

Roedder and Bodnar., 1980 Geologic and pressure determinations from fluid inclusion studies. Ann. Rev. Earth Planet Sci. V.8, pp.263-301.

Romberger, S.B., 1982. Transport of gold hydrothermal system at Temperatures up to 300 C, Geol. Soc. America Abstracts with Programs, V.14, pp.602.

Rose, A.W., Hawkes, H.E., and Webb, J.S., 1979. Geochemistry in Mineral exploration. (2nd edit.) Academ. Press pp.657.

Sassos, M.P., 1986. Mining Investment -1986. Eng. and Min. Jour. V.187, no.1, pp.25-33.

Schnorr, P., Creech, M.S., Kesler, S.E., and Kelly, W.C., 1984. Fluid inclusion gas halos as guides to exploration of hydrothermal minerals systems. Poster session at 113th AIME annual meeting. SEG program. Feb 26th - Mar.1 1984, Los Angeles, California.

Seward, T.M., 1982. Transport and deposition of gold in hydrothermal systems: Proceedings of Conference on Geology, Geochem. and Origin of Gold Deposits, Zimbabwe.

Seward, T.M., 1973. Thiocomplexes of gold and the transport of gold in hydrothermal ore solutions. Geochim et Cosmochim. Acta., V.37, pp.379-399.

Shepherd, T.J., 1981. Temperature - programmable, heating - freezing stage for microthermometric investigation of fluid inclusions. Econ. Geol., V.76, pp.1244-1247.

Shepherd, T.J., Rankin, A.H., and Alderton., D.H.M., 1985. A practical guide to fluid inclusion studies. (Blackie and Sons, Glasgow), pp.245.

Skinner, B.J., and Barton, P., 1973. Genesis of mineral deposits. Ann. Rev. Earth and Plan. Sci. V.1, pp.183-210.

Smith, T.J., Cloke, P.L., and Kesler, S.E., 1984. Geochemistry of fluid inclusions from the McIntyre - Hollinger gold deposit, Timmins, Ontario, Canada. Econ. Geol. V.79, pp.1265-1285.

Smith, T.J., and Kesler, S.E., 1985. Relation of fluid inclusion geochemistry to wall rock alteration and lithogeochemical zonation at the Hollinger - McIntyre gold deposit, Timmins, Ontario, Canada. C.I.M. Bulletin, V.78, No.876, pp.35-45.

Spooner, E.T.C., 1981. Fluid inclusion studies of ore deposits. Chapter 9 in Handbook to mineralogical Assoc. Canada Short Course in Fluid Inclusions.

Takenouchi, S., and Kennedy, G., 1964. The binary system H2O - CO2 at elevated temperatures and pressures. Am. Journ. Sci. V.262, pp.1054-1074.

Takenouchi, S., and Kennedy, G.C., 1965. The solubility of carbon dioxide in NaCl solutions at high temperatures and pressures. Am. Journ. Sci.,V.263, pp.445-454.

Theodore, T.G., and Nash., J.T., 1973. Geochemical and fluid zonation, Copper Canyon, Lander County, Nevada. Econ. Geol. V.68, pp.565-570.

Thompson, M., Rankin, A.H., Walton, S.J., Halls, C., and Foo, B.N., 1980. The analysis of fluid inclusion decrepitate by inductively coupled plasma atomic emission spectroscopy: an exploratory study. Chemical Geology, V.30, pp.121-133.

Thompson, M., and Howarth, R.J., 1978. A new approach to the estimation of analytical precision. Jour. of Geochem. Explorn. V.9, pp.23-30.

Thompson, M., and Howarth, R.J., 1976. Duplicate analysis in geochemical practice (2 parts). Analyst, 101, pp.690-709.

Thompson, M., and Walsh, J.W., 1983 . A handbook of inductively coupled plasma spectrometry. Blackie: Glasgow and London.

Troxel, B.W., and Morton, P.K., 1962. Mines and mineral resources of Kern County, California: Calif. Div. of Mines and Geol. County report No.1.

Tucker, W.B., and Sampson, R.J., 1940. Randsburg District. Calif. Div. Mines Rept. 29, pp.285-286.

Walthier, T.N., Sirvas, E., and Araneda, R., 1985. The El Indio gold - silver - copper deposit. Eng. and Min. Jour., V.186, No.10.

APPENDIX I

PETROGRAPHIC CRITERIA FOR FLUID INCLUSION ORIGIN
(from Roedder, 1984b)

Criteria for primary origin

I. Based on occurence in a single crystal, with or without evidence of direction of growth or growth zonation.

A. Ocurrence as a single inclusion (or small three - dimensional group of inclusions) in an otherwise inclusion - free crystal.

B. Large size relative to that of the enclosing crystal, e.g., with a diameter 0.1 that of crystal, and particularly several such inclusions.

C. Isolated occurrence, away from other inclusions, for a distance of 5 times the diameter of the inclusion.

D. Occurrence as part of a random, three-dimensional distribution throughout the crystal.

E. Disturbance of otherwise regular decorated dislocations surrounding the inclusion, particularly if they appear to radiate from it.

F. Occurrence of daughter crystals (or accidental solid inclusions) of the same phase(s) that occur as solid inclusions in the host crystal or as contemporaneous phases.

G. Occurrence along a twin plane, but note that secondary or pseudosecondary inclusions can behave similarly.

II. Based on occurrence in a single crystal showing evidence of direction of growth:

A. Occurrence beyond (in the direction of growth) and sometimes immediately before extraneous solids (the same or other phases) interfering with the growth, where the host crystal fails to close incompletely. (Inclusion may be attached to the solid or at some distance beyond, from imperfect growth).

B. Occurrence beyond a healed crack in an earlier growth stage, where new crystal growth has been imperfect.

C. Occurrence between subparallel units of a composite crystal.

D. Occurrence at the intersection of several growth spirals, or at the center of growth spiral visible on the outer surface.

E. Occurrence, particularly as relatively large flat inclusions, parallel to an external crystal face, and near its center (i.e., from 'starvation' of the growth at the center of the crystal face), e.g., much 'hopper salt'.

F. Occurrence in the core of a tubular crystal (e.g., beryl). This may be merely an extreme case of previous item.

G. Occurrence, particularly as a row, along the

boundary between two growth sectors.

III. Based on occurrence in a single crystal showing evidence of growth zonation (as determined by color, clarity, composition, X-ray darkening, trapped solid inclusions, etch zones, exsolution phases, etc.).

A. Occurrence in random three-dimensional distrbution, with different concentrations in adjacent zones (as from a surge of sudden feathery or dendritic growth).

B. Occurrence as subparallel groups (outlining growth directions), particularly with different concentrations in adjacent zones, as in previous item.

C. Multiple occurrence in planar array(s) outlining growth zone. Note that if this is also a cleavage direction, there is ambiguity.

D. Occurrence on a surface from an episode of etching that interrupted normal crystal growth.

IV. Based on growth from a heterogeneous (i.e., two-phase), or a changing fluid.

A. Planar arrays (as in III-C) or other occurrence in growth zones, in which the compositions or inclusions in adjacent zones are different (e.g., gas inclusions in one and liquid in another, or oil and water.

B. Planar arrays (as in III-C) in which trapping of some of the growth medium has occurred at points where

the host crystal has overgrowth and surrounded adhering globules of the imiscible dispersed phase (e.g., oil droplets or steam bubbles).

C. Otherwise primary - appearing inclusions of a fluid phase that is unlikely to be the mineral - forming fluid, e.g., mercury in calcite.

V. Based on occurrence in hosts other than single crystals (i.e., inter crystalline inclusions).

A. Occurrence on compromise growth surface between two nonparallel crystals. (These inclusions have generally leaked and could also be secondary).

B. Occurrence within polycrystalline hosts, e.g., as pores in fine grained dolomite, cavities within chalcedony - lined vugs in metal deposits or pegmatities. (These last two are among the largest inclusions, and have almost always leaked).

C. Occurrence in noncrystalline hosts (e.g., gas bubbles in amber vesicles in pumice).

VI. Based on inclusion shape or size.

A. In a given sample, large size and/or equant shape.

B. Negative crystal shape -- this is valid only in certain specific samples; in other samples, both primary and secondary or only the secondary inclusions may have negative crystal shape.

VII. Based on occurrence in euhedral crystals, projecting into vugs.

Criteria for secondary origin

I. Occurrence as planar groups outlining healed fractures (cleavage or otherwise) that come to the surface of crystal (note that movement of inclusions during recrystallization can cause dispersion -- Roedder, 1971a, Fig.11, see also II-C above).

II. Very thin and flat; in process of necking down (but note that necking down may occur either during temperature decline or isothermally, in primary, secondary or pseudosecondary inclusions).

III. Occurrence within a plane that differs compositionally from the rest of the crystal, e.g., in cathodoluminescene.

IV. Primary inclusions with filling representative of secondary conditions.

A. Located on secondary healed fracture; hence presumably refilled with later fluids (Kalyuzhnyi, 1971).

B. Decrepitated and rehealed after exposure to higher temperatures or lower external pressures than at time of trapping; new filling may have original composition but lower density.

V. Temperature of homogenization (Th) far below that of

adjacent presumed primary inclusions in the same growth zone (on the basis taht low -Th early primaries would be decrepitated by a much hotter later stage of growth; note, however, that late-stage primaries and pseudosecondaries can be at any lower temperature, and that barring decrepitation, primary inclusions can show an increase in Th with stage of formation).

Criteria for pseudosecondary origin

I. Same occurrence as secondary inclusions, but other end of the fracture visibly terminates at a growth surface within crystal. Frequently tapered in size, the largest inclusions being near the outer termination.

II. Generally more apt to be equant and of negative crystal shape than secondary inclusions in same sample (suggestive only).

III. Occurrence as a result of the covering of etch pits crosscutting growth zones.

APPENDIX II

GEOLOGY OF THE YELLOW ASTER MINE AREA (AFTER AMSELCO EXPLORATION INC.)

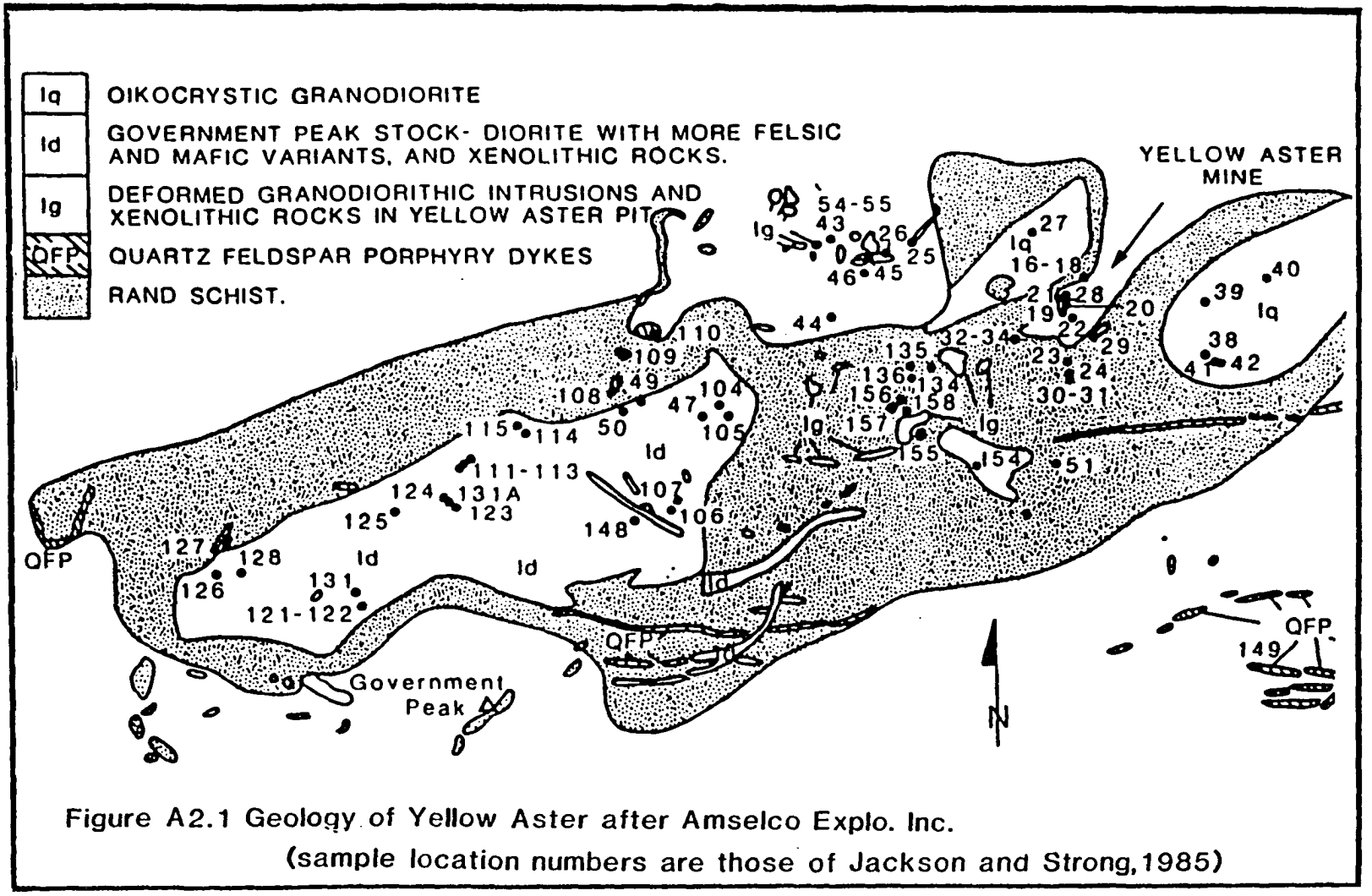

Figure A2.1 Geology of Yellow Aster after Amselco Explo. Inc.
(sample location numbers are those of Jackson and Strong, 1985)

APPENDIX III

GEOCHEMICAL ANALYSES FOR RANDSBURG WHOLE ROCKS

Table A.3-1 COMMERCIAL GEOCHEMICAL DATA FOR ROCKS OF YELLOW ASTER MINE-GOVERNMENT PEAK AREA

Sample	Description	Sb	W	Th	U	As	Mo	Au	Mn	Ag	Hg
YA.134	Phyllic granodiorite, W rim of YA pit	5.9	14	20.0	3.5	3159	<4	368	100	0.4	20
YA.135	" " " " " "	10.7	14	21.2	3.5	650	3	187	28	0.3	30
YA.136	" " " " " "	4.8	21	23.4	3.7	871	<2	629	15	0.5	15
YA.154	" " " " " "	3.4	18	11.3	4.0	332	2	546	130	0.2	20
YA.156	" " " " " "	<0.4	9	18.2	2.0	7292	<5	1216	8	0.6	20
YA.157	" " " " " "	0.5	87	12.9	1.5	6567	<4	404	4	0.4	10
YA.158	" " " " " "	8.4	24	11.8	1.5	2329	<4	324	62	0.5	10
YA.48	Fresh fine grained diorite, Gvt Pk St (GPS)	0.3	2958	8.4	2.8	2	<2	<6	645	<0.1	5
YA.105	" " " " " "	0.6	2088	10.0	2.7	11	<2	<6	700	<0.1	<5
YA.125	" " " " " "	0.4	1518	8.6	2.2	8	<2	<5	680	0.1	5
YA.130D	Fine grained diorite, Gvt Pk St	0.7	<2	9.9	2.1	73	<2	6	550	<0.1	30
YA.126	Decomposed med-gd diorite88, W end of GPS	1.2	3	3.1	1.5	105	<2	36	1000	0.2	15
YA.128	" " " " " "	4.2	3	5.8	2.1	79	<2	73	900	0.7	10
YA.129	" " " " " "	0.5	<2	10.6	2.0	15	<2	14	445	0.1	10
YA.131	" " " " " "	0.6	<2	5.6	1.5	24	<2	29	900	0.1	5
YA.131A	" " " " " "	0.9	<2	9.7	2.8	131	<2	11	645	<0.1	20
YA.0115P	" " " " " "	5.6	30	5.2	4.6	1543	<4	146	800	0.1	15
YA.122	Sericitised diorite, W end of GPS	5.9	13	15.2	3.6	159	<2	29	510	0.4	10
YA.0125P	Fract. zone with qtz veinlets in adit, GPS	11.8	48	9.5	4.5	1402	<4	507	625	0.2	20
YA.0127P	Altered fract. zone with calcite vein, GPS	5.9	22	14.5	3.5	826	3	266	700	0.1	10
YA.121	Limonitic fracture zone in GPS	19.5	114	8.8	3.8	1409	7	645	475	0.6	10
YA.1	Limonitic gouge & breccia, Jupiter tunnel	7.3	39	13.1	2.3	8123	<9	486	540	0.8	25
YA.3	" " " " "	12.0	35	10.8	3.2	1505	<4	599	205	0.2	140
YA.117	Breccia, Jupiter Fault, Jupiter tunnel	3.1	5	3.9	1.0	211	<2	61	100	0.3	25
RLSD	Sericitic gouge, Jupiter Fault, Rand Level	8.4	10	8.7	5.1	971	<3	1132	95	0.5	40
YA.9	Limonitic gouge, Rand Level	42.1	69	6.3	5.5	9000	<10	9333	2500	1.3	200
YA.9(dup)	" " " "	33.1	39	7.2	3.2	7331	<8	2260	1530	1.2	160
YA.11	Limonitic gouge, Rand Level	29.2	84	10.8	6.6	6139	<8	3827	740	0.7	10
YA.14	" " " "	26.4	21	5.4	2.9	2484	<5	388	650	0.4	60
YA.51	Fault gouge, in stope in RS, S of YA pit	13.9	13	8.7	5.9	2609	<4	172	750	0.5	20
YA.52	Fault gouge, Jupiter F., Midway Tunnel	12.9	29	13.7	6.8	2048	<4	1390	185	0.4	100
YA.54	Altered granod. in F. in adit NW of YA pit	5.6	11	20.6	4.5	629	<2	591	45	0.3	30
YA.0109P	Fault breccia in Rand Schist " " " "	8.2	13	17.1	5.2	1524	<4	455	170	0.6	5
YA.28	Fresh deformed granodiorite, YA pit	1.1	2688	7.4	2.9	2	<2	<5	600	0.2	200
YA.288	" " " " "	2.1	2338	9.4	3.0	14	<2	<5	660	0.1	85
Sample	Description	Sb	W	Th	U	As	Mo	Au	Mn	Ag	Hg

RESULTS ARE IN PPM EXCEPT FOR GOLD (Au) AND MERCURY (Hg) WHICH ARE IN PPB (see over for conversion to oz/ton)

cont GEOCHEMICAL DATA FOR ROCKS OF THE ROMEO (WEST) AND JULIETTE (EAST) PIPES-KELLY MINE AND 'BLUE HILL' AREAS

Sample	Description	Sb	W	Th	U	As	Mo	Au	Mn	Ag	Hg
YA.59	Sercts'd. QFP, altn. halo of Romeo (W) pipe	15.4	5	8.9	3.6	83	<2	158	26	0.5	75
YA.71	" " " " " " " "	21.1	9	9.6	3.7	508	3	63	38	0.2	25
YA.96	" " " " " " " "	4.0	3	9.6	4.2	26	<2	21	22	0.4	30
YA.72	Altered granod., " " " " " " "	56.7	37	5.3	1.7	28	<3	33	14	0.5	140
YA.73A	" " " " " " " "	55.9	79	4.5	1.7	23	<3	18	12	0.3	40
YA.65	Silicified breccia, Romeo (West) Pipe	22.2	8	7.2	1.5	126	<2	134	35	1.8	370
YA.66	" " " " " "	21.3	8	8.8	2.4	212	<2	218	25	2.3	180
YA.67	" " " " " "	20.3	5	5.8	2.8	95	<2	118	28	1.3	300
YA.79A	Juliette (East) rhyolite pipe	12.7	2660	17.2	4.6	38	<2	32	40	0.3	50
YA.81	" " " "	28.2	<2	14.1	5.1	76	<2	10	20	3.2	25
YA.83	" " " "	7.3	<2	15.0	5.3	32	<2	14	22	2.1	100
YA.98	Fault gouge, Kelly Mine gloryhole	490.0	17	6.5	<1.5	2286	<8	922	20	70.0	565
YA.100	Mn^2-rich siliceous gouge, Kelly gloryhole	60.6	23	6.0	1.9	2038	<5	712	12	8.1	225
YA.101	Qtz-pyrite vein, Kelly gloryhole dump	535.6	<4	4.3	<1.5	2138	<8	1542	38	41.0	180
YA.150a	Siliceous rhyolite breccia, Blue Hill	54.5	1136	6.2	1.7	<1	<2	10	12	0.1	>5000
YA.150b	" " " " "	103.9	23	8.2	2.9	35	2	72	26	0.4	3400
Sample	Description	Sb	W	Th	U	As	Mo	Au	Mn	Ag	Hg

RESULTS ARE IN PPM EXCEPT GOLD (Au) AND MERCURY (Hg) WHICH ARE IN PPB

1 oz/ton	= 34.3 ppm	= 34,300 ppb
0.1 oz/ton	= 3.43 ppm	= 3,430 ppb
0.05 oz/ton	= 1.72 ppm	= 1,720 ppb
0.01 oz/ton	= 0.34 ppm	= 340 ppb
0.005 oz/ton	= 0.17 ppm	= 170 ppb

* Sample ground in tungsten carbide mill
** Decomposed diorites contain variable amount of limonitic fractures

Abbreviations
Altn. = alteration
(Dup) = duplicate sample
F. = fault
Fract. = fracture
Granod. = granodiorite
Gvt Pk St = GPS = Government Peak Stock
Med-gd = medium-grained
QFP = quartz-feldspar porphyry ('Big Dyke')
Qtz = quartz
RS = Rand Schist
Sercts'd = sericitised
YA = Yellow Aster

Sb, W, Th, U, As, Mo, Au were analysed by Neutron Activation. Mn, Ag, Hg were analysed by Atomic Absorption

APPENDIX IV

EXPLANATION OF DATA SIGNIFICANCE TESTING AND CONTAMINATION EVALUATION TECHNIQUES FOR DICP ANALYSES (CONTAINING LOGIC LISTINGS FOR PROGRAMS USED)

Introduction

This appendix aims to briefly outline the techniques used to test the "significance" of DICP analyses. The large volume of data generated by DICP, i.e. a 36 element read out per sample, necessitated a system to establish the 'real' responses from those representing background levels.

The volume of data is aptly illustrated by the following example. Consider fifty samples prepared for analysis. Each sample generates a 36 element read out in millivolts (1800 pieces of information). These millivolt sample data contain residual background values which have to be removed ('stripped out') to give the background reduced millivolt values (3600 data pieces total). These raw millivolt data were often converted to equivalent ppm (5400) and the relative atomic proportions (7200). If element / element ratios are desired, the total rapidly exceeds 10,000 individual information units for 50 samples!

A combination of statistical evaluation and subjective overview was utilized to establish 'significance'. Following this, apparently real values were tested to elucidate the origin of the response i.e. whether decrepitate or contiminant derived.

Significance Testing

Although data for 36 elements are aquired for each sample, not all elements are present. Furthermore, approximately only 10 are at significant levels in most decrepitates (Hart, 1984).

If an element was not present in a sample decrepitate, its plasma response would be close to the value gained for blank tube analyses. Therefore a set of samples with no response (or very small ones) for a specific element would have approximately the same mean, standard deviation and therefore variance as that element in blank tubes.

The F-test (Davis, 1973) was applied to test the equivalence of sample and blank variances for each element. The F-test assumes two normal distributions are being used. The test was applied prior to the removal of the residual background values contained in the sample responses. The F-ratio between the sample and blank tube variances was calculated thus:

$$F=S1/S2$$

where S1 is the larger variance and S2 the smaller. The null hypothesis Ho was formulated thus:

$$Ho: S1 = S2$$

this states the parent population of the two samples hase

equal variance: the alternative hypothesis (Ha) states they do not.

$$Ha: S1 \neq S2$$

Tables A4.1A and B contain data for a typical analytical run. The F-ratios calculated are illustrated in Table A4.1B. The calculated F-ratio can be compared to the critical value of the F-ratio, with the stated degrees of freedom, at a chosen significance level i.e 1% (or =.01 in statistical notation).

For example:

at 0.01

for V1 = 22 and V2 = 8

then F = 5.36

This means that if the calculated F-ratio exceeds 5.36 for the conditions above, the null hypothesis is rejected. This infers that the variation in overall sample values (for a specific element) is significantly above that of blank tubes, and the element should be considered as being present in the decrepitates, though not necessarily derived from inclusion fluids.

This technique was found very useful in establishing the general response level of an element in the decrepitates. However, the F-test alone cannot distinguish between contiminant or decrepitate derived

Table A.4-1a and b.

a Analysis of Background Data Based on Millivolt Responses for Blank Tubes over a Small Time Interval (Values in mVs) for Some Elements

Element	Max.	Min.	Mean	St. Dev.	% Dev.	
Zn	8.42	7.89	8.15	.19	2.31	
Pb	204.20	194.70	201.10	3.26	1.62	
Fe	2.08	2.03	2.06	.018	.86	
S	33.08	26.61	28.68	2.07	7.21	*
Si	113.90	34.11	96.27	8.66	8.99	*
Na	25.20	23.57	24.57	0.54	2.18	
Ca	2.92	2.04	2.00	.03	1.04	
K	184.70	176.40	181.54	2.77	1.52	

* Note more erratic background of silica and sulphur.
Values based on 12 blank tubes over 30 mins.

b F-Test Ratios for Selected Elements (22 Samples Against Blanks)

Element	V_1	V_2	F-Test	Present at Levels above background
Zn	8	22	3.84	Yes
Pb	8	22	1.25	No
Fe	22	8	1322.90	Yes
S	22	8	50.2	Yes
Si	8	22	1.77	No
Na	22	8	1700.8	Yes
Ca	22	8	8.59	Yes
K	22	8	953.26	Yes

To pass test at = 0.01 when $V_1 = 22$, $V_2 = 8$, $F > 5.36$
$V_1 = 8$, $V_2 = 22$, $F > 3.45$

responses.

Blank Based Detection Limits

Table A4.1A illustrates the statistics for the analysis of 12 blank tubes 'en bloc' over a thirty minute period. The blank based detection limit for Fe was thus estimated at 0.036 millivolts (twice the positive standard deviation about the mean blank value for Fe). Programs DALART and DATAFIX were developed (Hart, 1984) to remove the residual background values for each element from samples. The 'background stripped' or real value for an elemental response could then be assessed in light of the magnitude of the blank based detection limit (Figure A4.1).

Programs DALART and DATAFIX remove the background value for an element from the sample responses, based on the values obtained (for a specific element) in the blank tube preceding and following a sample. The time of the blank tube analyses was recorded, with the element responses, onto floppy disc. The elemental drift between blank tubes was approximately linear with respect to time. A simple linear time-dependent correction was thus applied to the sample data 'sandwiched' between two blank tubes.

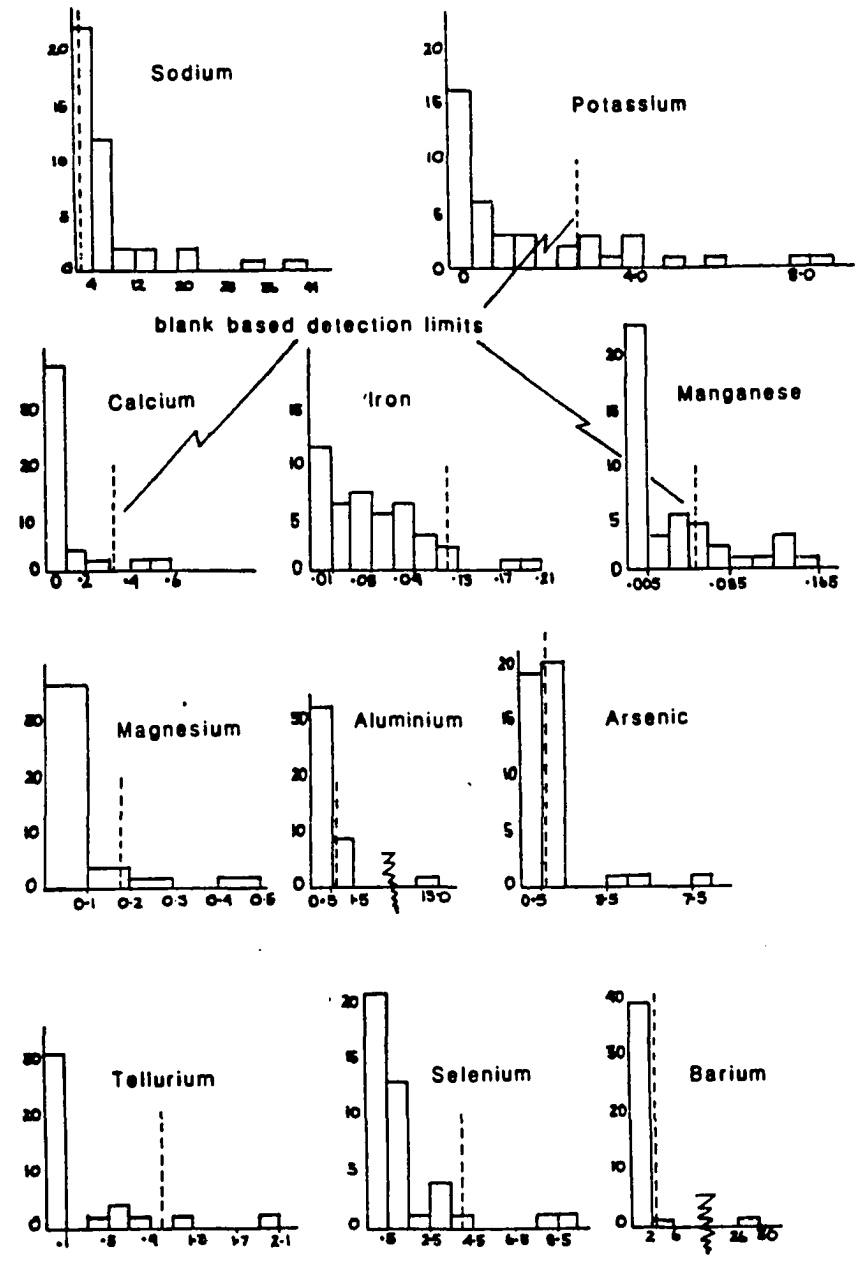

Figure A4-1 Histograms of DICP element responses

(Values in background reduced millivolts)

Contamination

The DICP technique for the analysis of fluid inclusions utilizes the temperature - induced explosive release of the contained phases. However, this destructive process commonly results in fragmentation of the host crystal. If these fragments are small enough (approximately 1μm) they could be supported by the argon carrier gas and taken into the plasma. Chryssoulis (1983a) identified two main DICP contamination sources:

i) by the introduction into the plasma, via the argon flow, of very small particles of either the host crystal or admixed contaminant.

ii) By sublimation from either host crystals or any admixed contaminant.

During this study, contamination was monitored using an integrated approach combining several techniques, some previously discussed, these were:

i) chromium channel response monitoring.

ii) Aluminium and rubidium channel response monitoring.

iii) Window integration analysis (Chapter 3).

iv) Precision estimation (Chapter 3).

Chromium Channel Technique

This approach assumes that chromium is absent from the fluids associated with felsic intrusives. Thus it is assumed that any variation in the chromium response for a sample is due to variation in the instrumental background. A plot of an element against chromium for each individual sample could ostensibly be used to discriminate between real and contaminant derived values (figure A4.2).

Aluminum-Rubidium Channels Technique

The aluminum and rubidium channels can be used to monitor the effects of feldspar and/or mica contamination. This was extensively investigated by Chryssoulis (1983b) who showed that presence of admixed alkali felspars had little effect on the analysis of fluid inclusions in quartz by DICP. However, the presence of biotite was shown to have a greater (though relatively minor) effect. Chryssoulis (1983a) clearly illustrates the main effect of feldspar/mica contamination of quartz analyte is dilution of the sodium channel response.

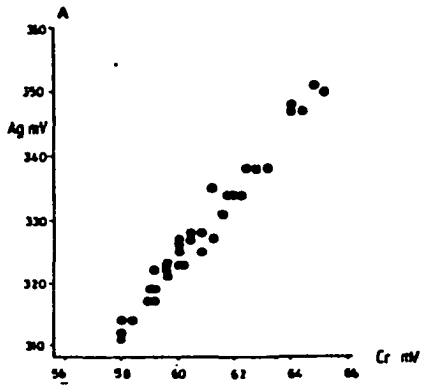

A. The linear trend for Ag shows no significant levels above background.

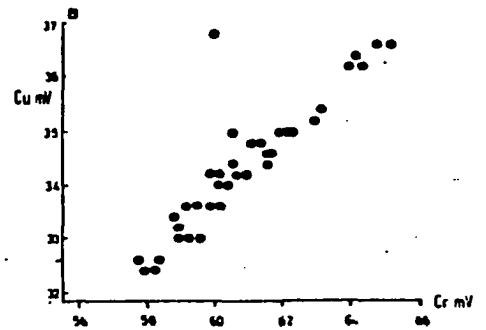

B. The results for Cu show a few samples above the background trend.

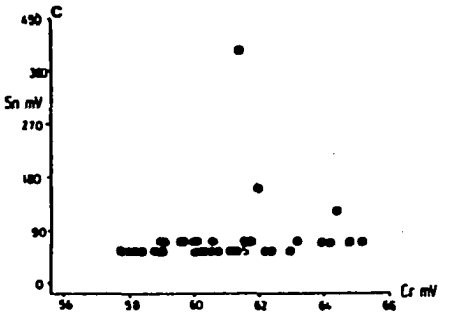

C. Three Sn values are significantly above background (the two highest values are from 10 NSW).

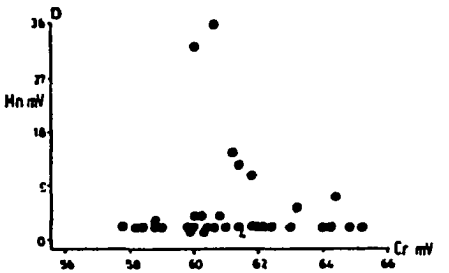

D. Mn is quite commonly detected in inclusions as shown by this plot.

FigureA4-2Contamination evaluation plot (elements against chromium technique)

PROGRAM DALART

```
      PROGRAM DALART (INPUT,OUTPUT,TAPE14=INPUT,TAPE15=OUTPUT)
      INTEGER STYPE (100),TIM1(100),CODE(100)
      REAL TIME (100),CREC(36),EL(100,36)
      N=1
  130 READ(14,00150,END=260,ERR=260)CODE(N),TIM1(N),STYPE(N)
     +,(EL(N,J),J=1,36)
  150 FORMAT(A4,16,5X,A5,10X,3(10F10.4/30X),6F10.4)
      TIME(N)=TIM1(N)
      D1=TIME(N)/10000
      ID=D1
      D1=ID
      D2=(TIME(N)-10000*D1)
      D2=D2/100
      ID=D2
      D2=ID
      D3=(TIME(N)-(D1*10000)-(D2*100)
      TIME(N)=(D1*3600)+(D2*60)+D3
      N=N+1
      GO TO 00130
  260 IN1=1
      DO 00340 I=2,N
      IF(STYPE(I).NE.   BLK)GO TO 340
      IN2=I
      DO 00320 L=1,36
      CREC(L)=(EL(IN2,L)-EL(IN1,L))/(TIME(IN2-TIME(IN1))
  320 CONTINUE
      DO 00390 J=IN1+1,IN2-1
      DO 00380 L=1,36
      EL(J,L)=EL(J,L)-EL(IN1,L)-(CREC(L)*(TIME(J)-TIME(IN1)))
  380 CONTINUE
  390 CONTINUE
      IN1=IN2
  340 CONTINUE
      DO 00440 I=1,N
      IF(STYPE(I).EQ.   BLK')GO TO 440
      WRITE(15,00150)CODE(I),TIM1(I),STYPE(I),(EL(I,J),J=1,36
  440 CONTINUE
      STOP
      END
```

PROGRAM DATAFIX

```
PROGRAM DATAFIX(INPUT=131B,OUTPUT,TAPE=INPUT,TAPE1,TAPE6,
+TAPE7=OUTPUT,TAPE8)

      **********************************************************************

            PROGRAM TO CORRECT D.I.C.P.ANALYSES FOR BACKGROUND.
            OUTPUT IN MILLIVOLTS, EQUIVALENT PARTS PER MILLION,
            MILLIVOLTS /(RELATIVE SENSITIVITIES), OR RELATIVE
            ATOMIC PROPORTIONS (MV/KG).

      **********************************************************************

       DIMENSION BMAX(36),BMIN(36),BSUM(36),BSQSUM(36),BMEAN(36),
      +BVAR(36),SMAX(36),SMIN(36),SSUM(36),SSQSULM(36),SMEAN(36),
      +SVAR(36),ITIME(36),ATW(36),ATWT(36)INUM(36),ISET(36)
       COMMON/SAMP/IDUM(12),DATA(12,36),XMS(12)ID(12),ITT,IOPT,LPT1,LPT2
       COMMON/TIMEX/TIME(12),YNORM(36)
       COMMON/TITLE/ITIT(36)
       DATA(ITIT(L),L=1,36)/2HSE,2HZN,2HSR,2HSB,2HPB,2HBI,2HCD,
      +2HBA,2HNI,2HB ,2HMN,2HFE,2HP 2HS ,2HMG,2HMO,2HSN,2HSI,2HAS,
      +2HNA,2HAL,2HV ,2HBE,2HCA,2HTE,2HCU,2HAG,2HLI,2HTI,2HCO,2HZR,
      +2HHG,2HK,2HRB,2HLA,2HCR/
       DATA (ATWK),K=1,36)/78.96,65.38,87.62,121.75,207.2,208.98,
      +112.40,137.34,58.71,10.81,54.938,55.847,30.974,32.06,24.305,
      +95.94,118.69,28.086,74.922,22.990,26.982,50.941,9.012,40.08,
      +127.60,63.546,107.868,6.941,47.90,58.933,91.22,200.59,39.098,
      +85.468,138.901,51.996/

      *     SET UP ELEMENT SET    *

       NUM=0
       PRINT,"ELEMENT SET:"
       WRITE(7,20) ((L,ITIT(L)),L=1,36)
    20 FORMAT(6(6(12,3X,A2,5X),/))
       PRINT,"CHANGE ELEMENT SET Y/N (FORMAT A1)?"
       READ(5.21) NOPT
    21 FORMAT(A1)
       IF(NOPT.EQ.1HN) GO TO 1001
       PRINT,"ENTER NUMBER OF ELEMENTS TO BE CHANGED, FREE FORMAT."
       READ(5,*)NUM
       PRINT,"ENTER INDICES OF ELEMENTS TO BE CHANGED, FREE FORMAT."
       READ(5,*) (INUM(NN),NN=1,NUM)
       PRINT,"ENTER NEW ELEMENTS, A2 FORMAT SEPARATED BY BLANKS."
       READ(5.22) (INSET(NN),NN=1,NUM)
    22 FORMAT(2(18(A2,X),/))
       DO 1005 NN=1,NUM
       INN=INUM(NN)
       ITIT(INN)=I SET(NN)
  1005 CONTINUE
       PRINT,"NEW ELEMENT SET:"
       WRITE(7,20) ((L,ITIT(L)0,L=1,36)

       *   SELECT OUTPUT OPTION   *

  1001  PRINT,"SUPPLY OUTPUT OPTION, FREE FORMAT."
```

```
      PRINT,"FOR OUTPUT IN MILLIVOLTS, ENTER:0"
      PRINT,"FOR OUTPUT IN EQU.PPMS., ENTER:1"
      PRINT,"FOR OUTPUT IN MILLIVOLTS CORRECTED FOR RELATIVE"
      PRINT "SENSITIVITIES, ENTER: 2"
      PRINT,"FOR OUTPUT AS RELATIVE ATOMIC PROPORTIONS, ENTER: 3"
      READ(5,*) IOPT
      PRINT,"OUTPUT IN COLUMNS, Y/N ?"
      READ(5,21) LPTI
      PRINT,"OUTPUT IN BLOCK FORM, Y/N ?"
      READ(5,21) LPT2

      *   SET CORRECTION FACTORS FOR CONVERSION TO    *
      *   "EQU. PP.", MILLIVOLTS/(RELATIVE SENSITIVITIES),   *
      *   OR RELATIVE ATOMIC PROPORTIONS.    *

      IF(IOPT.NE.0) GO TO 1002
      DO 1015 K=1,36
 1015 YNORM(K)=1.0
      GO TO 1006
 1002 PRINT,"ENTER SENSITIVITIES FOR THE ELEMENTS,"
      PRINT,"FREE FORMAT."
      READ(5,*) (YNORM(K),K=1,36)
      IF(IOPT.EQ.1) GO TO 1003
      SODIUM=YNORM(20)
      00 1025 K=1,36
      YNORM(K)=YNORM(K)/SODIUM
 1025 CONTINUE
 1003 PRINT,"CORRECTION FACTORS:"
      WRITE(7,30) (YNORM(K),K=1,36)
   30 FORMAT(6(6F10.2/))
      IF(IOPT.NE.3) GO TO 1006
      IF(NUM.LE.0) GO TO 1004
      PRINT,"ENTER ATOMIC WEIGHTS, FREE FORMAT."
      READ(5,*) (ATWT(NN),NN=1,NUM)
      DO 1035 NN=1,NUM
      INN=INUM(NN)
      ATW(INN)=ATWT(NN)
 1035 CONTINUE
 1004 DO 1045 K=1,36
 1045 YNORM(K)=YNORM(K)*ATW(K)*.1E-2

      *   WRITE OUT HEADING TO TAPE 6    *

 1006 IF(IOPT.EQ.0) WRITE (6,40)
      IF(IOPT.EQ.1) WRITE (6,50)
      IF(IOPT.EQ.2) WRITE (6,50)
      IF(IOPT.EQ.3) WRITE (6,70)
   40 FORMAT(1H1/////20X,"PLASMA READINGS IN MILLIVOLTS"/)
   50 FORMAT(1H1/////20X,"PLASMA READINGS IN EQUIVALENT PPM."/)
   60 FORMAT(1H1/////20X,"PLASMA READINGS IN MILLIVOLTS CORRECTED FOR ",
     +/20X,"RELATIVE SENSITIVITIES."/
   70 FORMAT(1H1/////20X,"PLASMA READINGS EXPRESSED AS RELATIVE  ",
     +/20X,"ATOMIC PROPORTIONS (MV/KG).")

      *   READ IN FIRST BLANK FROM TAPE1.    *
```

```
      REWIND 1
      NBLANK=1
      IBLANK=1
      ITT=0
      IC=1
      TIME(IC)=0.0
      READ(1,10) (ITIME(M),M=1,3),IDUM(IC),XMS(IC),DATA(IC,J),J=1,36)
   10 FORMAT (4X,312,4X,A6,F10.3,10F10.0/3(30X,10F10.0/))
      ZTIME+(FLOAT(ITIME(1)))*60.0+FLOAT(ITIME(2))+
     +(FLOAT(ITIME(3)))/60.0

      *    SET STATISTICAL COUNTERS.    *

      DO 5 J=1,36
      SMAX(J)=0.0
      SMIN(J)=.1E6
      SSUM(J)=0.0
      SSQSUM(J)-0.0
      BMAX(J)=DATA(IC,J)
      BMIN(J)=DATA(IC,J)
      BSUM(J)=DATA(IC,J)
      BSQSUM(J)=DATA(IC,J)**2
    5 CONTINUE

      *    READ IN SAMPLES BETWEEN BLANKS    *

      ISAMP=0
  301 IC=IC+1
      READ(1,10) (ITIME(M),M=1,3),IDUM(IC),XMS(IC),DATA(IC,J),J=1,36)
      IF(EOF(1).NE.0.0) GO TO 101
      TIME(IC)=(FLOAT(ITIME(1)))*60.0+FLOAT(ITIME(2))+
     +(FLOAT(ITIME(3)))/60.0-ZTIME
      IF(TIME(IC).LE.0) TIME(IC)=TIME(IC+1440.
      IF(IDUM(IC).EQ.6H BLANK) GO TO 201
      IF(IOPT.EQ.0) CALL ASTAT(IC,SMAX,SMIN,SSUM,SSQSUM)
      ITT=ITT+1
      ISAMP=ISAMP+1
      ID(ISAMP)=IC
      GO TO 301

      *    COMPENSATE FOR BACKGROUND    *

  401 CALL FIX(ISAMP,IC)
      IOLD=IC
      NBLANK=1

      *  SET UP NEXT FIRST BLANK    *

      IC=1
      TIME(IC)=TIME(IOLD)
      UDUM(IC)=IDUM(IOLD)
      XMS(IC)=XMS(IOLD)
      DO 15 J=1,36
   15 DATA(IC,J)=DATA(IOLD,J)
```

```
      ISAMP=0
      GO TO 301
  101 CONTINUE
      WRITE(7,80) ITT
      WRITE(7,90) IBLANK
   80 FORMAT(///20X,"TOTAL NUMBERS OF SAMPLES EQUALS   ",14)
   90 FORMAT(///20X,"TOTAL NUMBER OF BLANKS EQUALS     ",14///)
      IF(ITT.EQ.0.OR.IOPT.NE.0) GO TO 501

      *   ANALYSIS OF BACKGROUND AND SAMPLE DATA.   *

      WRITE (7,100)
  100 FORMAT(///20X,"ANALYSIS OF BACKGROUND DATA (MILLIVOLTS):")
      CALL BSTAT(IBLANK,BMAX,BMIN,BSUM,BSQSUM,BMEAN,BVAR)
      WRITE(7,110)
  110 FORMAT(///20XX,"ANALYSIS OF SAMPLE DATA (MILLIVOLTS:",
     +"UNCORRECTED):")
      CALL BSTAT(ITT,SMAX,SMIN,SSUM,SSQSUM,SMEAN,SVAR)
      WRITE(7,120)
      DO 35J=1,36
      IF(SVAR(J).LT.BVAR(J)) GO TO 86
      F=SVAR(J)/BVAR(J)
      N1=ITT-1
      N2=IBLANK-1
      GO TO 87
   86 F=BVAR(J)/SVAR(J)
      N1=IBLANK-1
      N2-ITT-1
   87 N=N1+N2
      B=FLOAT(IBLANK)
      S=FLOAT(ITT)
      SPSQ=((B-1.)*BVARC(J)+(S-1.)*SVARC(J))/(B+S-2.)
      SP=SQRT(SPSQ)
      X=SQRT(1./B+1/S)
      T=(BMEAN(J)-SMEAN(J))/SP*X)
      WRITE(7,130) ITIT(J),N1,N2,F,N,T
   35 CONTINUE
  120 FORMAT(///13X,"V1",3X,"V2",4X,"F-TEST",14X,"V",4X,
     +"T-TEST',/X,"ELEMENT:")
  130 FORMAT(5X,A2,3X,215,F10.2,10X,15,F10.2)
  501 STOP
      END

      *   SUBROUTINE FIX CORRECTS THE DATA   *
      *   FOR BACKGROUND   *

      SUBROUTINE FIX(IS,IC)
      COMMON/SAMP/IDUM(12),DATA(12,36),XMS(12),ID(12),ITT,IOPT,LPT1,LPT2
      COMMON/TIMEX/TIME(12),YNORM(36)
      IF(IS.EQ.0) RETURN
      XO=TIME(1)
      XN=TIME(IC)
      DO 1 J=1,36
      YO=DATA(IC,J)
      YN=DATA(IC,J)
```

```
      SLOPE=(YN-YO)/(XN-XO)
      C=YO
      DO 2 I=1,IS
      I1=ID(I)
      X=TIME(I1)-XO
      Y=SLOPE*X+C
      DATA(I1,J=DATA(I1,J)-Y
      IF(DATA(I1,J).LT.0) DATA(I1,J)=0.
      DATA(I1,J)=DATA(I1,J)/(YNORM(J)*XMS(I1))
    2 CONTINUE
    1 CONTINUE
      IF(LPT1.NE.1HN) CALL CPRINT(IS)
      IF(LPT2.EQ.1HY) CALL BPRINT(IS)
      RETURN
      END

      *   SUBROUTINE CPRINT WRITES THE DATA OUT IN   *
      *   COLUMNS.   *

      SUBROUTINE CPRINT(IS)
      COMMON/SAMP/IDUM(12),DATA(12,36),XMS(12),ID(12),ITT,IOPT,
     +LPT1,LPT2
      COMMON/TITLE/ITIT(36)
      DO 3 I=1,IS
    3 ID(I)=ITT-IS+I
      WRITE(6,30) (ID(I),I=1,IS)
      WRITE(6,40) (IDUM(I),I=2,IS+1)
      WRITE(6.50)
      IF(IOPT.EQ.1) GO TO 101
      DO 4 J=1,36
      WRITE(6,10) ITIT(J),(DATA(I,J)I=2,IS+1)
    4 CONTINUE
      GO TO 201
  101 DO 5 J=1,36
      WRITE(6,20) ITIT(J),(DATA(I,J),I=2,IS+1)
    5 CONTINUE
  201 CONTINUE
   10 FORMAT(5X,A2,3X,10F10.2)
   20 FORMAT(5X,A2,3X,10E10.3)
   30 FORMAT(///11X,10(2X,T4,4X))
   40 FORMAT(3X,"SAMPLE NO:",10(A6,4X))
   50 FORMAT(/X,"ELEMENT:")
      RETURN
      END

      *   SUBROUTINE BPRINT WRITES THE DATA OUT IN   *
      *   BLOCK FORM.   *

      SUBROUTINE BPRINT(IS)
      COMMON/SAMP/IDUM(12),DATA(12,36),XMS(12),ID(12),ITT,IOPT,LPT1,LPT2
      DO 5 I=2,IS+1
      IF(IOPT.NE.1) WRITE(8,10) IDUM(I),(DATA(I,J),J=1,36
      IF(IOPT.EQ.1) WRITE(8.20) IDUM(I),(DATA(I,J),J=1,36
    5 CONTINUE
   10 FORMAT(A6,4X,9F10.2/3(10X,9F10.2/))
```

```
20 FORMAT(A6,4X,9E10.3/3(10X,9E10.3/))
   RETURN
   END

   *   SUBROUTINE ASTAT CALCULATES THE MAXIMUM AND MINIMUM   *
   *   VALUES FOR EACH ELEMENT IN THE SAMPLES AND IN THE     *
   *   BLANKS: AND KEEPS RUNNING TOTALS OF THE INTENSITY     *
   *   AND THE SQUARE OF THE INTENSITY.   *

   SUBROUTINE ASTAT(IC,XMAX,XMIN,XSUM,XQSUM)
   COMMON/SAMP/IDUM(12),DATA(12,36),XMS(12),ID(12),ITT,IOPT,LPT1,LPT2
   DIMENSION XMAX(36),XMIN(36),XSUM(36),XSQSUM(36)
   DO 5 J=1,36
   IF(DATA9IC,J).GT.XMAX(J)) XMAX(J)=DATA(IC,J)
   IF(DATA(IC,J).LT.XMIN(J)) XMIN(J)=DATA(IC,J)
   XSUM(J)=XSUM(J)+DATA(IC.J)
   XSQSUM(J)=XSQSUM(J)+DATA(IC,J)**2
 5 CONTINUE
   RETURN
   END

   *   SUBROUTINE BSTAT CALCULATES THE MEAN AND STANDARD     *
   *   DEVIATION FOR EACH ELEMENT AND WRITES THEM OUT TO     *
   *   TAPE 7.   *

   SUBROUTINE BSTAT(N,MAX,XMIN,XSUM,XSQSUM,XMEAN,XVAR)
   DIMENSION XMAX(36),XMIN(36),XSUM(36),XSQSUM(36),XMEAN(36),
  +XVAR(36)
   COMMON/TITLE/ITIT(36)
   WRITE(7,10)
   X=FLOAT(N)
   DO 5 J=1,36
   XMEAN(J)=XSUM(J)/X
   XSUMSQ=XSUM(J)**2
   XVAR(J)=(X*XSQSUM(J)-XSUMSQ)/(X*(X-1.))
   SDB=SQRT(XVAR(J))
   RSDB=SDB*100./XMEAN(J)
   WRITE(7.20) ITIT(J),XMAX(J),XMIN(J),XMEAN(J),SDB,RSDB
 5 CONTINUE
10 FORMAT(15X,"MAX",5X,"MIN,6X,"MEAN",5X,"ST.DEV.",5X," % DEV.",
  +/X'"ELEMENT:")
20 FORMAT(5X,A2,3X,2F10.2,3F10.3F10.2)
   RETURN
   END
```

APPENDIX V

LOGIC LISTING FOR THE PROGRAM TO PRODUCE CURVES FOR THE ESTIMATION OF XCO2 IN FLUID INCLUSIONS (FIGURE 5.3)

Introduction

The program listed was developed in conjunction with fellow student Roger Burleigh, and its final form owes much to his computing skill. The idea to develop a graph from which the molar proportion of carbon dioxide in three phase fluid inclusions could be rapidly estimated, providing TH CO2 and degree of fill have been estimated, was first discussed at Imperial College, London.

The estimation of mole proportion carbon dioxide in a three phase fluid inclusion is time consuming when dealing with moderate to large data sets. Program MOLECO constructs a series of curves which predict the molar proportion of carbon dioxide for any combination of degree of fill between 0.1 to 0.9 and TH CO2 between 0°C and 31.1°C (to either liquid or gas) for pure water and carbon dioxide inclusions.

Calculation of the mole proportion of carbon dioxide requires reference to three separate graphs if the technique outlined in the Mineralogical Association of Canada short course in fluid inclusions handbook, is used (Burruss, 1981, p61). Program MOLECO uses the same fundemental assuptions outlined by Burruss (1981), these are:

a) at temperatures greater than 31.1°C but less than 50°C

the coexisting phases are pure end members. This is assumed to be reasonable because the solubility of water in carbon dioxide is less than 0.6 mole % and that of carbon dioxide in water, less than 3 mole % at the temperature range and pressures considered i.e. less than 500 bars. However the program can be easily modified to account for the mutual solubilities if desired.

b) The bulk molar volume (or bulk density) of an inclusion is linear combination of the end member components i.e.

$$VB = X1.V1+X2.V2 \quad cm^3/mole$$

where X1 and X2 are the mole fraction of the first and second pure component phase respectively. V1 and V2 are the molar volumes of these pure component phases and VB the bulk molar volume. The bulk density of the inclusion can be estimated using the relationship:

$$1/VB \times 1000 = (moles/liter)$$

C) At temperatures less than 40 °C, water is incompressible and the internal pressure within an inclusion is fixed by the isochore for the one-phase carbon dioxide fluid at the specified temperature.

Program MOLECO contains an option for estimating the mole proportion of carbon dioxide in carbon - dioxde - water - sodium chloride inclusions. The bulk density of the brine solution calculated by the program results in a minor underestimation (<1% at < 10 wt % sodium chloride compared to the density values of Weast (1984). This relatively insignificant discrepancy results from electro -striction effects not considered in the prgram.

The mole proportion of carbon dioxide is calculated thus, (for pure carbon dioxide and water inclusions):

$$XCO2 = \frac{\text{Moles CO2}}{\text{Moles CO2 + Moles H2O}}$$

The number of moles of each component present is a function of the volumetric proportion of each component (carbon dioxide and aqueous liquid) observed at 40 °C and the estimated density of each pure component. It should be noted that the largest source of possible error in the estimation of mole proportion carbon dioxide is that associated with the initial volumetric estimate of phases.

PROGRAM MOLECO

```
      DIMENSION XCG(34),RG(17),RL(17)
      CHARACTER*4 TRAY(8),YRAY(8),LYARAY(1)
      CHARACTER*2 DEGREE(9)
      INTEGER G,R,S,TIWORD,OWORD,IYWORD,
     1 OYTOT,TYTOT,IYTOT
      DATA (TRAY(R),R=1,8)/'28  ','24  ','20  ','16  ','12  ','8   ',
     1 '4   ','0   '/
      DATA (YRAY(S),S=1,8)/'0   ','4   ','8   ','12  ','16  ','20  ',
     1 '24  ','28  '/
      DATA (LYARAY(K),K=1,1)/'31.1'/
      DATA (DEGREE(J),J=1,9)/'.1','.2','.3','.4','.5','.6','.7','.8','.9'/
      REAL DG(17)/.0955,.102,.109,.1175,.126,.134,.143,.155,.166,.18,.197,
     1 .212,.234,.254,.291,.345,.4/
      REAL DL(17)/.912,.901,.891,.88,.869,.857,.845,.83,.811,.795,.772,
     1 .75,.724,.7,.652,.6,.4/
      REAL YG(34)/0,2,4,6,8,10,12,14,16,18,20,22,24,26,28,30,31.1,
     1 31.1,32.2,34.2,36.2,38.2,40.2,42.2,44.2,46.2,48.2,50.2,52.2,
     1 54.2,56.2,58.2,60.2,62.2/
      PRINT *,'INPUT WEIGHT % SALT'
      READ *,WTSALT
      CALL REGIS (1,1)
      CALL COMPRS
      CALL NOBRDR
      CALL PHYSOR(.75,3.75)
      CALL AREA2D(6.5,6.5)
      YAXIS=6.5
      YORIG=0.
      YSTP=2.0
      YMAX=62.2
      XAXIS=6.5
      XORIG=0.0
      XSTP=.1
      XMAX=1.0
      CALL XNAME('MOLAR PROPORTION CO2; XCO2',26)
      CALL YTICKS(0)
      CALL XTICKS(10)
      CALL GRAF(XORIG,XSTP,XMAX,YORIG,YSTP,YMAX)
      VTSA=(WTSALT*10)/(2.16)
      VTS=(100.-WTSALT)*10.
      Z=1000./(VTSA+VTS)
C
C     DO LOOP FOR CURVE TRACING
C
      DO 2 F=10,90,10
        T=0
        DO 1 I=1,17
        MG=(F*Z)+((100-F)*DG(I))
        D1=10*MG
        RG(I)=D1/1000
        WCG=((100-F)*DG(I))*100/MG
```

```
            WHG=(F*Z)*100/MG
            WHGA=WHG*(1-(WTSALT/100))
            WNACL=WHG*(WTSALT/100)
            PHG1=WHGA/18.015
            PNACL=WNACL/58.52
            PCG=WCG/44
            XCG(I)=PCG/(PCG+PHG1+PNACL)
C
C            SAME CALCULATIONS FOR CO2
C            HOMOGENISE TO LIQUID
C
            ML=(F*Z)+((100-F)*DL(I))
            D2=10*ML
            RL(I)=D2/1000
            WCL=((100-F)*DL(I)*100)/ML
            WHL=(F*Z)*100/ML
            WHLA=WHL*(1.-(WTSALT/100))
            WNACLL=WHL*(WTSALT/100)
            PHL1=WHLA/18.015
            PNACLL=WNACLL/58.52
            PCL=WCL/44
            T=35-I
            XCG(T)=PCL/(PCL+PHL1+PNACLL)
1          CONTINUE
C           CALL DASH
            CALL RASPLN(1)
            CALL CURVE(XCG,YG,34,0)
C           CALL RESET('DASH')
          CALL HEIGHT(.07)
          CALL CWIDTH('CONDENSED')
          XPOS=(XCG(28)*6.5)-.2
          YPOS=6.0
          G=F/10
          CALL MESSAG(ZREF(DEGREE(G)),2,XPOS,YPOS)
2          CONTINUE
         CALL RESET('HEIGHT')
         CALL RESET('CWIDTH')
          OAXIS=(6.5/2.)*(28./31.1)
          YORIG=0.
          OWORD=1
          OYTOT=8
          YPOS=0.0
          XPOS=0.0
          CALL YAXANG(0.)
          CALL YTICKS(4)
          CALL YLBAXS(ZREF(YRAY),OWORD,OYTOT,OAXIS,'CO2 Homo. Tc Gas; Deg. C.',
         1 25,XPOS,YPOS)
          YAXIS=(6.5/2.)*(28./31.1)
          TIWORD=1
          TYTOT=8
```

```
      YPOS=6.5-((6.5/2.)*(28./31.1))
      XPOS=0.
      CALL YLBAXS(ZREF(TRAY),TIWORD,TYTOT,YAXIS,'CO2 Homo. To Liq.; Deg. C.'
     1 ,26,XPOS,YPOS)
      XPOS=-.425
      YPOS=(6.5/2.)-.065
      YAXIS=1.
      IYTOT=1
      IYWORD=1
     CALL MESSAG(ZREF(LYARAY),4,XPOS,YPOS)
      XPOS=5.3
      YPOS=6.0
     CALL MESSAG('DEGREE OF$',9,XPOS,YPOS)
      XPOS=5.3
      YPOS=5.75
     CALL MESSAG('FILLING$',7,XPOS,YPOS)
      XPOS=5.3
      YPOS=5.5
     CALL MESSAG('LIQUID$',6,XPOS,YPOS)
      XPOS=0.0
      YPOS=6.5
      CALL STRTPT(XPOS,YPOS)
      CALL CONNPT(6.5,YPOS)
      XPOS=6.5
      YPOS=6.5
      CALL STRTPT(XPOS,YPOS)
      CALL CONNPT(XPOS,0.0)
      XPOS=0.1
      YPOS=3.25
      CALL DASH
      CALL STRTPT(XPOS,YPOS)
      CALL CONNPT(6.5,YPOS)
      CALL MESSAG('GRAPH FOR THE ESTIMATION OF XCO2$',32,1.0,-1.)
      CALL MESSAG('BASED ON HOMOGENISATION TEMPERATURE$',35,.85,-1.2)
      CALL MESSAG('OF CO2 IN CO2-H2O INCLUSIONS$',28,1.2,-1.4)
C     CALL MESSAG('CURVE =',7,3.7,.75)
C     CALL REALNO(WTSALT,1,'ABUT','ABUT')
C     CALL MESSAG(' Wt.% NaCl',10,'ABUT','ABUT')
C     CALL RESET('DASH')
C     CALL DASH
C     CALL STRTPT(3.2,.755)
C     CALL CONNPT(3.6,.755)
       CALL ENDPL(0)
       CALL DONEPL
       END
```

APPENDIX VI

ADDITIONAL MICROTHERMOMETRIC DATA

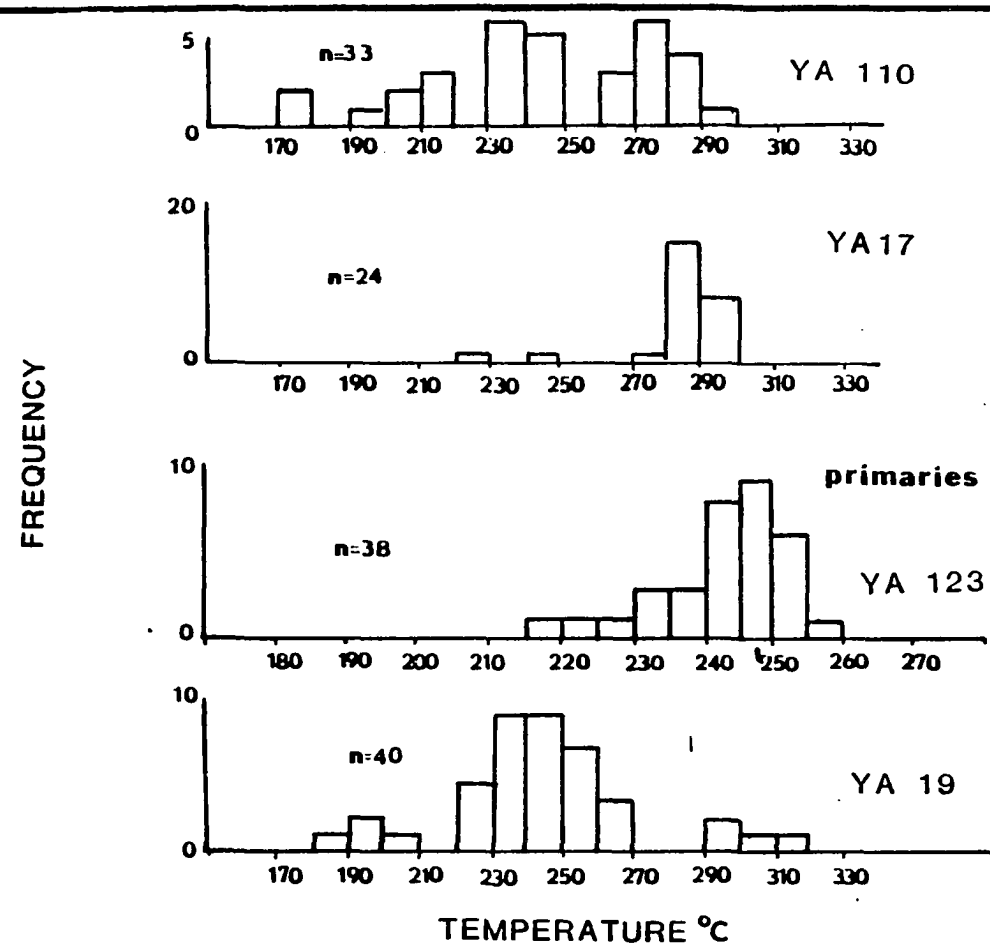

Figures A6.1,2,3 and 4 Histograms of TH for quartz veins (Type 3 inclusions)

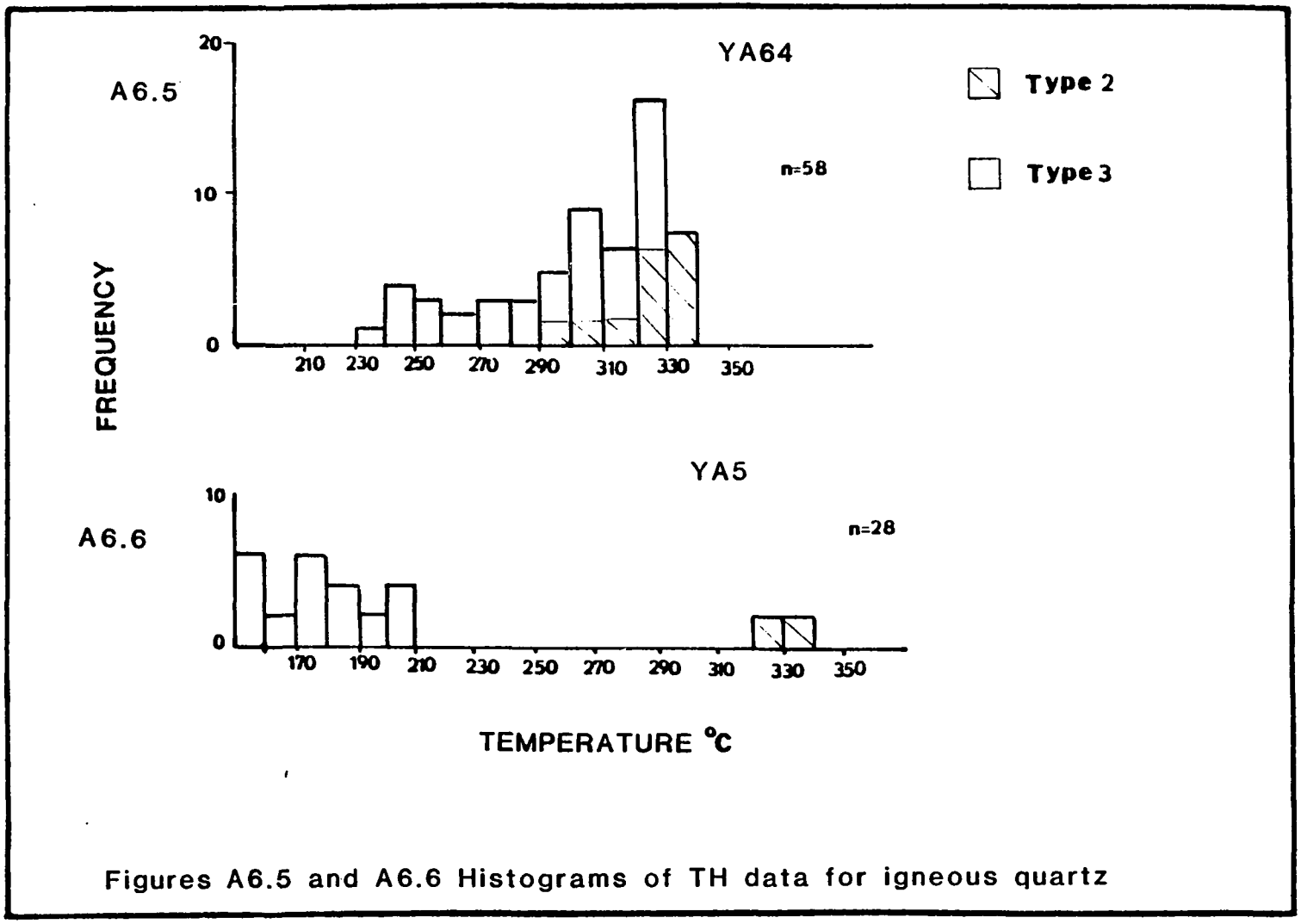

Figures A6.5 and A6.6 Histograms of TH data for igneous quartz

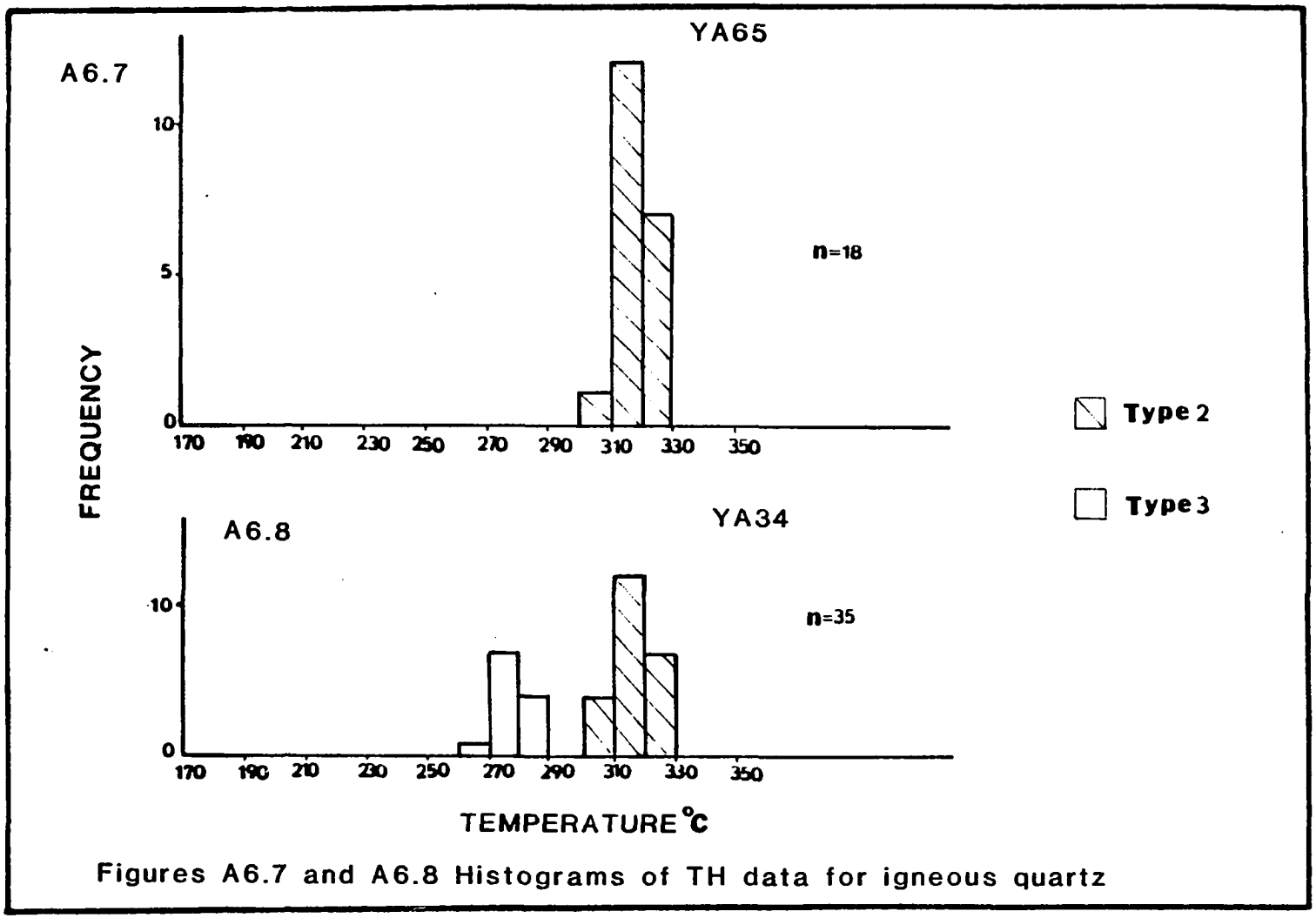

Figures A6.7 and A6.8 Histograms of TH data for igneous quartz

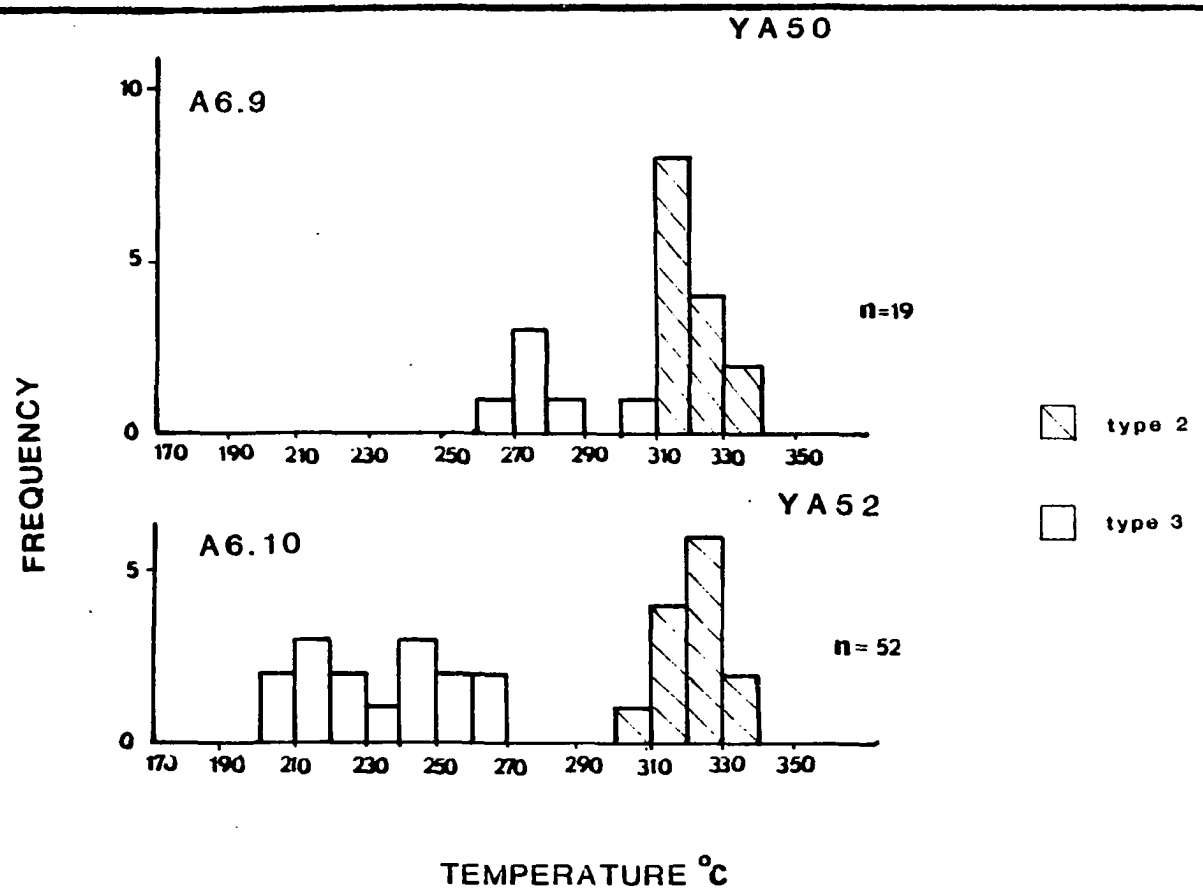

Figures A6.9 and A6.10 Histograms of TH data for quartz from the EW granodiorite

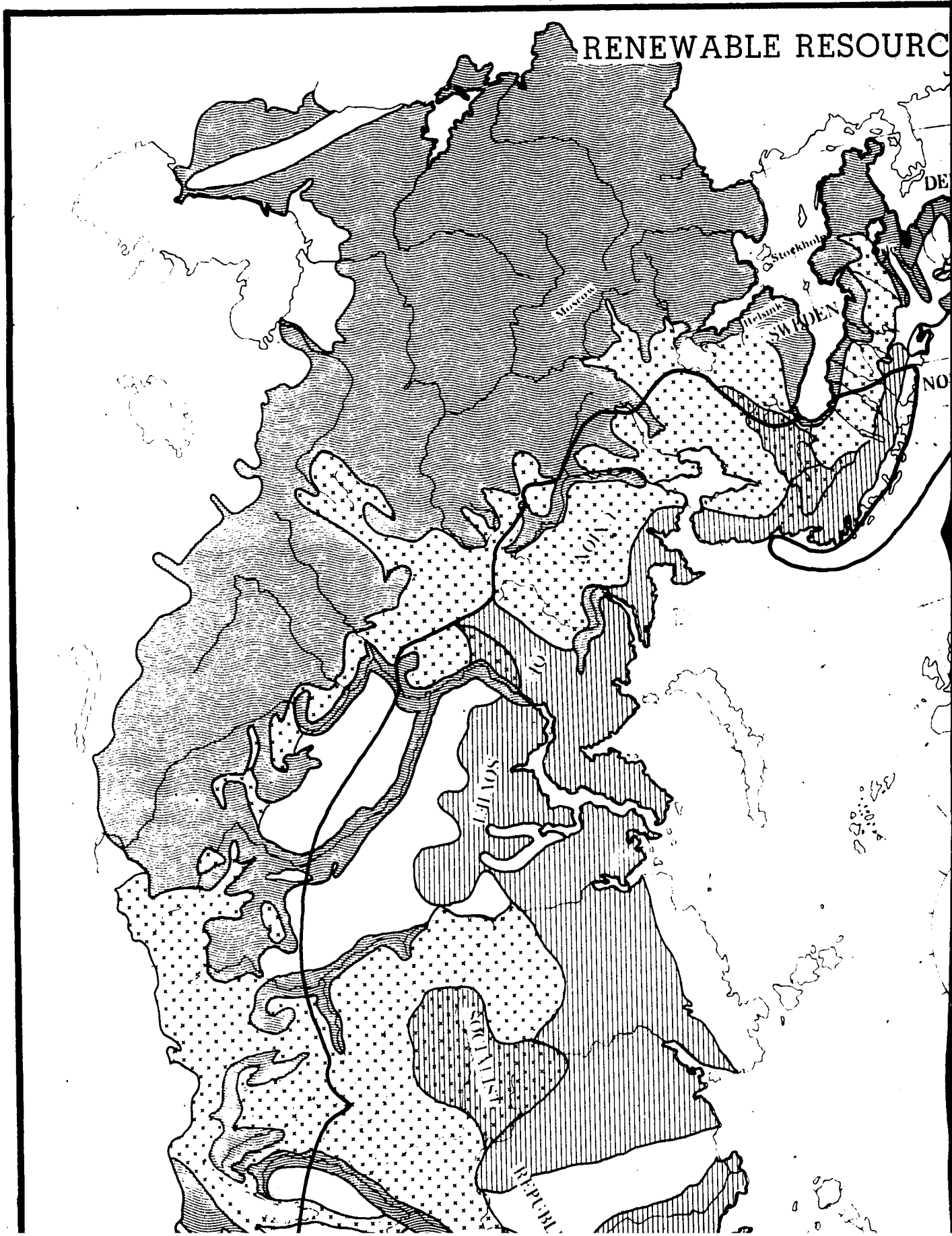

RESOURCES OF THE CIRCUMPOLAR NORTH

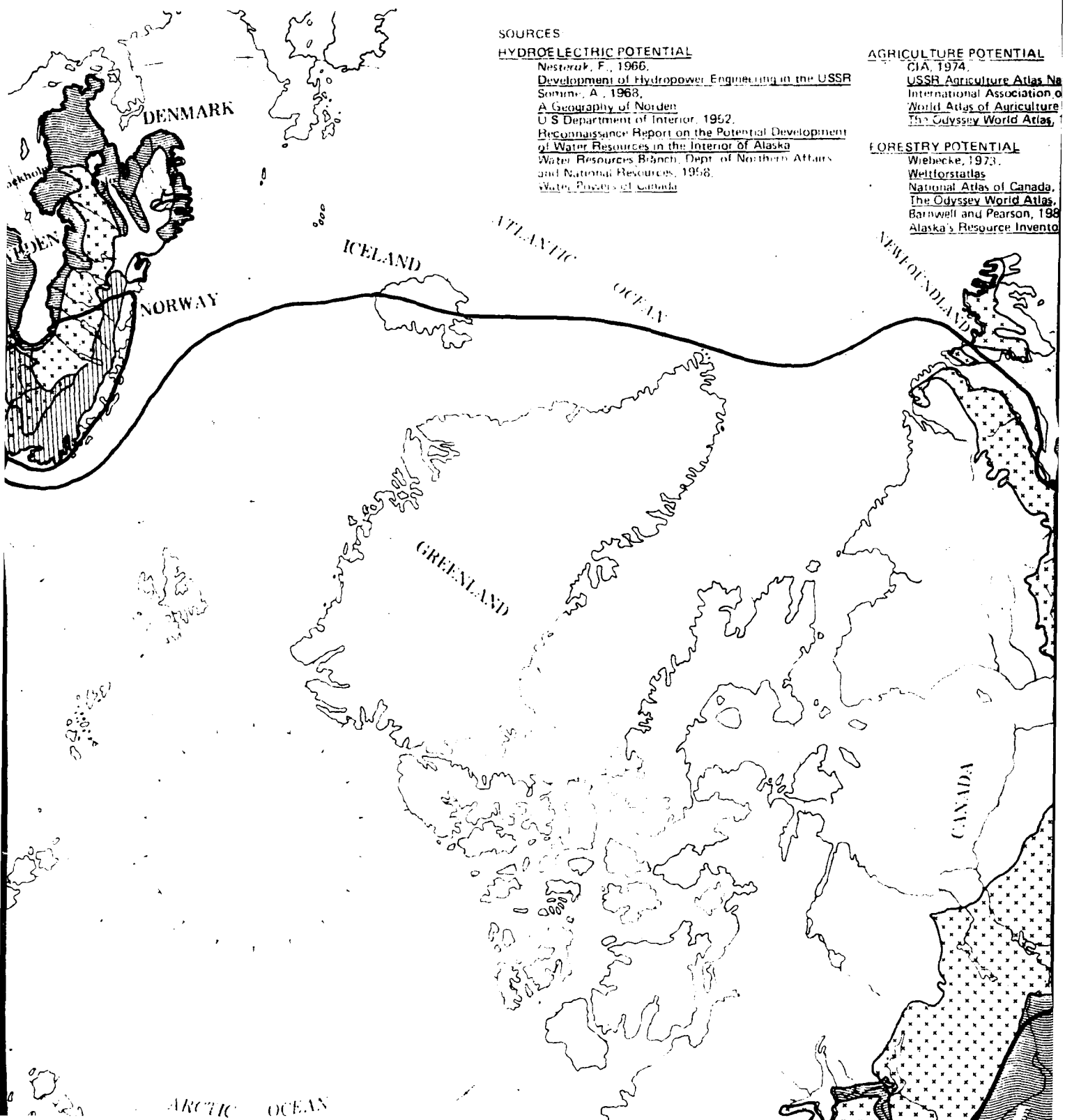

SOURCES

HYDROELECTRIC POTENTIAL

Nesterak, F., 1966.
Development of Hydropower Engineering in the USSR
Somme, A., 1968.
A Geography of Norden
U S Department of Interior, 1952.
Reconnaissance Report on the Potential Development of Water Resources in the Interior of Alaska
Water Resources Branch, Dept. of Northern Affairs and National Resources, 1958.
Water Powers of Canada

AGRICULTURE POTENTIAL

CIA, 1974.
USSR Agriculture Atlas Na
International Association o
World Atlas of Agriculture
The Odyssey World Atlas,

FORESTRY POTENTIAL

Wiebecke, 1973.
Weltforstatlas
National Atlas of Canada,
The Odyssey World Atlas,
Barnwell and Pearson, 198
Alaska's Resource Invento

CIRCUMPOLAR NORTH

SOURCES

HYDROELECTRIC POTENTIAL

Nesteruk, F., 1966.
Development of Hydropower Engineering in the USSR
Somme, A., 1968,
A Geography of Norden
U S Department of Interior 1952,
Reconnaissance Report on the Potential Development of Water Resources in the Interior of Alaska
Water Resources Branch, Dept. of Northern Affairs and National Resources, 1968
Water Powers of Canada

AGRICULTURE POTENTIAL

CIA, 1974,
USSR Agriculture Atlas National Atlas of Canada
International Association of Agriculture Economics, 1969,
World Atlas of Agriculture
The Odyssey World Atlas, 1974

FORESTRY POTENTIAL

Wiebecke, 1973,
Weltforstatlas,
National Atlas of Canada, 1975
The Odyssey World Atlas, 1974
Barnwell and Pearson, 1984,
Alaska's Resource Inventory

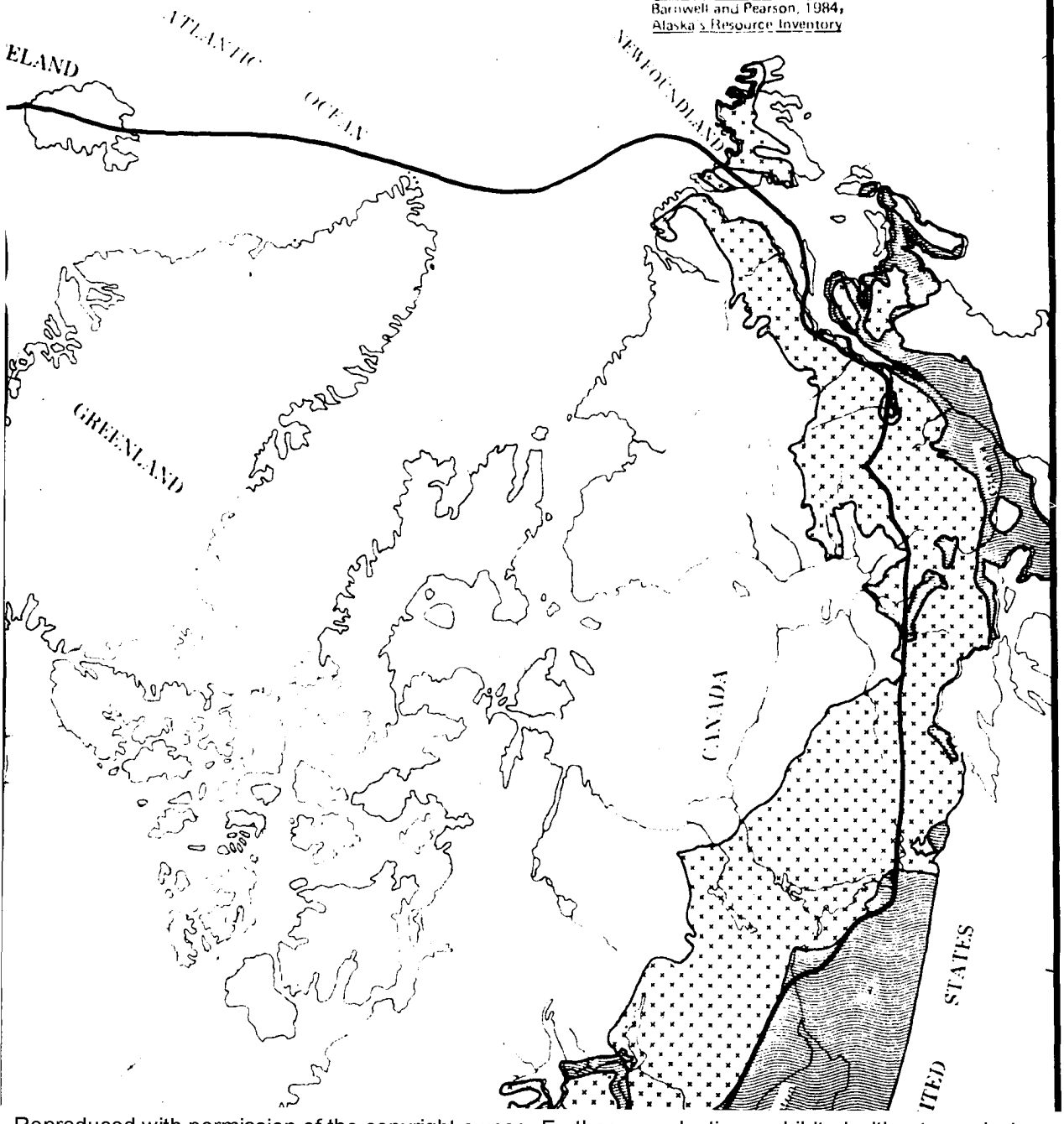

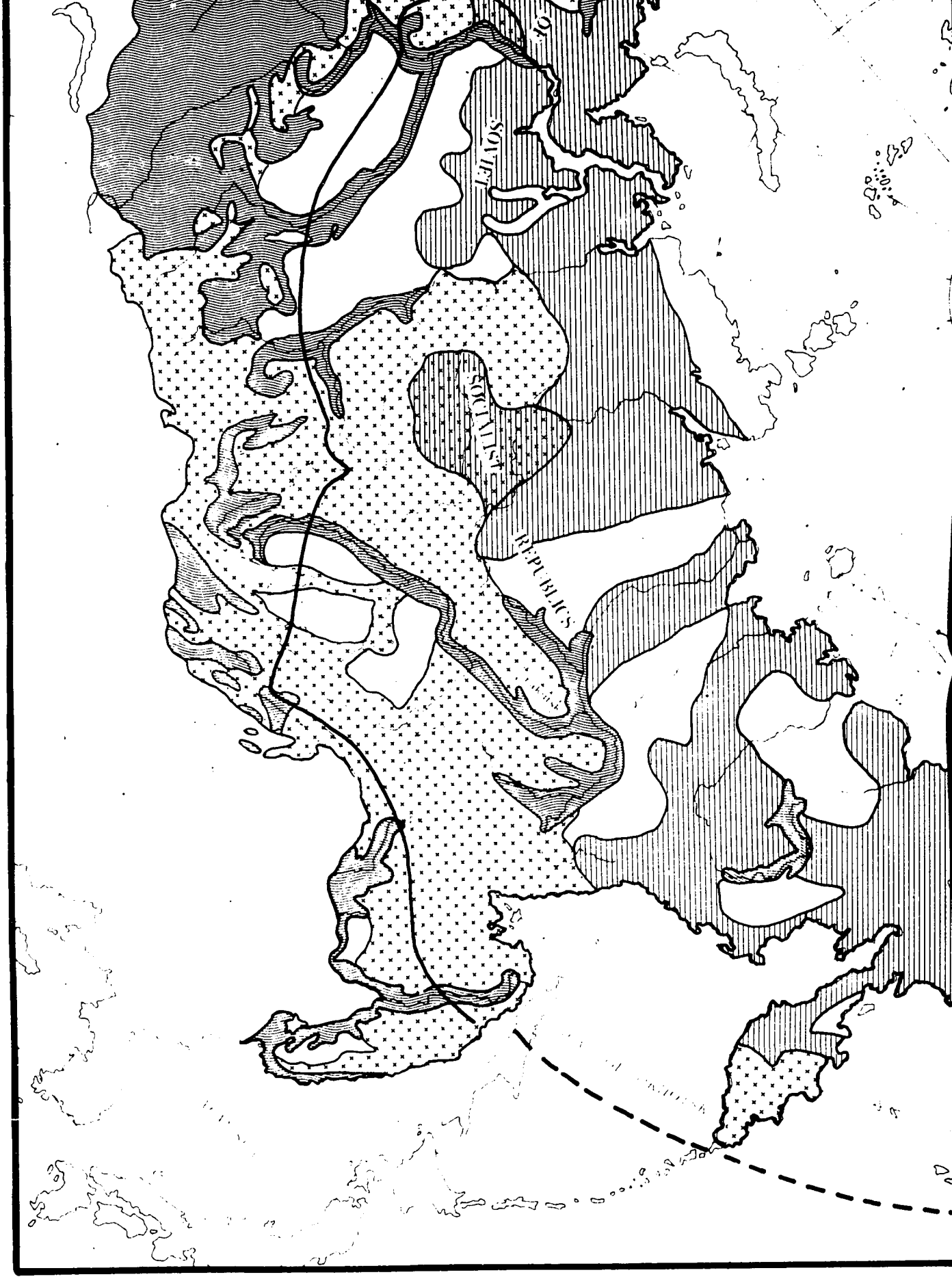

Figure 2: F

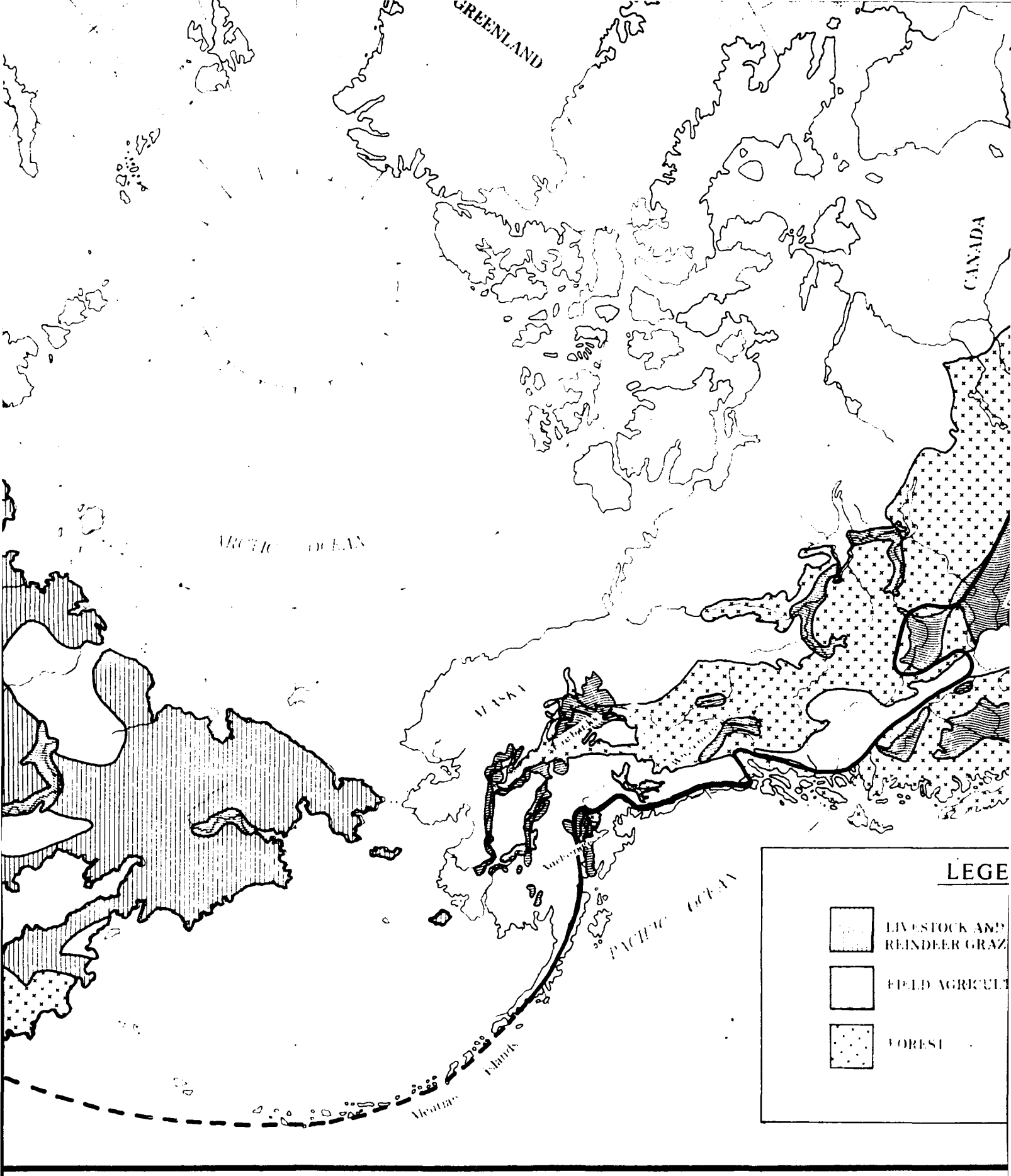

Figure 2: Renewable resources of the northlands

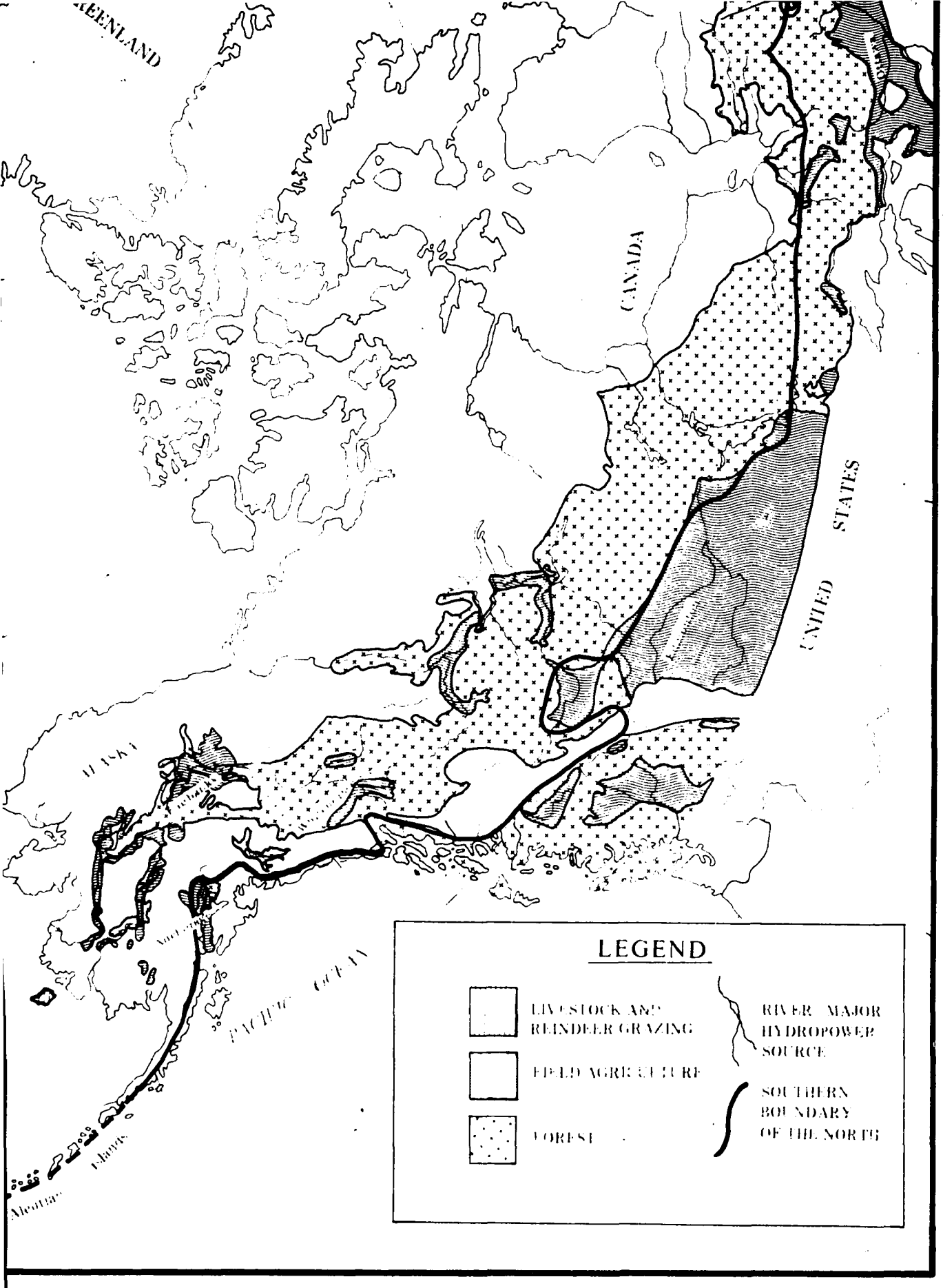

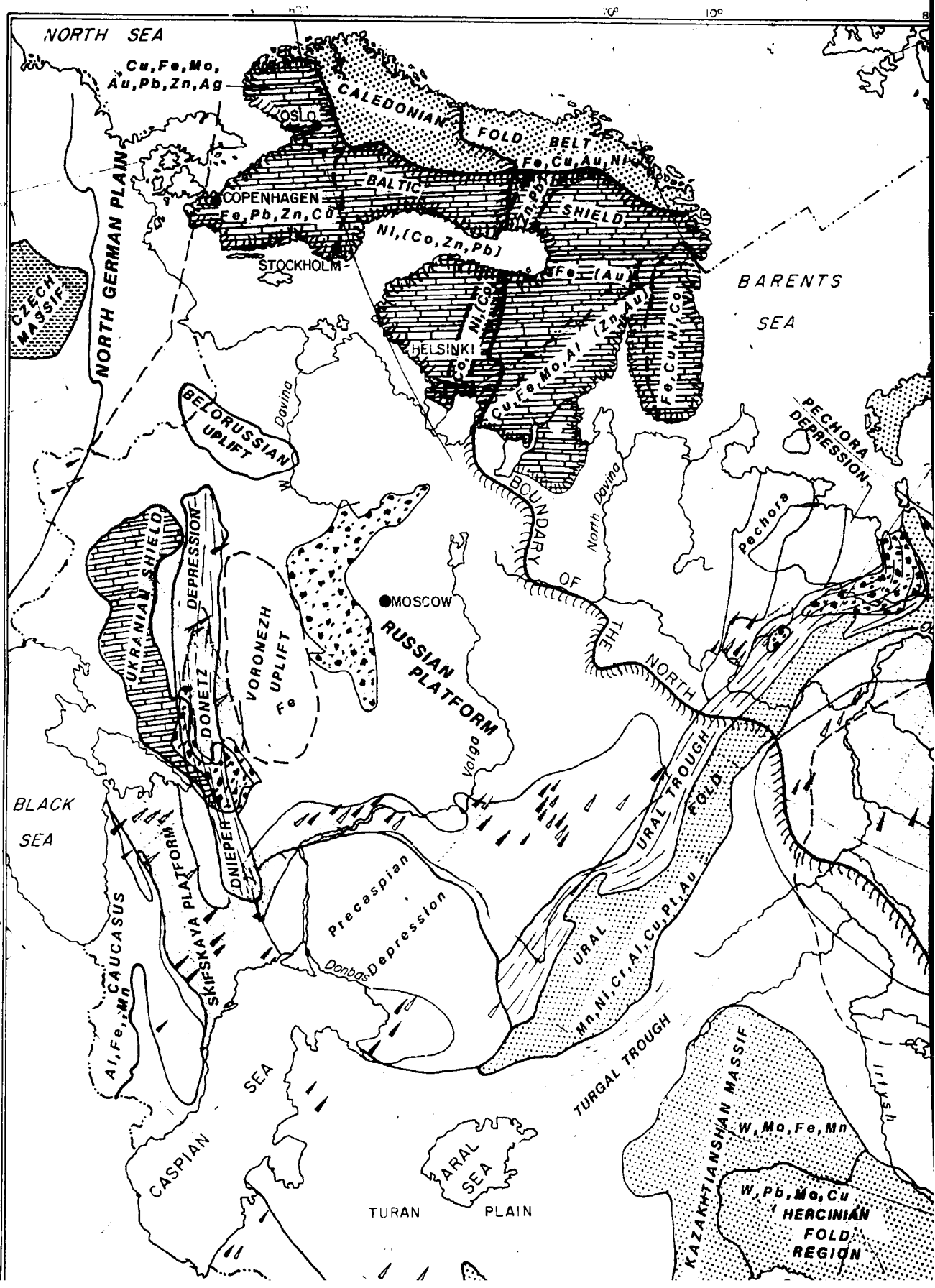

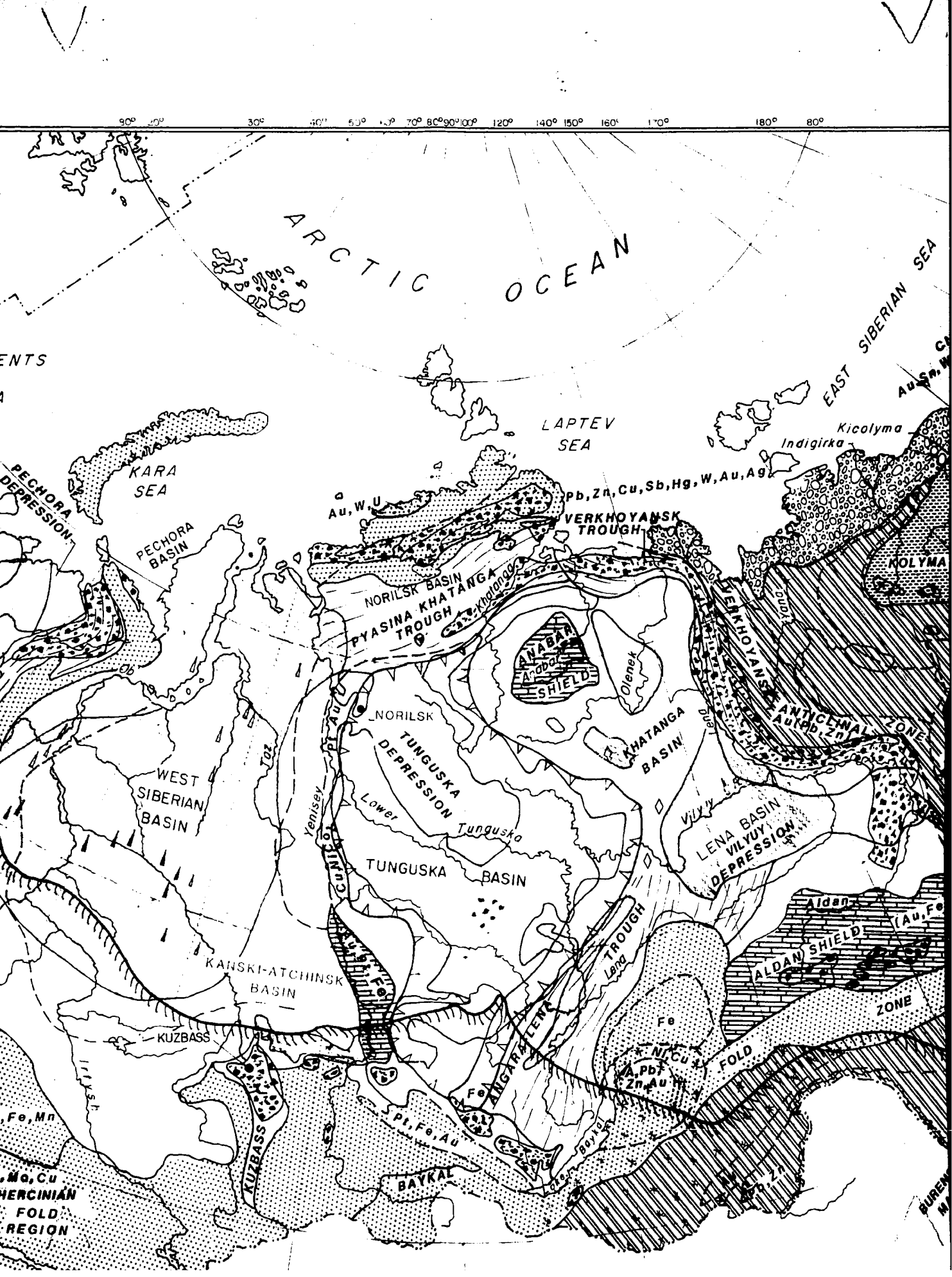

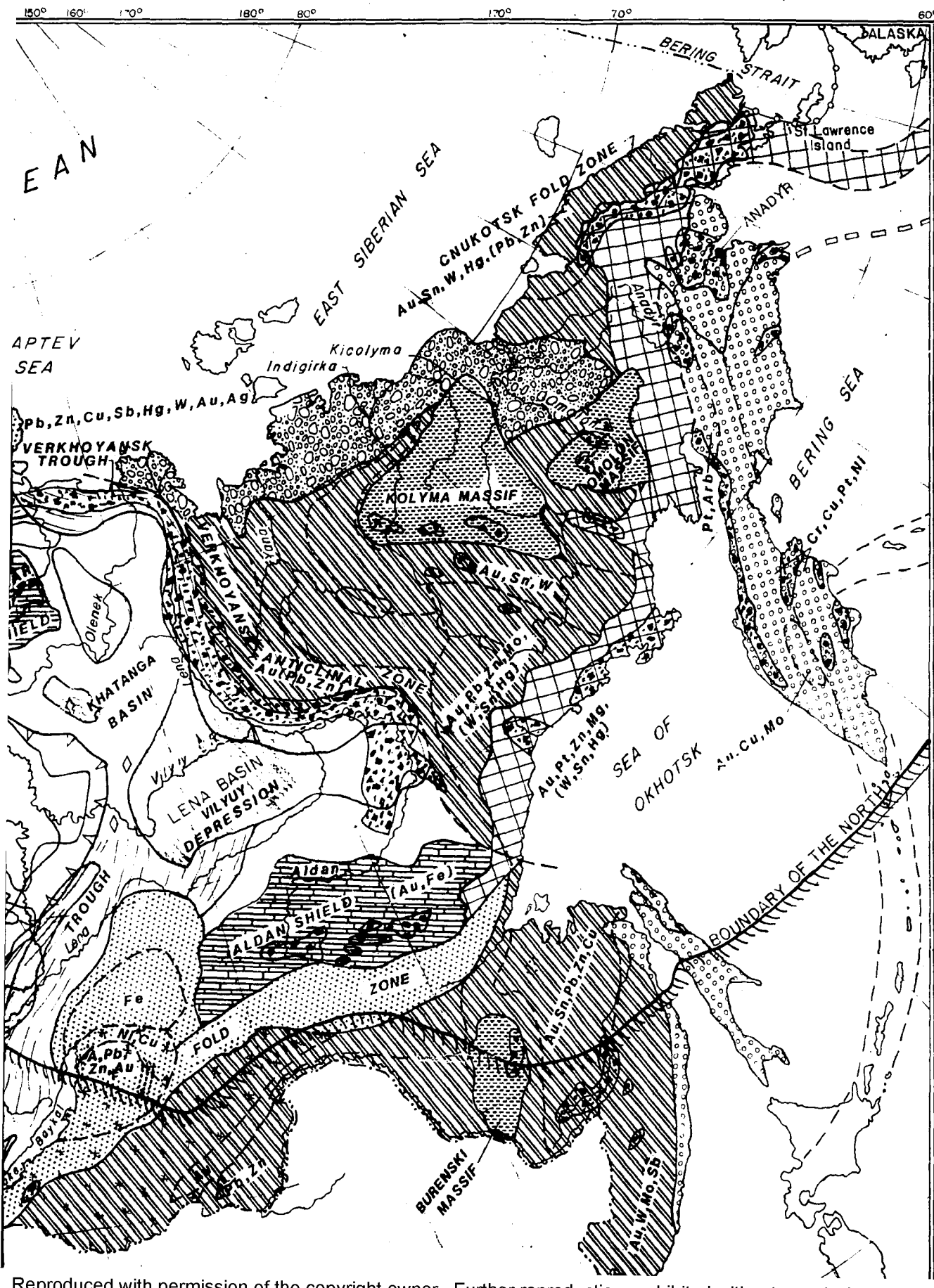

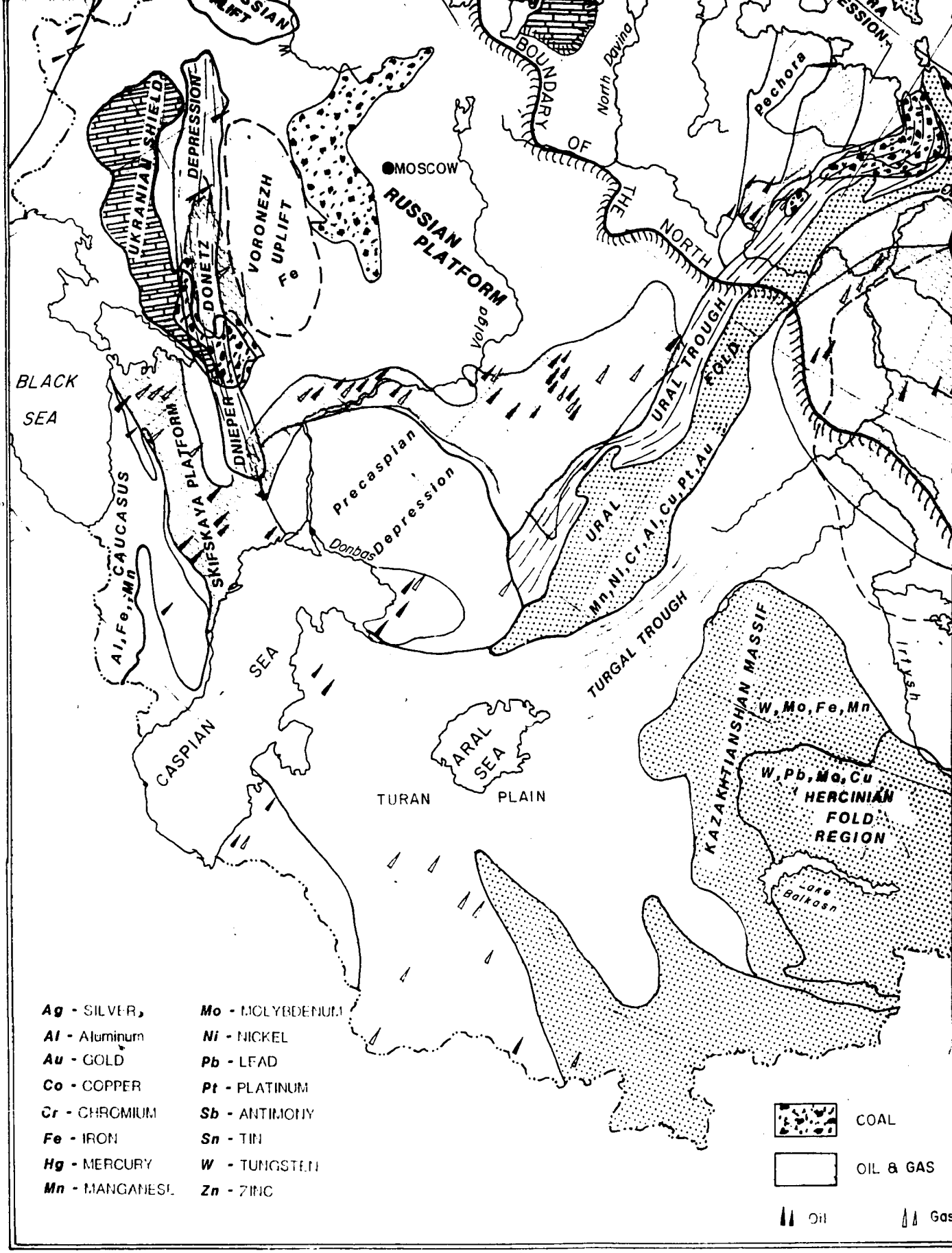

Figure 3:

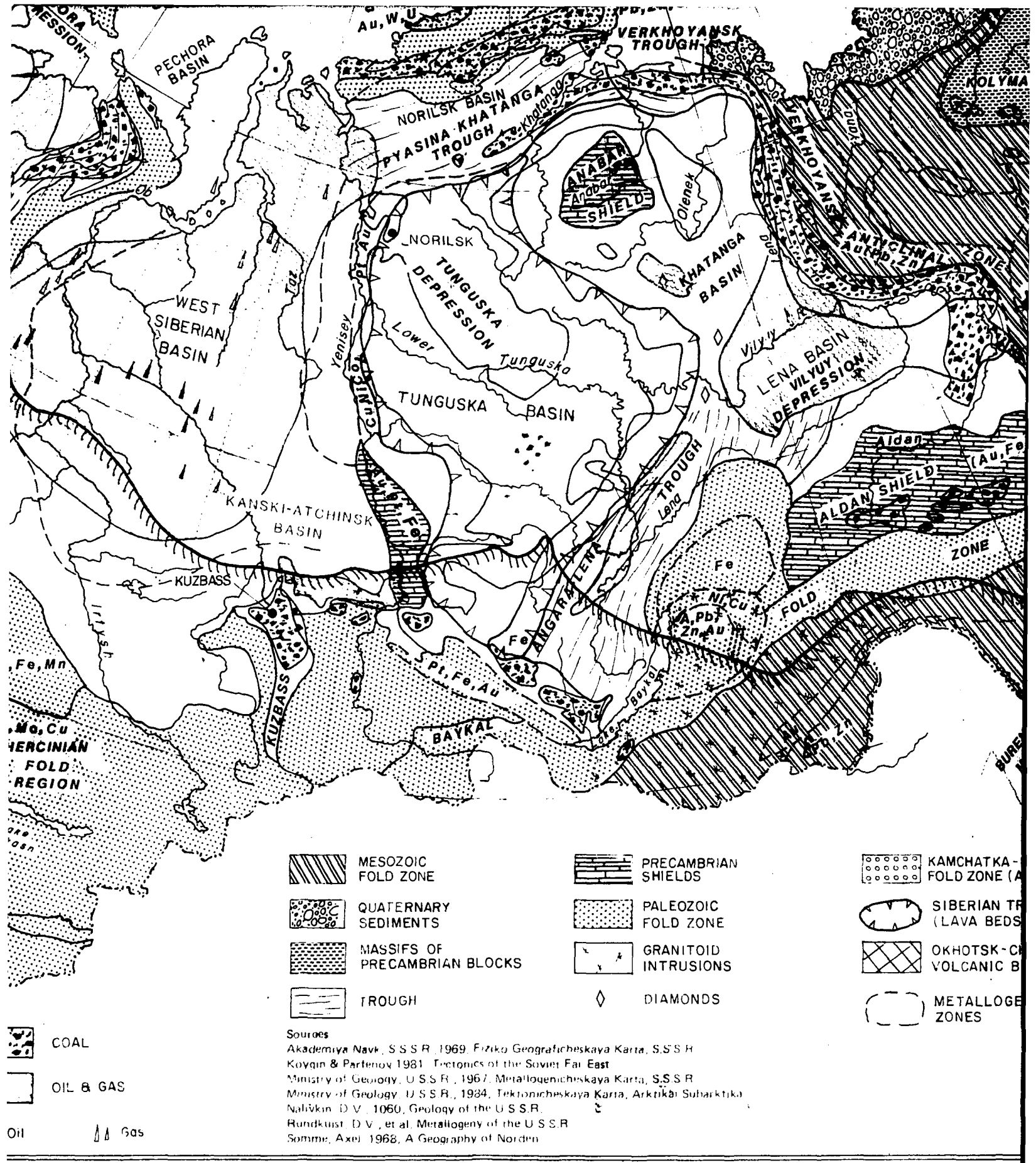

Sources

Akademiya Navk, S.S.S.R. 1969, Fiziko Geograficheskaya Karta, S.S.S.R.

Koygin & Parfenov 1981, Tectonics of the Soviet Far East

Ministry of Geology, U.S.S.R., 1967, Metallogenicheskaya Karta, S.S.S.R.

Ministry of Geology, U.S.S.R., 1984, Tektonicheskaya Karta, Arktikai Subarktika

Nalivkin, D.V., 1960, Geology of the U.S.S.R.

Rundkvist, D.V., et al, Metallogeny of the U.S.S.R.

Somme, Axel, 1968, A Geography of Norden

Figure 3: Geotectonic features and mineral zones, Eurasian Northlands

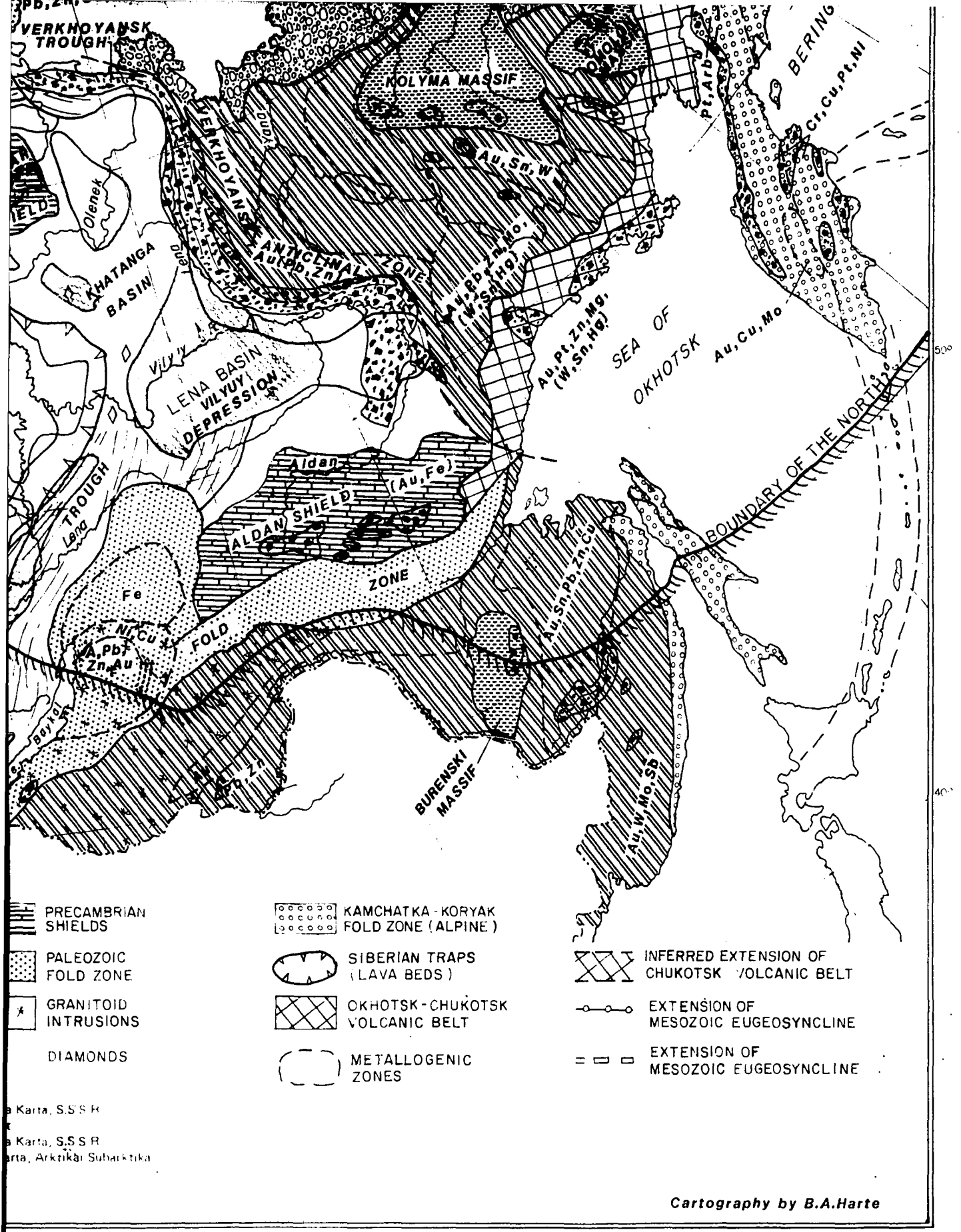

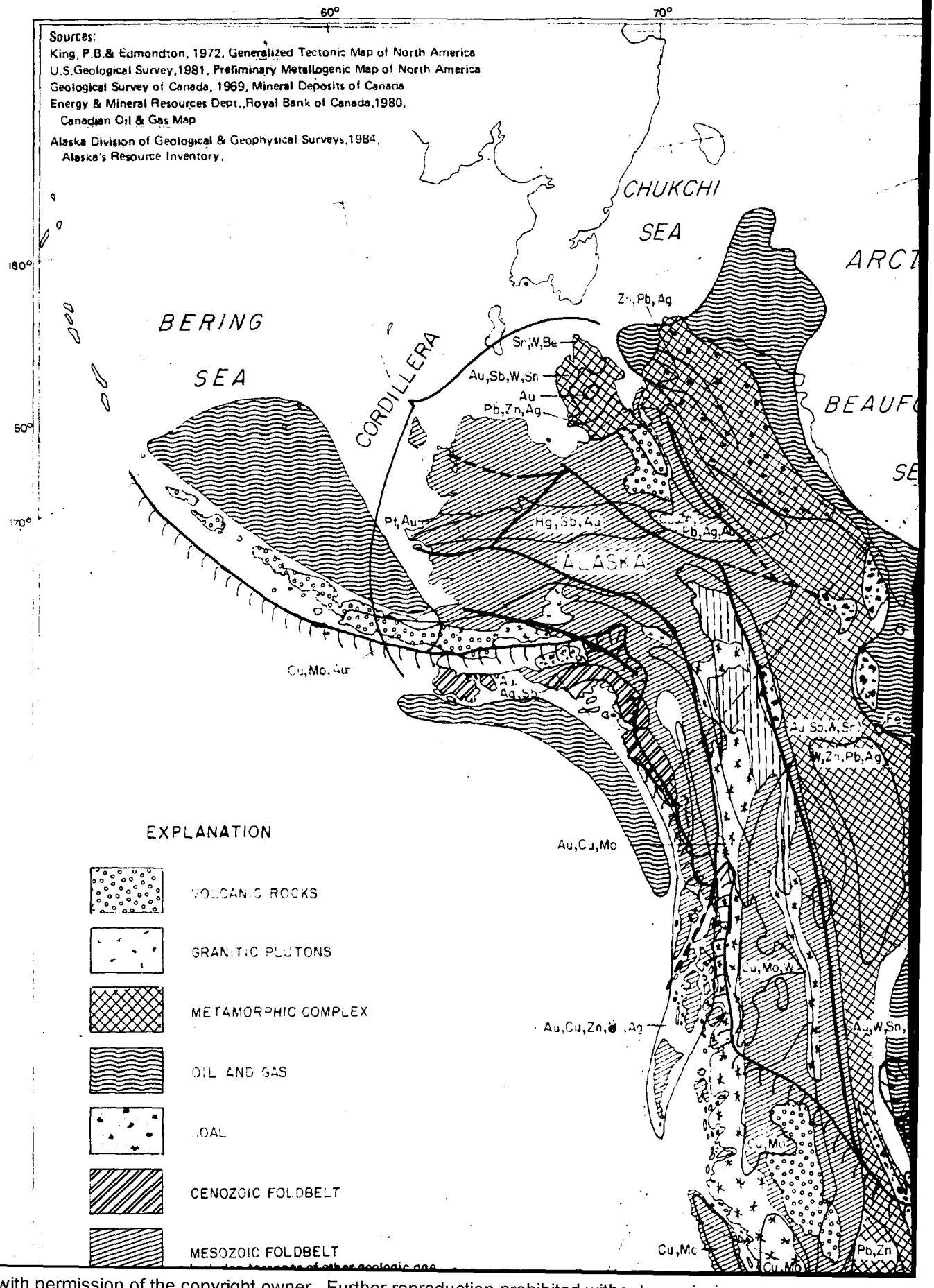

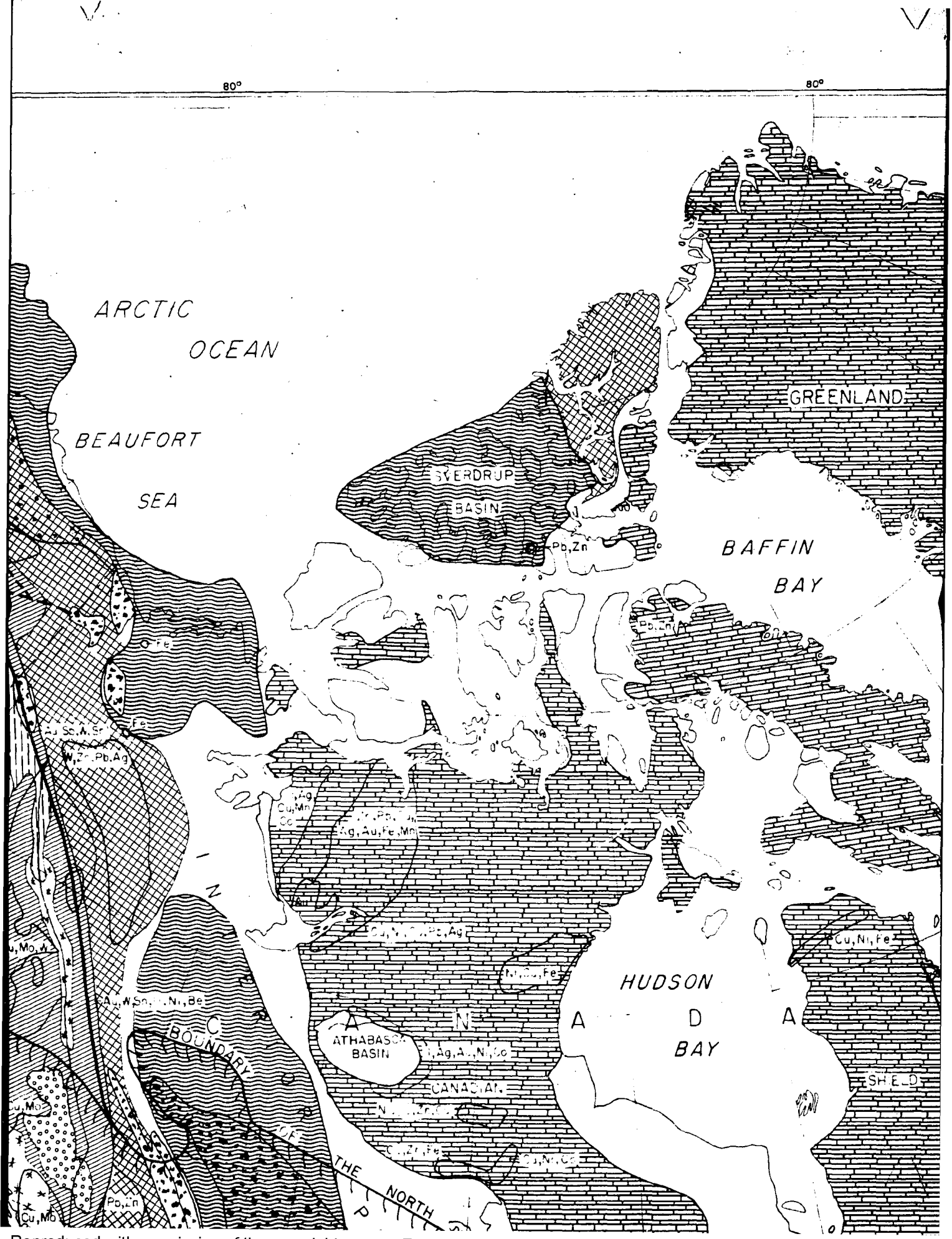

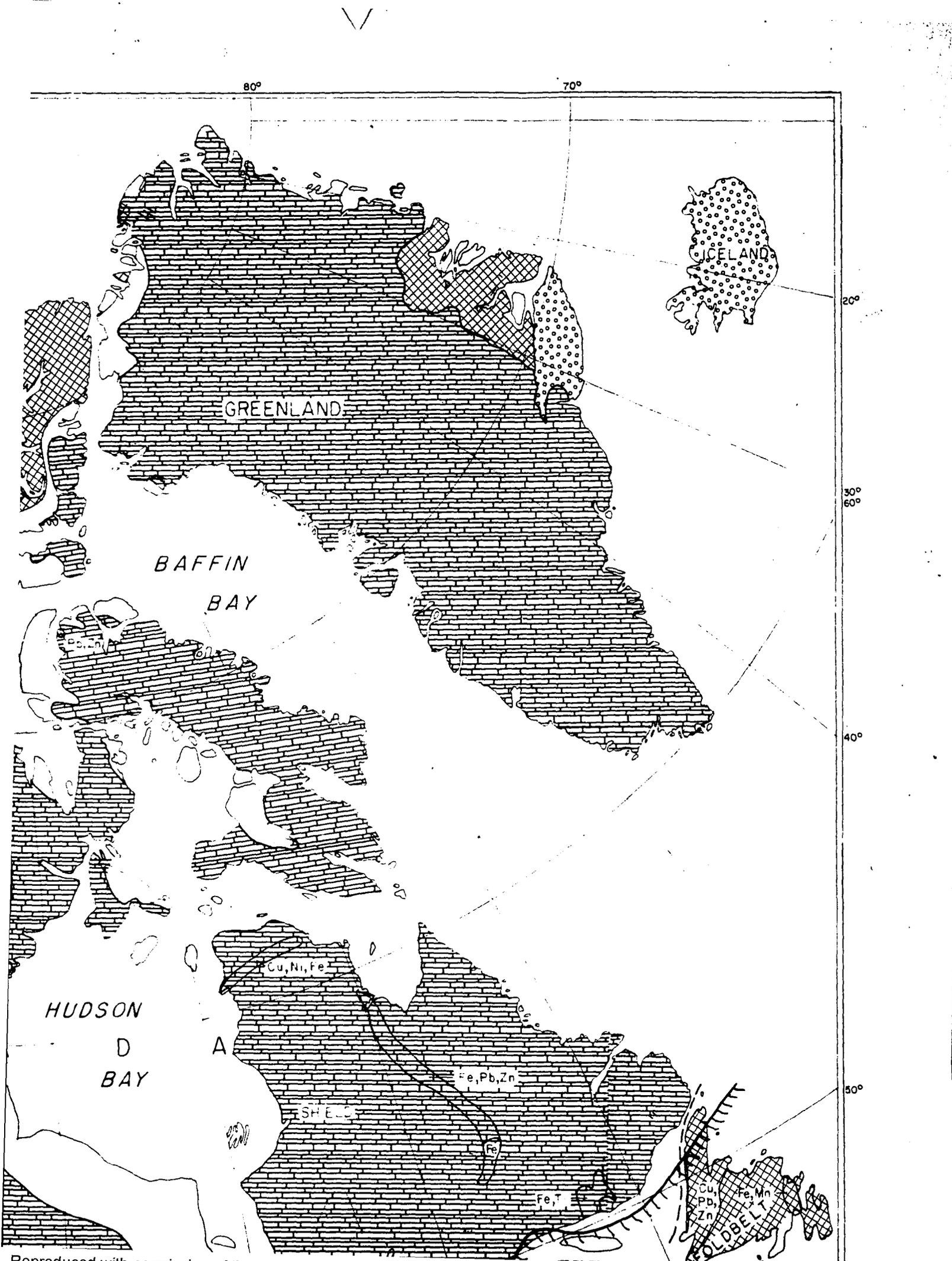

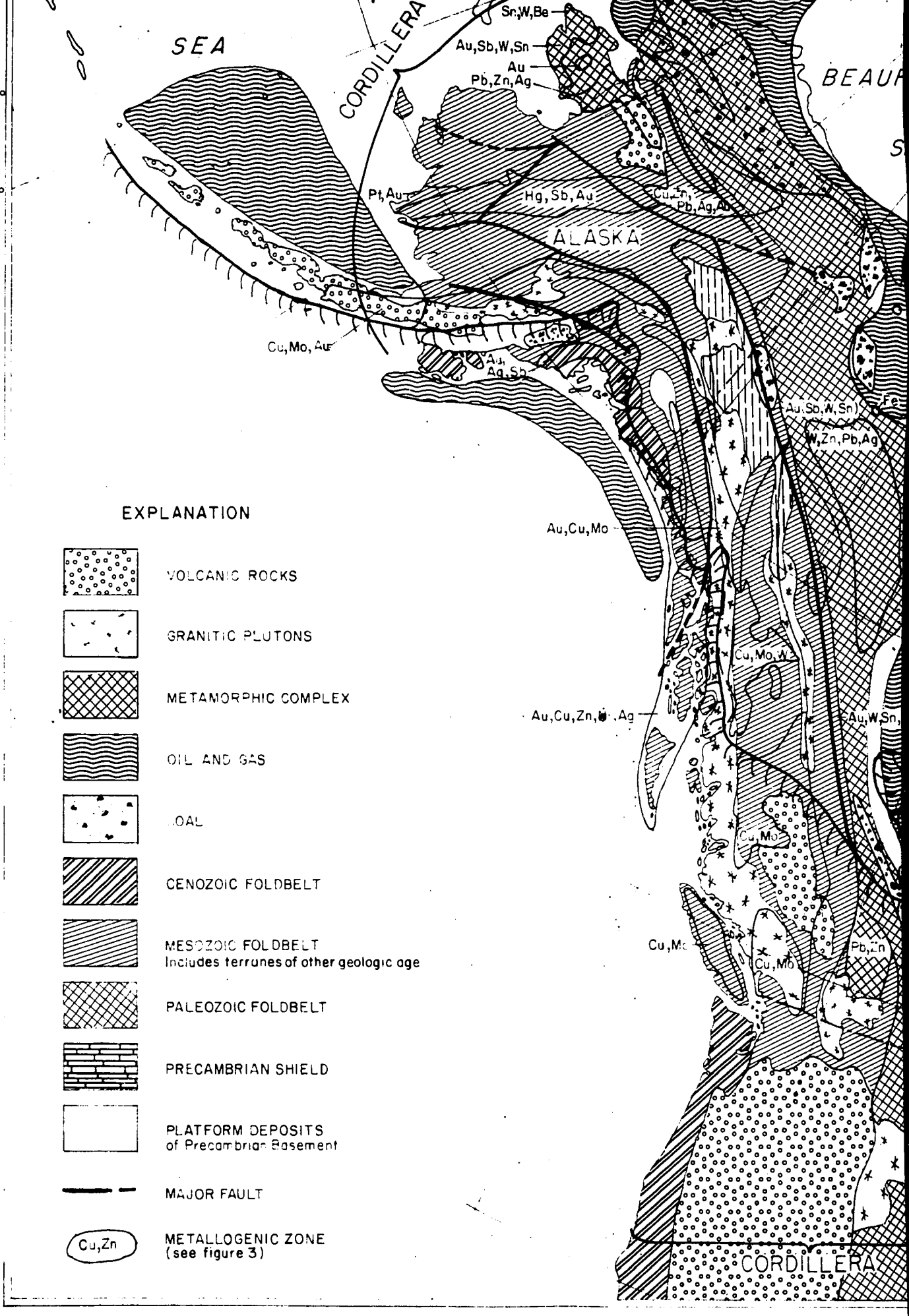

Figure 4

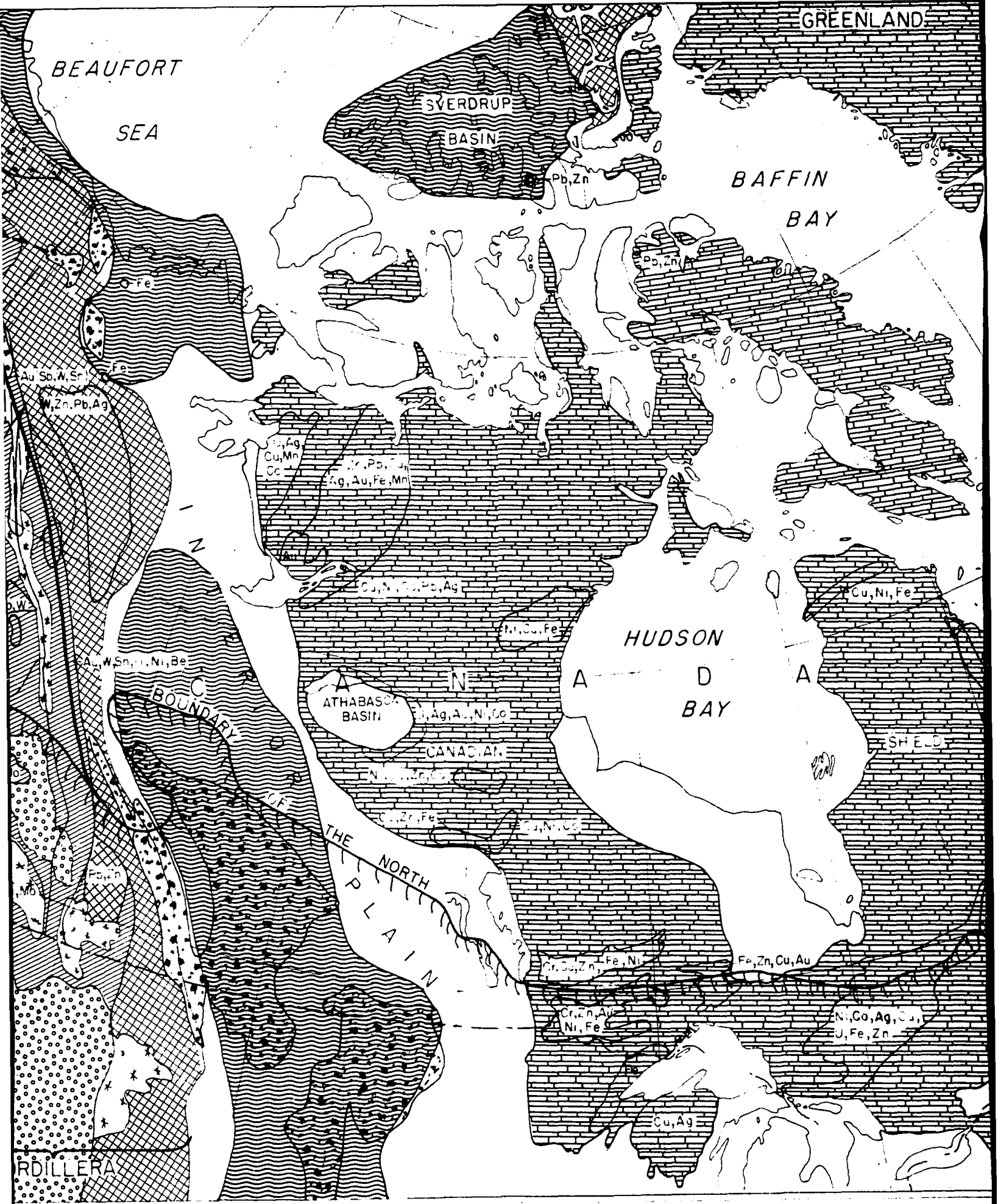

Figure 1. Geotectonic features and mineral zones, North American Northlands